DTIC FILE COPY

SECURITY CLASSIFICATION OF THIS PAGE

REPORT DOCUMENTATION PAGE

Form Approved OMB No. 0704-0188

1a. REPORT SECURITY CLASSIFICATION

AD-A219 183

1b. RESTRICTIVE MARKINGS
NONE

3. DISTRIBUTION/AVAILABILITY OF REPORT
APPROVED FOR PUBLIC RELEASE; DISTRIBUTION UNLIMITED.

5. MONITORING ORGANIZATION REPORT NUMBER(S)
AFIT/CI/CIA-89-161

6a. NAME OF PERFORMING ORGANIZATION	6b. OFFICE SYMBOL (If applicable)	7a. NAME OF MONITORING ORGANIZATION
AFIT STUDENT AT Univ of Oxford		AFIT/CIA

6c. ADDRESS (City, State, and ZIP Code)

7b. ADDRESS (City, State, and ZIP Code)
Wright-Patterson AFB OH 45433-6583

8a. NAME OF FUNDING/SPONSORING ORGANIZATION	8b. OFFICE SYMBOL (If applicable)	9. PROCUREMENT INSTRUMENT IDENTIFICATION NUMBER

8c. ADDRESS (City, State, and ZIP Code)

10. SOURCE OF FUNDING NUMBERS

PROGRAM ELEMENT NO.	PROJECT NO.	TASK NO.	WORK UNIT ACCESSION NO.

11. TITLE (Include Security Classification) (UNCLASSIFIED)
STRUCTURE-PROPERTY RELATIONS IN ALUMINIUM-LITHIUM ALLOYS

12. PERSONAL AUTHOR(S)
DAVID JOHN NICHOLLS

13a. TYPE OF REPORT	13b. TIME COVERED	14. DATE OF REPORT (Year, Month, Day)	15. PAGE COUNT
THESIS/DISSERTATION	FROM _____ TO _____	1989	156

16. SUPPLEMENTARY NOTATION
APPROVED FOR PUBLIC RELEASE IAW AFR 190-1
ERNEST A. HAYGOOD, 1st Lt, USAF
Executive Officer, Civilian Institution Programs

17. COSATI CODES		
FIELD	GROUP	SUB-GROUP

18. SUBJECT TERMS (Continue on reverse if necessary and identify by block number)

19. ABSTRACT (Continue on reverse if necessary and identify by block number)

DTIC ELECTE FEB 15 1990 S D

90 02 14 064

20. DISTRIBUTION/AVAILABILITY OF ABSTRACT	21. ABSTRACT SECURITY CLASSIFICATION
☒ UNCLASSIFIED/UNLIMITED ☐ SAME AS RPT. ☐ DTIC USERS	UNCLASSIFIED

22a. NAME OF RESPONSIBLE INDIVIDUAL	22b. TELEPHONE (Include Area Code)	22c. OFFICE SYMBOL
ERNEST A. HAYGOOD, 1st Lt, USAF	(513) 255-2259	AFIT/CI

DD Form 1473, JUN 86 Previous editions are obsolete. SECURITY CLASSIFICATION OF THIS PAGE

AFIT/CI "OVERPRINT"

STRUCTURE-PROPERTY RELATIONS IN ALUMINIUM-LITHIUM ALLOYS

David John Nicholls

Merton College

Oxford University

A thesis submitted for the degree of Doctor of Philosophy at the University of Oxford, Trinity term, 1989.

TABLE OF CONTENTS

ABSTRACT

David J. Nicholls
Merton College

D. Phil Thesis
Trinity term, 1989

Structure-Property Relations in Aluminium-Lithium Alloys

This work describes the effect of microstructure on the behaviour of small fatigue cracks in the two Al-Li-Cu-Mg-Zr alloys 8090 and 8091. The slip distribution in these alloys was varied through thermo-mechanical processing. Although slip distribution affected tensile, cyclic and long fatigue crack behaviour, it did not affect small fatigue crack behaviour due to low levels of closure and reduced slip reversibility near to a free surface. Similarly, underageing and overageing had no effect on small fatigue crack behaviour. Therefore, small fatigue crack growth is concluded to be insensitive to precipitate size and distribution. Due to differences in grain size, small fatigue cracks in 8091 were observed to propagate twice as slowly as in 8090.

Small fatigue cracks grew more rapidly than long fatigue cracks under the same nominal ΔK and displayed no threshold behaviour. This was shown to be due to the combined effects of the low closure levels, high applied stresses and proximity to the surface. Corrections to ΔK to account for these factors were shown to be less effective than using ΔJ as a correlating parameter. None of these factors affected the suitability of ΔK for characterizing microstructural effects. Small and long fatigue crack data were comparable when plotted versus calculated plastic zone size.

Low cycle fatigue behaviour was shown to be related to small fatigue crack behaviour and similar microstructural effects were observed. Total rather than plastic strain was identified as the critical parameter when comparing small fatigue crack and LCF behaviour. Small fatigue crack growth behaviour was shown to be inconsistent with the plastic work accumulation criterion for the exhaustion mechanism of fatigue. Finally, because of low ΔK's and the lack of closure, fatigue mechanisms may be easier to study in small cracks than in long cracks.

Acknowledgements

John Donne wrote that "no man is an island unto himself". Similarly, research projects are not done in isolation. For the help that they gave me in the course of this research, I would like to particularly thank the following people:

Professor Sir Peter Hirsch who provided the laboratory facilities.

Colonel C.A. Fisher and the U.S. Air Force Academy who gave me the opportunity to study at Oxford.

Dr. J.W. Martin, my supervisor, for his invaluable advice and encouragement throughout the project.

Dr. C. Peel and Dr. D.W. McDarmaid of the Royal Aircraft Establishment at Farnborough who supplied the alloys and participated in several helpful discussions.

Mr J. Short, Mr D. Pinfold, Mr J.W. Bryant, Mrs T. Godfrey, Mr R. Cripps and the other members of the laboratory workshops for their skilled and willing help.

Miss H. Peacock, Mr. A. Uguz, Dr. X. Xia, Dr A. Tekin, Mr. M Henderson and all members of the JWM group, for their friendship and assistance.

My parents who have always been willing to help.

Lastly, but by no means leastly, I would like to thank my wife, Cynthia, for her support, encouragement, beauty, charm and help with the wording of this sentence.

David J. Nicholls

Preface

This thesis is an account of research carried out in the Department of Metallurgy and Science of Materials at the University of Oxford between October 1987 and September 1989. The work reported is original and is not substantially the same as any thesis submitted in this or any other university. The work of other authors, when included in the text, has been acknowledged and the source given in an alphabetical list of references at the end of the thesis.

CHAPTER 1

FRACTURE, FATIGUE AND SMALL CRACK GROWTH

1.1 INTRODUCTION

In the 19th century there was an alarming increase in the number of accidents due to the failure of a structural component. The number of people killed in railroad accidents in Great Britain, for example, increased to about two hundred per year between 1860 and 1870 (Broek, 1978). Most of these accidents were caused by the brittle fracture of a wheel, an axle or a rail. Factors that led to this increase in structural failures included a greater number of structural applications for materials and the higher design stresses that were possible with a better understanding of mechanics.

Gradually, it was discovered that many failures were due to the presence of a flaw within the material. Some flaws were introduced during the manufacturing process and could be eliminated through improved production methods. Other flaws, initially insignificant, grew sufficiently under cyclic loading to cause fracture. This process, not initially understood, was known as fatigue. Nowadays, calculation of the life of structures subject to cyclic loading is recognized as an essential part of design. Nevertheless, Duga et al (1983) have estimated that fracture and fatigue still cost the U.S. $119 billion each year, approximately half of which could have been saved with currently available techniques.

The work contained in this thesis was done to explore the behaviour of small fatigue cracks in the aluminium-lithium (Al-Li) alloys 8090 and 8091. The practical significance of the growth in fatigue of small, or indeed any, cracks is that knowledge of their behaviour is required for accurate estimates of design life.

Therefore, the next topic to be discussed will be how design life calculations have been made in the past and how they are made today. This will be followed by a description of fracture mechanics and its application to prediction of the rate of crack growth. Having established the framework of fracture mechanics that contains the subject of small fatigue cracks, the literature relating specifically to small fatigue cracks will be reviewed. Because of the large amount of literature concerning small cracks, the objective of this review will be to summarise the current understanding of small fatigue crack behaviour and to provide a framework for the experimental results to be discussed later rather than to review the literature exhaustively.

1.2 DESIGN LIFE CALCULATION

Wöhler (1860) was one of the first to develop a technique for calculating the design life of a structure. As part of his investigation of the brittle fracture of railroad wheel axles, he plotted the maximum stress during cyclic loading versus the number of cycles to failure. Such a plot is known today as an S-N curve and is still widely used. Since Wöhler, the usefulness of S-N curves has been enhanced with the development of empirical extensions, such as Goodman diagrams which account for the effect of mean stress and Miner's Rule which accounts for variable amplitude loading.

Any design method based on S-N diagrams uses data generated from smooth, polished specimens. This means that the time required for a specimen to fail includes both the time to initiate a crack and the time to propagate that crack to failure. If a crack already exists in a structure, then the structure will fail after only the

amount of time required for the crack to propagate to a critical size. The implicit inclusion of the time required for crack initiation makes it difficult for S-N curves to account for pre-existing flaws. Unfortunately, the time required for crack initiation is often a large proportion of the total life and so pre-existing flaws dramatically reduce structural life.

A well known accident illustrating this point is the crash of a U.S. Air Force F-111 in 1968. This aircraft had been designed using S-N data that, combined with full-scale prototype testing, indicated that the wing root could be expected to last about 40,000 flight hours. In actual fact, an aircraft lost a wing after only 100 hours in flight. The failure investigation showed that the accident was caused by a pre-existing flaw which was undetected during the manufacturing process.

Such accidents spurred interest, especially in the nuclear and aerospace communities, in developing better design techniques. It was recognised that any design technique which hoped to improve on S-N curves must assume the existence of pre-existing flaws. Or, in other words, the design life must be defined as the length of time required for the most damaging pre-existing flaw to grow enough to cause catastrophic failure of the component. In order to calculate this period of time the following three facts must be known:

1. the size of the pre-existing flaw
2. the size of a flaw that will cause structural failure
3. the rate of crack growth in between these two extremes.

"Damage tolerant" design, so called because the structure is tolerant of flaws up to a defined size, was developed as an improvement to the use of S-N curves and centres around the calculation of these three facts. The size of the pre-existing flaw is

usually defined as the size of flaw that would just be detectable by inspection. The size of flaw that will cause structural failure is calculated from the theory of fracture mechanics. Finally, the rate of crack growth is calculated empirically from laboratory test specimens.

In practice, components designed to be "damage tolerant" are periodically inspected for cracks throughout their service life. If a crack long enough to grow to a critical size before the next inspection is found, the component is either removed from service or repaired. If no crack sufficiently large is found then the component is returned to service until the next inspection. The length of the inspection interval is chosen such that cracks too small to be detected in an inspection cannot become critical before the next inspection.

1.3 FRACTURE MECHANICS

The success of damage tolerant design hinges on the ability to extrapolate crack growth behaviour in laboratory specimens to crack growth behaviour in structures. Fracture mechanics had already been successfully used to calculate the critical crack length for a given structure. Therefore, it was natural to suspect that it could also be used to calculate crack growth rates. In 1961, Paris et al correlated the rate of fatigue crack growth for a variety of geometries using the fracture mechanics concept of the stress intensity factor (K). The use of K to predict the crack growth behaviour in structures from laboratory specimens has been highly successful but there are conditions in which it requires adaptation or might be totally inappropriate. The topic of this thesis, small crack growth, is one such area. The purpose of this section is to

summarise the theory of fracture mechanics and its application to predicting crack growth rates.

1.3.1 THE GRIFFITH CRITERION

One approach to modelling the mechanical behaviour of a crack is to treat it as a stress concentration - the analysis of which is well established. A crack may be modelled as a very narrow elliptical hole. The expression for the stress concentration due to an elliptical hole is $\sigma = \sigma_{nom}[1 + 2(L/R)]$ (Inglis, 1913). L and R are the half length and the radius of curvature at the narrow part of the ellipse, respectively. If the ellipse is narrowed to model a crack then R approaches zero and the stress at the crack tip approaches infinity. Unfortunately, as all cracks would have stresses approaching infinity, it is useless to model a crack as a stress concentration from a design standpoint. Another approach is required.

Griffith (1920) resolved the problem by considering crack growth from an energy standpoint. Regardless of the stresses, for a crack to grow in an elastic material there must be sufficient energy to create the new crack face surfaces. This energy is supplied by the release of strain energy associated with the increase in structural compliance as the crack grows. The Griffith criterion below is derived by equating the strain energy release rate to the rate of surface energy required by the advancing crack. E is the Young's modulus, γ_s is the surface energy, a is one half of the crack length, and σ_{crit} is the stress required to propagate the crack.

$$\sigma_{crit} = \left(\frac{2E\gamma_s}{\pi a}\right)^{1/2}$$

Irwin (1948) and Orowan (1948) later extended this equation to materials which could deform plastically by adding an energy term for the plastic deformation. Subsequently, this equation has been more commonly expressed with an energy source term instead of the energy sink term (γ_s). The energy source term is the strain energy release rate, named G in honour of Griffith. Substituting G for $2\gamma_s$ in the previous equation we get, after rearrangement, the result below showing that G is a function of the applied stress and crack length.

$$G = \frac{\pi a \sigma^2}{E}$$

When G reaches a critical value (denoted G_c) fracture will occur. Irwin (1964) further extended the usefulness of the theory by calculating the strain energy release rate in terms of the change in compliance of the cracked component. While this theory made some useful contributions, its application was limited because the principle of superposition could not be applied and so complicated crack geometries could not be modelled by superposing solutions for simpler ones.

1.3.2 THE STRESS INTENSITY FACTOR

The stress intensity factor (K) was first proposed by Irwin (1957) as a convenient way to calculate G. K, however, eventually became more important than G, primarily because K solutions could be superposed to calculate K for a complicated loading situation or geometry. Like the stress concentration approach, K is related to the stresses around the crack tip. The stresses around the tip of a crack under remote, uniaxial tension in an elastic solid are given by the following equations. θ and r are the angle and the radial distance respectively of the point of interest from the crack tip. σ

is the applied stress.

$$\sigma_{xx} = \sigma \left[\frac{\pi a}{2\pi r}\right]^{1/2} \cos\theta/2\ [1 - \sin\theta/2\ \sin3\theta/2] + \text{higher order terms}$$

$$\sigma_{yy} = \sigma \left[\frac{\pi a}{2\pi r}\right]^{1/2} \cos\theta/2\ [1 + \sin\theta/2\ \sin3\theta/2] + \text{higher order terms}$$

$$\tau_{xy} = \sigma \left[\frac{\pi a}{2\pi r}\right]^{1/2} \sin\theta/2\ \cos\theta/2\ \sin3\theta/2 + \text{higher order terms}$$

Close to the crack tip the higher order terms are negligible. Neglecting these terms and defining K as $K = Y\sigma(\pi a)^{1/2}$ where Y is a geometric factor (equal to unity for a remotely loaded crack in an infinite plate) the previous equations become

$$\sigma_{xx} = \frac{K}{[2\pi r]^{1/2}} \cos\theta/2\ [1 - \sin\theta/2\ \sin3\theta/2]$$

$$\sigma_{yy} = \frac{K}{[2\pi r]^{1/2}} \cos\theta/2\ [1 + \sin\theta/2\ \sin3\theta/2]$$

$$\tau_{xy} = \frac{K}{[2\pi r]^{1/2}} \sin\theta/2\ \cos\theta/2\ \sin3\theta/2$$

Three points should be recognised. Firstly, although the stresses are still infinite at the crack tip (in agreement with the stress concentration approach) K is not infinite. The singularity is caused by r equalling zero at the crack tip. Secondly, every term except K is a function of only r and θ. This means that the distribution of stresses around a crack is the same for all cracks but that the overall intensity of these stresses is determined by K. K, which is a function of the applied stresses, the specimen geometry, and the crack length, can be used in design as a measure of the stress field around a crack. Finally, comparison of the equations for K and for G indicates that the two are related. The relationship for plane stress is

$$G = \frac{K^2}{E}$$

Just as there is a critical value of G that causes fracture, there is a critical value of K associated with fracture called K_c. K_c is a function of specimen thickness as shown in Figure 1.1. Because of the desirability of a criterion for fracture that is independent of geometry, published values of K_c are normally taken from the plateau of Figure 1.1 (i.e. under plane strain conditions). Furthermore, it is important to specify the mode of loading (see Figure 1.2). Thus, K_{Ic} is defined as the plane strain fracture toughness under mode I loading. K_{IIc} and K_{IIIc} are similarly defined for their respective modes of loading.

1.3.3 PLASTIC ZONE SIZE

The equations for the stress field around a crack tip were derived assuming that the material was perfectly elastic. In reality there will be plastic yielding at the crack tip. For the stress field equations still to estimate accurately the stresses around the crack tip, the plastic zone must be small in comparison with both the crack length and the overall specimen dimensions. If this small scale yielding assumption is not satisfied then K cannot be used. Therefore, it is important to estimate the size of the plastic zone.

A first estimate of the plastic zone size may be made by setting σ_{yy} in the crack stress field equations equal to the yield stress and θ equal to zero. This gives the result (when rearranged)

$$r_p = \frac{1}{2\pi}\left(\frac{K_I}{\sigma_y}\right)^2$$

However, local yielding near the crack tip leads to a redistribution of the stresses as illustrated in Figure 1.3. Setting the areas of the two shaded regions equal to one another the following equation can be derived for a condition of plane stress.

$$r_p = \frac{1}{\pi}\left(\frac{K_I}{\sigma_y}\right)^2$$

Alternatively, the Dugdale model has been used to derive this very similar expression for plastic zone size (Kanninen and Popelar, 1985).

$$r_p = \frac{\pi}{8}\left(\frac{K_I}{\sigma_y}\right)^2$$

In plane strain the smallest principal stress is tensile rather than zero so the stress required to yield the material is increased. Based on an estimate that the yield stress was increased by the square root of three, Irwin (1968) derived the following equation for the size of the plastic zone under plane strain conditions.

$$r_p = \frac{1}{3\pi}\left(\frac{K_I}{\sigma_y}\right)^2$$

Combining the equations for the state of stress at the crack tip with a yield criterion such as the Von Mises yield criterion, it is possible to calculate the plastic zone size as a function of θ. The plastic zones for plane stress and plane strain conditions are graphically illustrated in Figure 1.4.

In the case of a fatigue crack there is, in addition to the plastic zone described above, a reversed plastic zone in which material is alternately plastically stretched and compressed. This zone arises through the following mechanism. When K is maximum all of the material is in tension but only the material within the plastic zone is plastically deformed. As K is reduced to its minimum value, the material outside the plastic zone, while elastically contracting, compresses the plastically deformed material within the plastic zone. Near the crack tip, where the plastic strains were the greatest in tension, the compressive stresses are the highest and may exceed the compressive yield strength. Thus, when K is a minimum, there

is a small zone where material is plastically deformed in compression. The cycle repeats when K increases again. Paris (1964) suggested that the size of the reversed plastic zone is given by the following equation.

$$r_p = \frac{1}{8\pi}\left(\frac{\Delta K}{\sigma_{ys}}\right)^2$$

1.3.4 ELASTIC-PLASTIC FRACTURE MECHANICS

Because there are applications where the small scale yielding assumption is not valid, elastic-plastic parameters have also been developed. The best known are the crack tip opening displacement (CTOD) and the J integral.

The CTOD concept is based on the fact that, when the net section is near to yielding, additional applied stress affects only the crack tip strains, not the crack tip stresses. Consequently, the crack tip blunts and the crack faces at the crack tip separate. Wells (1963) postulated that there is a critical value of this separation displacement required for crack advance. The main problem with this approach is the experimental difficulty of measuring the separation of the crack faces at the crack tip.

The J integral (Rice, 1968) is defined by the following line integral around the crack tip.

$$J = \int_{\Gamma} w\, dy - T\frac{\partial u}{\partial x} ds$$

T is the traction vector, u is the displacement vector in the x direction, w is the strain energy density, and y is perpendicular to the crack line. Physically, J is a measure of the potential energy change associated with the growth of a crack in a non-linear, elastic solid. Because J is path-independent, any convenient path may be chosen to integrate over as long as the crack tip is surrounded. As

a result, J is easier to calculate than CTOD.

Although strictly J is defined for a non-linear, elastic material, it can nevertheless be applied to elastic-plastic materials. The main reason for this is that the stress-strain behaviour of non-linear, elastic materials and elastic-plastic materials is the same if the stress is monotonically increased. If the stress is decreased, of course, the stress-strain curve for a non-linear elastic material would retrace its path while the stress strain curve for an elastic-plastic material would decrease linearly to some permanent offset (see Figure 1.5). This raises certain issues when J is applied to fatigue which will be discussed in section 1.4.4. The application of J to elastic-plastic materials does, however, modify the physical meaning of J. For elastic-plastic materials, J is the work required for the deflection of the solid rather than the change in potential energy associated with crack growth.

1.3.5 APPLICATION OF FRACTURE MECHANICS TO FATIGUE

As noted in section 1.3.3, the size of the reversed plastic zone is related to ΔK. Inasmuch as fatigue crack growth is the result of accumulated damage at the crack tip, it is perhaps not surprising that the rate of crack growth is related to ΔK. To find this relation, Paris et al (1961) plotted the rate of crack growth (da/dN) vs ΔK producing a curve similar to that in Figure 1.6. Two particularly noteworthy aspects of this curve are the linear region, upon which the well-known Paris "law" is empirically based, and the threshold region, where the crack growth rate dramatically decreases resulting in a threshold ΔK below which no crack growth occurs.

The importance of this work was that it established ΔK as a parameter that could correlate fatigue crack growth rates for

different geometries. Therefore, it could be used to predict crack growth rates in structures from data generated on laboratory test specimens. In addition, the Paris law ($da/dN = A\Delta K^m$) provided a relation that could be integrated to calculate the number of cycles required for a given amount of crack growth. This is exactly what is required for damage tolerant design approaches and ΔK is now widely used for predicting fatigue crack growth rates in structures.

Perhaps because of ΔK's widespread use, there is significant concern when ΔK-based approaches fail to predict crack growth rates. Often, failure is associated with the presence of large scale yielding because LEFM equations no longer describe the stresses around the crack tip. For such cases ΔJ, an elastic-plastic parameter, has been used. The concept of crack closure has been used to describe several irregularities in crack growth behaviour including the existence of ΔK_{th} and the dependence of crack growth rate on the stress ratio. Because crack closure has also been used to rationalize small crack behaviour, it will now be briefly described.

The concept of closure was first proposed by Elber (1970). He showed that a fatigue crack closes (i.e. the crack faces touch) at values of K above K_{min} even when K_{min} is tensile. Once the crack has closed the actual value of K at the crack tip ceases to decrease as the applied stress falls. Consequently, the effective ΔK at the crack tip is given by $\Delta K_{eff}=K_{max}-K_{cl}$ rather than $\Delta K=K_{max}-K_{min}$. The overall effect of closure is to reduce the driving force and so to reduce the crack growth rate.

Several mechanisms that have been proposed for closure are illustrated in Figure 1.7. All of these mechanisms result in the contact of the crack faces before the minimum load is reached. In plasticity-induced closure, proposed by Elber (1970), the material in

the plastic zone remains extended producing a plastic "wake". Roughness-induced closure, initially suggested by Cooke and Beevers (1974), applies when the crack path is zig-zag or serrated. In such a case, the peaks on the mating surfaces tend to interfere with each other which again means that the crack surfaces come into contact for values of K higher than K_{min}. In oxide-induced closure, first suggested by Paris et al (1972), newly created fracture surfaces oxidize. If the thickness of the oxide layer is comparable to the crack opening displacement the crack surfaces are prematurely brought into contact. Viscous fluid-induced closure only applies when the crack is submerged in a liquid and phase transformation-induced closure has been mainly associated with toughened ceramics. As they are irrelevant to the materials and conditions used in this work, they will not be discussed further.

As alluded to earlier, the growth of small cracks is anomolous when compared to the growth of long cracks under nominally the same ΔK. Having briefly described the design methodology used to predict structural life and the importance of ΔK in predicting crack growth rates, discussion will now focus on small fatigue crack behaviour and on the explanations for it.

1.4 SMALL FATIGUE CRACK PROPAGATION

It is appropriate to begin by formally defining what is meant by the term "small" crack. Firstly, there is the question of how many dimensions of a crack must be small for it to be considered small. That is, there is a distinction between a semicircular surface crack that is small in all of its dimensions and a through-the-thickness crack that is small in its length alone. The latter type of crack is commonly called "short" as opposed to "small".

Secondly, there is the question of what measure is used to class a crack as small. Suresh and Ritchie (1984) have suggested that types of cracks may be defined by considering what the crack length is small in relation to. A "mechanically" small crack's length is comparable to the size of its plastic zone. A "microstructurally" small crack's length is comparable to some relevant microstructure of the material (usually the grain size). A crack is considered to be "physically" small when it is less than about 0.5 mm in length. Finally, a "chemically" small crack is that propagates anomalously rapidly because of the unusual accessibility of the tip of the crack to the environment. Environmental effects are beyond the scope of this thesis, so chemically small cracks will not be discussed further.

1.4.1 BEHAVIOUR OF SMALL CRACKS

As was first noted by Pearson (1975), small cracks grow up to two orders of magnitude faster than long cracks under nominally the same ΔK. Furthermore, small cracks often grow under loading conditions that are well below the threshold ΔK required for long cracks. A useful perspective on the threshold behaviour of small cracks was provided by Kitagawa and Takahashi (1976). They observed that the non-propagation of cracks smaller than about 0.5 mm was determined by the endurance limit stress (σ_e) rather than ΔK_{th}. This suggested that small crack behaviour might link S-N behaviour and crack propagation behaviour based on fracture mechanics. As is illustrated in the schematic Kitagawa-Takahshi diagram shown in Figure 1.8, the non-propagation of cracks larger than a_o is determined by ΔK_{th}. For cracks smaller than a_o, σ_e is the critical parameter and ΔK_{th}, no longer a material property, decreases with crack length. The crack length associated with the

transition from long to small crack behaviour may be calculated by equating σ_e to the stress associated with the non-propagation of a long crack i.e.

$$\Delta\sigma = \frac{\Delta K_{th}}{Y(a)^{1/2}}$$

The resulting expression for the transitional crack length is

$$a_o = \left(\frac{\Delta K_{th}}{Y \Delta \sigma_e} \right)^2$$

El Haddad et al (1979) used these ideas in an attempt to extend the usefulness of ΔK to the small crack regime. An effective ΔK was defined as $\Delta K_{eff} = Y\sigma(a+a_o)^{1/2}$ where a_o is the transitional crack length just discussed. El Haddad felt that the addition of a_o to the actual crack length reflected the effect of the decreased constraint associated with surface grains on the stress required for deformation. He did not, however, provide a theoretical basis for the expression for a_o and so it remains empirical.

Although Kitagawa-Takahashi diagrams and El Haddad's effective length concept provide useful descriptions of small fatigue crack behaviour, they do not actually explain the behaviour of small cracks. After a brief discussion of the relevance of small cracks, work done on physically, mechanically and microstructurally small cracks will be reviewed. For the purposes of organization the various type of small cracks will be discussed separately. Many small cracks, however, are small by more than one definition and so more than one explanation is often required to account for their behaviour.

1.4.2 RELEVANCE OF SMALL CRACKS

For the behaviour of a crack to be relevant to damage tolerant design it must be detectable by inspection. Smith (1986) has pointed

out that most non-destructive testing techniques can only reliably find cracks more than 0.5 mm long. On this basis, the practical relevance of small cracks would appear to be limited. As Wanhill (1986) points out, however, some applications, such as engine disks, are very highly stressed which means that the critical crack length will be very small. Therefore, only small crack growth behaviour will be relevant. Furthermore, improved inspection methods have been developed that are capable of detecting small cracks in such components (Blom, 1986).

In addition, there are applications where alternatives to damage tolerant design are or might be used. ΔK_{th} has been used, in engine blades, for example, to define an operating stress below which fatigue is not a concern (Blom, 1986). ΔK_{th} is only a material property for long cracks and its use for applications containing small cracks is likely to be highly non-conservative as small cracks have much lower thresholds. Also, various probalistic analyses for durability are now under development (Nicholas, 1989) that will use statistical distributions of assumed crack sizes well into the small crack regime.

Small cracks may also be a link between S-N behaviour and crack growth behaviour as characterized with fracture mechanics. The relation between the threshold behaviour of small cracks and the endurance limit in S-N curves has already been discussed. In addition, as was pointed out by Taylor and Knott (1981), the anomolously fast growth rate of small cracks is probably necessary to explain how very small defects in polished S-N specimens can grow enough to cause failure. Finally, it has been recognised for a number of years that low cycle fatigue behaviour is dependent on crack propagation behaviour. In these specimens the propagating

cracks are very small and so small crack behaviour is likely to be more applicable than long crack behaviour.

1.4.3 PHYSICALLY SMALL CRACKS.

Much of the work on physically small cracks has been on "short" as opposed to "small" cracks. Typically, short cracks are made by growing a long crack and then machining away most of the material that the crack has passed through. It seems clear through the work of many investigators (Suresh and Ritchie, 1984) that the differences in short and long crack behaviour are due to the lack of closure in short cracks. Closure levels are reduced in short cracks because, although the crack surfaces may touch, there is very little area over which to generate significant closure forces. Viewed in this sense, it is the behaviour of long cracks that is anomalous because to calculate the true crack driving force, ΔK must be corrected for closure.

As evidence supporting this idea it appears that, when closure is taken into account, long and short cracks obey the same crack propagation law in the Paris regime (Breat et al, 1983). The lack of closure also explains the lower or non-existent threshold of short cracks. Several studies (Vecchio and Hertzberg, 1985) suggest that the threshold ΔK observed in long cracks is due to plasticity-induced closure generated by the load shedding used in approaching low ΔK levels. In short cracks the plastic wake is removed and so the ΔK threshold would be expected to disappear. Also consistent with this idea is the observation that, as the short crack propagates, the plastic wake is reformed and the closure stresses are redeveloped. When the plastic wake is fully reformed, the closure stresses rise and the rate of crack growth approaches that

found in long cracks.

Recent years have also seen the development of techniques to directly measure closure in small cracks (eg Larsen, 1987). Such studies show that closure is reduced in small cracks but not completely absent. Interestingly, the level of closure appears to depend on the length of the crack so that K_{max}/K_{cl} remains approximately constant. In this respect, small crack behaviour is unlike that of long cracks where K_{max}/K_{cl} typically approaches unity near threshold. This may partially explain Kitagawa and Takahashi's (1976) finding that non-propagation of a small crack is a function of its length.

1.4.4 MECHANICALLY SMALL CRACKS

As stated before, a mechanically small crack is one in which the plastic zone is comparable in size to the crack itself. Typically, all the dimensions of the crack are considered, so mechanically small cracks tend to be "small" rather than "short". An understanding of the behaviour of mechanically small cracks is important since many small cracks are mechanically small. The crack growth behaviour of mechanically small cracks is distinct from both long and "short" cracks. Mechanically small cracks not only grow below threshold, but they also grow at much higher rates than would be expected if the Paris regime for long cracks is extrapolated.

In order to assess whether a crack is mechanically small, the size of the plastic zone may be calculated using one of the equations referenced in section 1.3.3 such as

$$r_p = \frac{1}{\pi}\left(\frac{K_I}{\sigma_y}\right)^2$$

In actual fact, this type of equation tends to underestimate the

plastic zone size associated with small cracks and thus can fail to identify many mechanically small cracks. In part, this failure may stem from microstructural factors. For example, the plastic zone may be completely bounded by a single grain implying violation of the homogeneous, continuum assumption implicit in the use of K. Partly, however, this failure must be due to the high stresses (typically 60 to 90% of the yield strength) required to propagate very small cracks. Because of high average stresses, the equations for the stress field around a crack tip must retain higher order terms that are usually insignificant. Based on calculations of the J integral using the finite element method, Trantina and deLorenzi (1982) have suggested that K will no longer accurately represent the stress field around a crack when σ/σ_{ys} is greater than 0.7.

The lack of similitude between long and small cracks has been emphasized by experimental measurements of the plastic deformation associated with both long and small cracks. Lankford et al (1984) have measured the plastic zone size and CTOD for small cracks using scattered electron channelling patterns and stereo-imaging. They found that for small cracks the plastic zone was usually comparable in size to the crack itself. On this basis, they argued that the small scale yielding assumption, implicit with the use of ΔK, was violated More recently, Davidson and Lankford (1986) have found that mechanically small cracks are distinct from long cracks in the following ways.

1. The distribution of strains near the crack tip for short cracks is different than for long cracks and the strains are higher for equivalent ΔK's.
2. The CTOD is dependent on crack length although the crack tip strains were not.

3. The reversed plastic zone is almost as large as the overall plastic zone.
4. The strain fields associated with each end of the crack interact.
5. The material around the crack continues to deform - even when the crack tip is past.

As ΔK fails to correlate the strains and the CTOD's of mechanically small cracks with those of long cracks, it appears that ΔK may be inappropriate as a correlating parameter for the crack growth behaviour of mechanically small cracks.

To solve the problems associated with the amount of plasticity around the crack tip, the use of J (an elastic-plastic parameter) has been suggested (Hudak and Chan, 1986). As alluded to in section 1.3.4, the application of J to fatigue is not straightforward because of cyclic unloading of the crack. To circumvent the no-unloading restriction implicit in J, Lamba (1975) proposed a ΔJ integral where each term in the J integral is replaced by its respective range as shown below.

$$\Delta J = \int_{\Gamma} \Delta w \, dy - \Delta T \frac{\partial \Delta u}{\partial x} ds$$

An issue to be resolved is whether ΔJ is path independent. A necessary condition for the path independence of ΔJ is that the relationship between the strain range and the stress range must be independent of the deformation history. This condition is not satisfied by elastic-plastic materials under cyclic loading. To circumvent this problem, the cyclic stress-strain curve, which is independent of the deformation history, is used to relate the stress and strain ranges. There is also a certain physical appeal to this approach since it is reasonable to think of the material ahead of the

crack tip as a miniature low cycle fatigue specimen.

Nevertheless, this issue is still controversial. From careful measurements of the strains on various paths around the crack tip, Chan and Lankford (1988) have shown that ΔJ is path dependent due to closure for long cracks and microstructural effects for small ones. Despite this, Dowling (1977) and Davidson (1988) have successfully used ΔJ to correlate long and small crack growth rates. In addition, El Haddad and Miettinen (1982) have incorporated ΔJ and small crack growth in a fracture mechanics model for predicting low cycle fatigue lifetimes.

Another parameter currently receiving consideration is S, the strain energy density. Vecchio and Hertzberg (1985) have been able to correlate long and mechanically short crack data using ΔS for Astroloy. It should be noted that these data were for short cracks rather than small. The use of ΔS to characterize crack growth rates is not as well accepted as ΔJ primarily because of its failure to predict the direction of crack growth. As Hudak and Chan (1986) point out, however, this failure may be due to the difficulty of performing the tests and the sensitivity of the strain field to kinking or branching of the crack.

1.4.5 MICROSTRUCTURALLY SMALL CRACKS

Like mechanically small cracks, microstructurally small cracks are small rather than short. Similarly, microstructurally small cracks not only grow below the threshold observed in long cracks but also grow at higher rates than extrapolations from the Paris regime of long cracks. Unlike mechanically small cracks, however, the anomalous growth rates of microstructurally small cracks derive from the ability of microstructurally small cracks to exploit local

weaknesses. Among the microstructural features examined for their effect on small crack growth are crystallographic orientation, grain size, and precipitate size.

Crystallographic orientation undoubtedly has an important role in determining the rate at which small cracks grow. Small cracks grow crystallographically because their small size enables them to follow the slip planes which have the least resistance to cyclic slip (Suresh, 1983). Because the resistance to crack growth is lessened, small cracks grow very quickly. The effects of crystallographic orientation are seen clearly in textured material where there are preferred directions for crack growth. The angle between these preferred directions and the loading axis determines the mode of loading which, in turn, affects the rate of crack growth. Furthermore, when a crack enters a new grain, it changes direction to follow the new slip plane. Texture can determine the relative orientations of the grains and thereby the magnitude of the change in direction. Suresh (1983) has shown that such deflection processes can have a significant effect on the effective ΔK even discounting roughness-induced closure.

A related phenomenon is the dependence of the growth rate of small cracks on grain size. When a small crack approaches a grain boundary, the rate of growth is slowed or, in some cases stopped completely (Newman and Beevers, 1986). It follows that if the grain size is smaller, the distance between grain boundaries will be less and a small crack will encounter grain boundaries more often. The expectation, then, is that smaller grain sizes will lead to a slower rate of crack growth. In support of this hypothesis, Brown et al (1984) have observed that small crack propagation rates decreased by a factor of two when the grain size was decreased by an order

of magnitude. Other workers (such as Gerdes et al, 1984) have found similar effects. Retardation and near arrest of crack growth as a function of grain size is illustrated in Figure 1.9.

There is more than one possible mechanism by which grain boundaries can retard crack growth. As alluded to before, crack growth may be slowed by changes in crack direction required by the crystallographic orientation of the new grain. A second possibility is that the encapsulation of a crack within a single grain changes the driving force propagating the crack. In support of this idea, it has been observed that the CTOD of small cracks, a visible sign of the driving force, depends only on grain size and is independent of crack length and the applied stress (Morris, 1980). A third possibility is that the slip bands associated with the crack are blocked by the grain boundaries. Models based on slip band blocking have been able to predict grain size effects, threshold stress intensities for small cracks and whether small cracks will propagate at the root of a notch (Tanaka et al, 1981 and Tanaka, 1986). In addition, slip band blocking provides a physical explanation for El Haddad's a_o term discussed in section 1.4.1 (Tanaka and Nakai, 1983).

This relation between small fatigue crack growth rate and grain size is not always found, however. When comparing two Al 7075-T6 alloys with different grain sizes, Zurek et al (1983), observed slower small fatigue crack growth rates in the larger grained material. This was attributed to increased plasticity-induced closure. Brown and King (1986) noted that the evidence supporting lower small crack growth rates in smaller grained materials was generated on materials with a planar slip mode. Therefore, they suggested that the effect of grain size may be dependen.. on the

degree of slip planarity.

The distribution of precipitates can influence the crack growth rate by affecting the uniformity of slip distribution. Coherent precipitates may be sheared by dislocations making further slip on that plane more favourable and resulting in highly localized slip bands. It has been suggested that, in long fatigue cracks, this leads to slow crack propagation rates and high ΔK thresholds because of improved reversibility of slip in the slip bands and high closure stresses associated with the rough, crystallographic, fracture surfaces (Brown and King, 1986). In small cracks, only the reversibility of slip is likely to be important as closure stresses are low. The limited experiments in this area have had conflicting results. Some work has shown that precipitate size affects small cracks similarly to long ones (Bolingbroke and King, 1986). That is, crack propagation rates are slower in underaged material where the precipitates are easily sheared and slip is localized. Other work, however, has found no relation between precipitate size and distribution and small fatigue crack growth rates (eg Gungor and Edwards, 1989).

Persistent slip bands (PSB's) are another potentially important microstructural feature because small cracks often propagate within them (W.J. Baxter, 1986). Plastic strains within PSB's are 10-100 times greater than the applied strain and the microstructure within the PSB may be very different from that within the matrix at large. Dissolution of precipitates, for example, has been observed. Both of these effects are likely to influence the growth rate of small cracks.

In this discussion of microstructurally small cracks, the parameter correlating crack growth rates has been ΔK. As with mechanically small cracks, there are some doubts as to whether ΔK

is a suitable parameter. The continuum assumption implicit in the use of ΔK is probably violated. In addition, the crack driving force, as evidenced by the dependence of CTOD on grain size, may be different for microstructurally small cracks. Finally, the material's resistance to crack growth may differ when a crack is encapsulated within a single anisotropic grain (Chan and Lankford, 1988). Chan (1987), noting that cracks tend to initiate in grains where a low Taylor factor implies more yielding, has suggested a correction to ΔK that directly incorporates the Taylor factor. This model has successfully predicted small crack growth rates and retardation at grain boundaries in Astroloy.

Chan's model included the effects of closure and large scale yielding in addition to the effect of microstructural dissimilitude. It is worthwhile noting, at the close of this discussion of small fatigue crack behaviour, that the small cracks studied in this work will similarly be "small" in more than one sense. This point will influence the discussions of the experimental results in Chapters Four and Five. In the next chapter, the physical metallurgy and mechanical behaviour of aluminium-lithium alloys will be discussed with particular reference to the particular alloys studied in this work (8090 and 8091). At the conclusion of Chapter Two, the research objectives of this work will be described.

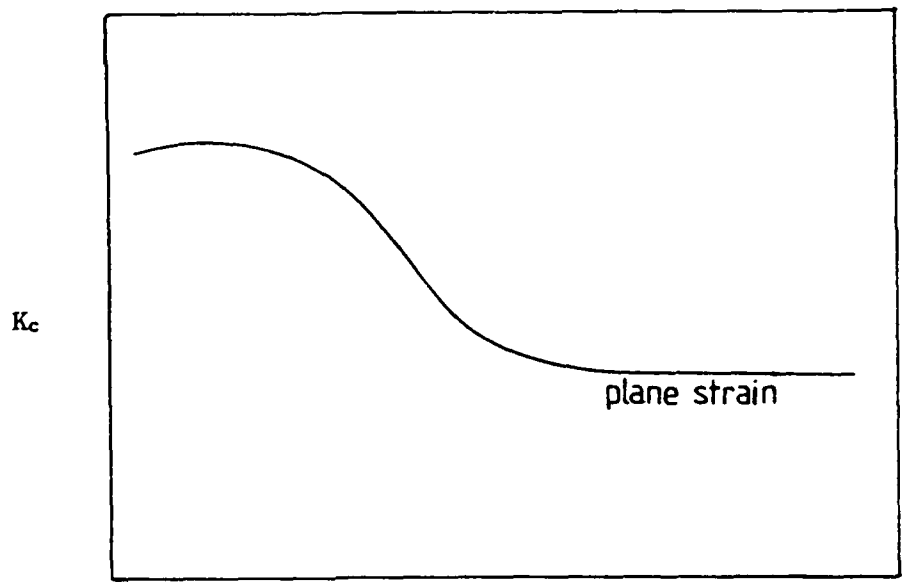

Figure 1.1 K_c versus thickness of material.

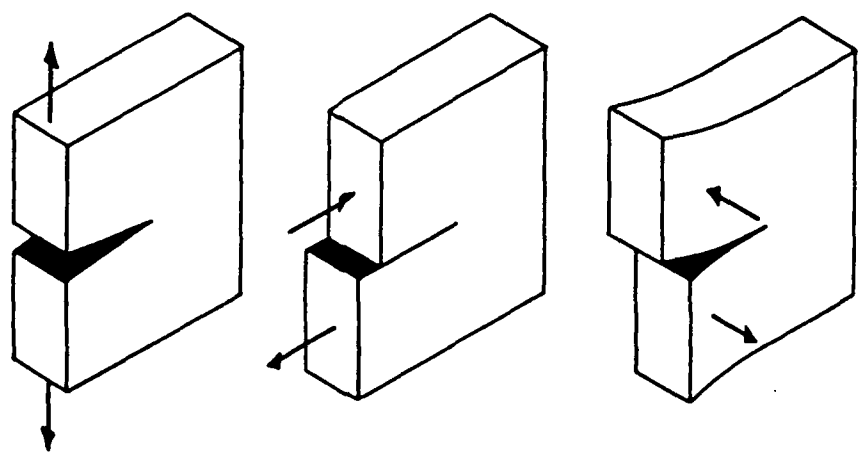

Figure 1.2 Modes of loading (after Ewalds and Wanhill, 1985)

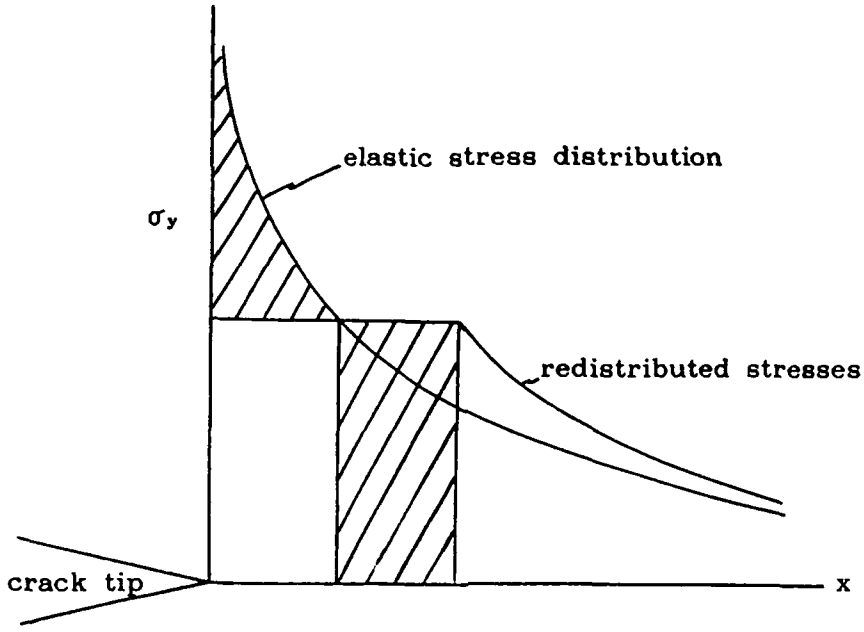

Figure 1.3 Redistribution of stresses ahead of the crack tip.

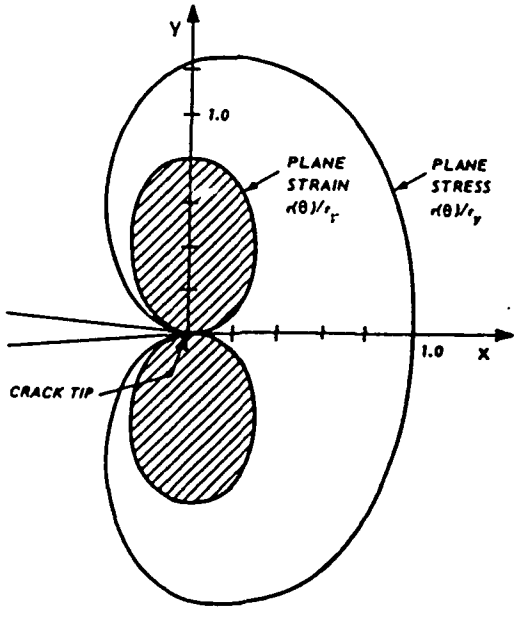

Figure 1.4 Plane stress and plane strain plastic zones (after Ewalds and Wanhill, 1985)

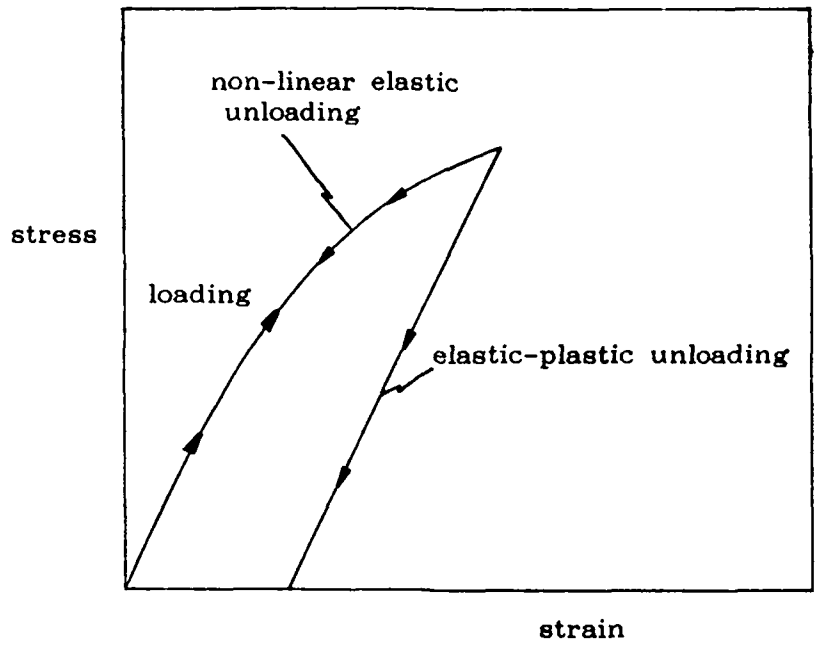

Figure 1.5 Comparison of stress-strain curves for nonlinear elastic and elastic-plastic materials.

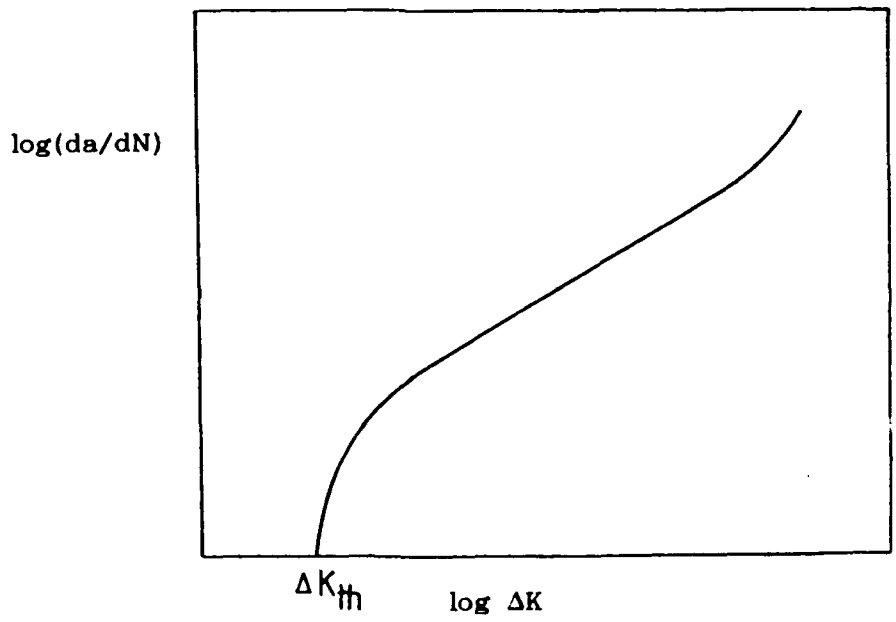

Figure 1.6 Schematic of a da/dN versus ΔK curve.

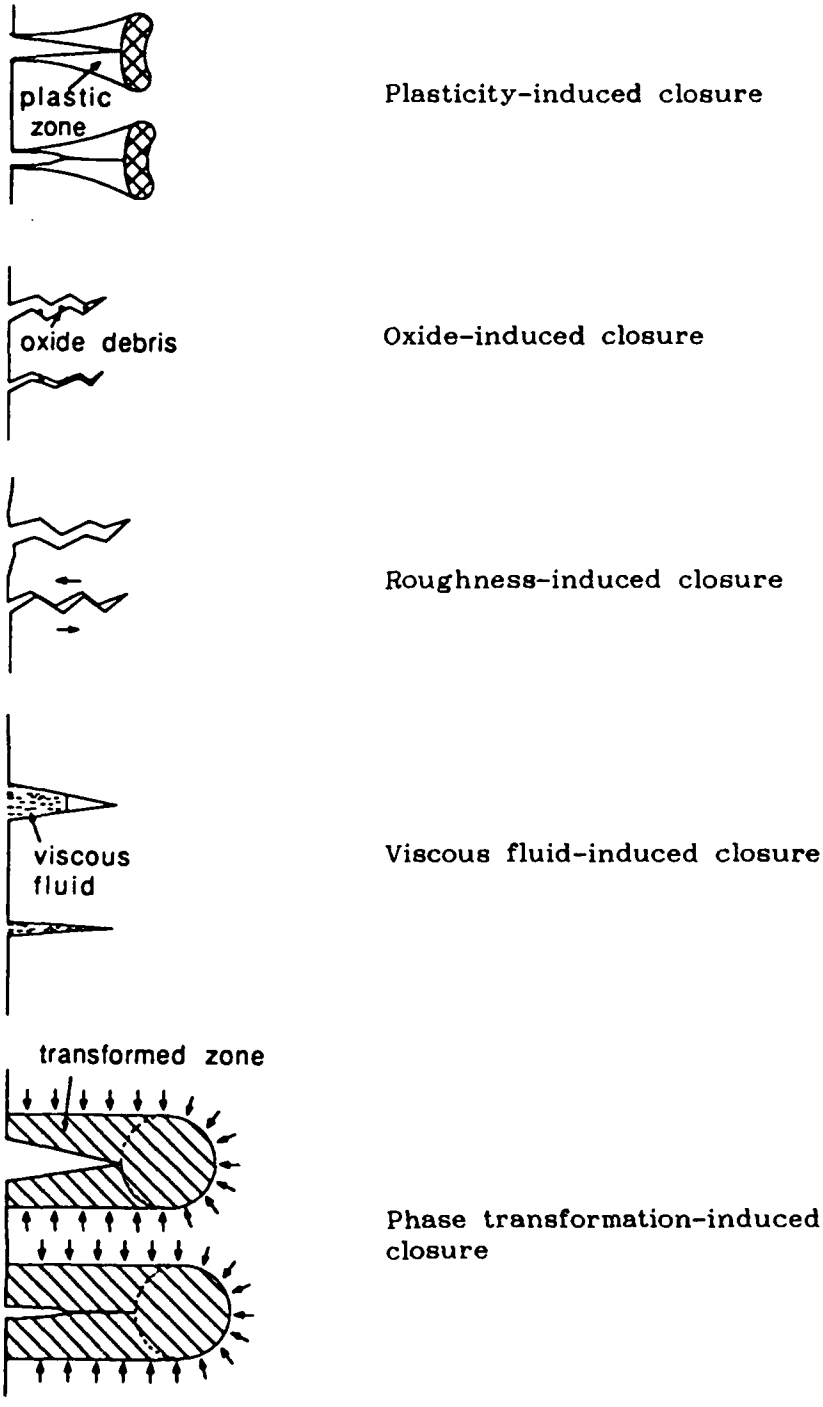

Figure 1.7 Mechanisms for closure (after Suresh and Ritchie, 1986).

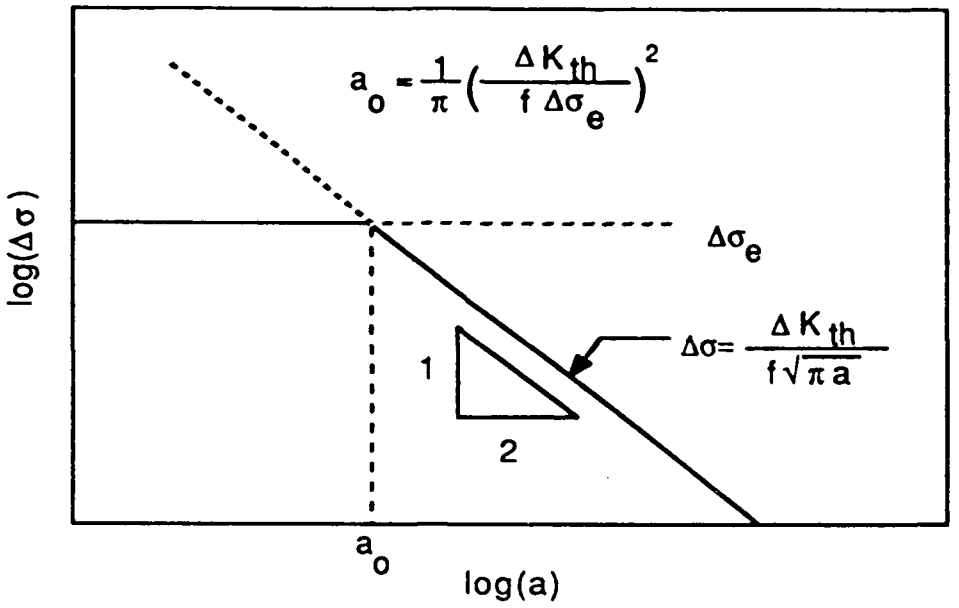

Figure 1.8 Schematic of a Kitagawa-Takahashi diagram (after Larsen, 1987).

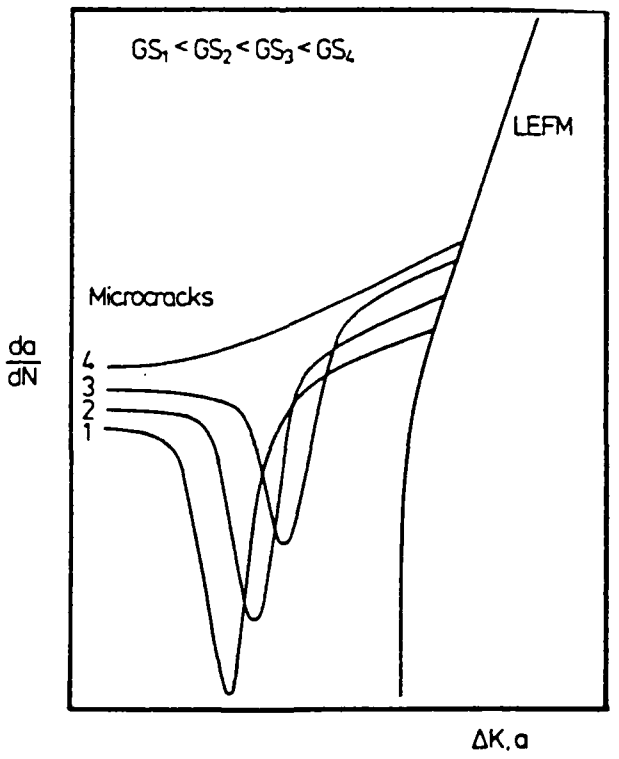

Figure 1.9 Dependence of crack growth rate on grain size (after Lankford, 1982).

CHAPTER 2

ALUMINIUM-LITHIUM ALLOYS

2.1 INTRODUCTION

The major applications for aluminium-lithium (Al-Li) alloys are in the aerospace industry. For this reason, this discussion of Al-Li alloys will begin with a description of the requirements for aircraft materials and the role which Al-Li alloys may play in future aircraft. The discussion will then focus on the phases found in the 8090 and 8091 alloys and the formation of those phases. Explanations for the mechanical behaviour of Al-Li alloys will then be discussed with particular emphasis again on 8090 and 8091 as the alloys studied in this work. Finally, the research objectives of this work will be discussed.

2.2 AIRCRAFT STRUCTURAL MATERIALS

Since the beginning of flight, low structural weight has been of overriding importance to all aircraft. In high performance aircraft, such as fighters, low structural weight translates into higher manoeuverability and acceleration. In cargo-carrying aircraft, such as airliners, low structural weight increases cargo capacity and/or reduces fuel requirements. To reduce structural weight, aircraft components must be designed for high stresses, requiring materials with high yield strengths. Similarly, to prevent buckling in compressively loaded components and excessive elastic deformation, stiff materials are required. The total weight of a component also depends on the density of the material that the component is made from. So, strength, stiffness and low density are all primary requirements for aircraft structural materials.

These requirements are reflected in the historical choice of aircraft materials. The earliest aircraft were made of wood and fabric in kite-like structures. Because of higher stiffness and homogeneity, steel was gradually introduced. Steel, in turn, was replaced by aluminium for most applications due to aluminium's lower density and today, aircraft are mostly aluminium. The Boeing 767, for example, is 81% aluminium by weight (Quist et al, 1984).

Composite materials now threaten the dominance of aluminium alloys. Generally, composite materials offer a 20% increase in specific stiffness over conventional aluminium alloys and a similar reduction in component cost due to lower assembly costs and a better "buy/fly" ratio. The buy/fly ratio refers to the weight of the material bought compared to the weight of the final component. A disadvantage of composite materials, for many manufacturers, is that they require capital investment for new equipment such as tape laying machines and autoclaves. A second disadvantage is that the anisotropic nature of composite materials complicates design and lowers damage tolerance to out-of-plane loading. Nevertheless, composites have been used in a variety of aircraft ranging from the Harrier to the Boeing 737 and there are projections that composite materials will make up as much as 65% of future subsonic aircraft (Quist et al, 1984).

Other materials are being developed that also have better properties than conventional aluminium alloys. Chief among these are the Al-Li alloys which, like composite materials, offer about a 20% increase in specific stiffness. Figure 2.1 shows alternative projections of the materials composition of future aircraft. Al-Li alloys offer the advantage that components made out of Al-Li alloys may be produced using the same techniques already used for

conventional aluminium alloys. Future production costs may be further reduced with the the use of superplastic forming technology. Like composites, however, Al-Li alloys historically have had low ductility and fracture toughness. Like composites, this disadvantage can be overcome with design techniques that account for the low fracture toughness as was done in the Al-Li alloy (2020) components on the Vigilante RA-5C. Alternatively, microstructural modifications may be used to improve fracture toughness and ductility.

With significant commercial applications at stake, there continues to be a great deal of research to develop improved Al-Li alloys and composite materials. In the U.K. three alloy design targets for Al-Li alloys have been set based on straight substitution for conventional aluminium alloys. These design targets are:

(1) Medium strength - equivalent to 2014-T6.

(2) Damage tolerant - equivalent to 2024-T3.

(3) High strength - equivalent to 7075-T6.

The rationale for the straight substitution approach is based on damage tolerance (Peel et al, 1986). To take full advantage of a stronger material, high stress levels must be used. These high stress levels, coupled with the tendency toward low fracture toughness in high strength alloys, diminish the damage tolerance of the structure - perhaps unsafely. If, however, a substitution is made where the main difference is in lower density then weight is reduced without affecting damage tolerance.

The alloys used in this work, 8090 and 8091, were developed by Alcan International in conjunction with the Royal Aircraft Establishment (RAE) at Farnborough to meet these design targets. With appropriate heat treatment 8090 meets the first two targets while 8091 meets the last.

2.3 THE PHYSICAL METALLURGY OF ALUMINIUM-LITHIUM ALLOYS

As part of the effort to develop improved Al-Li alloys, there has been a great deal of work defining the phases present and their formation. In this section, the part of that work relevant to 8090 and 8091 (the Al-Li-Cu-Mg-Zr alloys used in this work) will be summarized. The nominal compositions of 8090 and 8091 in weight % are given below (Miller et al, 1987).

Alloy	Li	Cu	Mg	Zr	Al
8090	2.2-2.7	1.0-1.6	0.6-1.3	0.04-0.16	Bal.
8091	2.4-2.8	1.6-2.2	0.5-1.2	0.08-0.16	Bal.

The phases that have been observed in this composition range are the matrix α, and the precipitates δ', δ, S, T_1, β' I, and C. In the discussion of the individual phases that follows, much of the material reviewed is specific to 8090 and 8091 but some has been deduced from the general behaviour of Al-Li alloys.

2.3.1 THE α SOLID SOLUTION

The α solid solution is, of course, FCC. Because it is the matrix from which other phases form there is not a great deal to be said about its formation or morphology. The fact that no more than 3.6 wt% lithium can be maintained in solid solution (see the binary phase diagram in Figure 2.2) sets an upper limit for the concentration of lithium in commercial alloys. This solubility is further depressed in those Al-Li alloys where magnesium is added for strength. The α matrix also has, on its own accord, an important mechanical role in Al-Li alloys. It has, for example, been shown to contribute the bulk of the improved modulus which makes application of Al-Li alloys so attractive (Noble et al, 1982).

2.3.2 THE δ PHASES

The precipitation sequence of the δ phases is (Silcock, 1959)

supersaturated solid solution -> δ' -> δ

The metastable FCC δ' has the crystal structure of an $L1_2$ superlattice in which the eight corner sites are occupied by lithium and the six face sites are occupied by aluminium (see Figure 2.3). The resulting stoichiometry is Al_3Li. The orientation relation between δ' and the matrix α is cube-cube. Because of the very small lattice misfit and the similarity between the structure of δ' and α, δ' precipitates rapidly and homogeneously as small, coherent spheres. Nucleation appears to be independent of lattice defects such as dislocations.

Once nucleation has occurred, the δ' coarsens in accordance with Lifshitz-Slyosov-Wagner kinetics and the particle radius is proportional to the cube root of time (Kulwicki and Sanders, 1984). Particle sizes follow a Weibull distribution. However, preferential coarsening of the precipitate particles has been noted at the grain boundaries (Niskanen and Sanders, 1982) - perhaps due to a higher rate of diffusion.

With further ageing, δ is formed. Currently, it is thought that the δ particles are not metamorphosed δ' particles but form independently on high angle grain boundaries (Flower and Gregson, 1987). As the δ precipitates grow, they remove lithium from nearby δ' particles, thus destroying them. This mechanism increases the width of the δ' precipitate-free zone adjacent to the grain boundaries. Excessive deformation in this δ' free zone and cracking of the δ particles are thought to lead to increased brittleness in Al-Li alloys containing δ (Vasudevan and Doherty, 1987). As a result,

typical commercial heat treatments avoid the formation of δ which leaves δ' as the major strengthening precipitate in Al-Li alloys. The BCC δ has the stoichiometry AlLi and its orientation relationship is

$$(0\bar{1}1)\delta//(1\bar{1}2)_{Al};\quad (100)\delta//(110)_{Al};\quad (011)\delta//(\bar{1}11)_{Al}.$$

2.3.3 THE S PHASES

S phase (Al_2CuMg) is face-centred and orthorhombic with a unit cell size of a=4.00Å, b=9.23Å, c=7.14Å. It precipitates as rods thickening to laths on {210} planes in <001> directions. Silcock (1959) found the orientation relationship

$$[100]_S//[100]_{Al}\ ;\ [010]_S//[0\bar{2}1]_{Al}\ ;\ [001]_S//[012]_{Al}$$

S phase precipitation in Al-Cu-Mg alloys is preceded by precipitation of the metastable S' phase. Since S' and S differ only in their respective lattice parameters, they can be confused in the absence of accurate lattice parameter measurements. In Al-Li-Cu-Mg alloys, where such measurements have not been made, the precipitate formed is often called S' as that is the phase formed with similar heat treatments in Al-Cu-Mg alloys. This nomenclature will be used in this work. As a practical matter, it may not be important to differentiate between them as their structural similarity implies similar behaviour (Gupta et al, 1987). While there is evidence that S' is preceded in ternary Al-Cu-Mg alloys by Gunier-Preston zone formation followed by S'' formation, there is no evidence, as yet, for this sequence of events in Al-Li-Cu-Mg alloys (Flower and Gregson, 1987).

For homogeneous nucleation of S' to occur, the required ageing conditions are such that the δ' precipitates are overaged and there is excessive precipitation at the grain boundaries. Therefore, in conventional heat treatments, the S' phase is precipitated

heterogeneously. The nature of the precipitation sites is influenced by the strong lithium to vacancy binding energy (Flower and Gregson, 1987). Vacancy condensation and the formation of dislocation loops and helices on quenching is inhibited by this strong binding energy. In the absence of these heterogeneous nucleation sites, the S' precipitates instead on grain boundaries, subgrain boundaries, and dislocations.

The S' phase is an important strengthening precipitate for 8090 and 8091. In addition, it is thought to homogenise slip. The density of S' phase nucleation sites may be increased by stretching the material before artificial ageing, thereby increasing the number of dislocations. The ability of the S' phase to homogenise slip is enhanced by the increase in the number of nucleation sites as the distribution of S' phase particles is itself more uniform. Thus, a pre-ageing stretch is used to increase toughness and to develop more isotropic properties.

For applications where a pre-ageing stretch is not feasible, a duplex ageing cycle has been suggested (Flower and Gregson, 1987). The homogeneous precipitation of S' is dependent on the density of free vacancies which, in turn, is a function of the solution treatment temperature and the temperature used for the first stage of the duplex age. During a low temperature natural age, δ' particles grow. As these precipitates grow, they incorporate lithium. The vacancies, which were originally strongly bound to the lithium, are released. These vacancies can then condense to form nucleation sites for the S' phase during subsequent ageing. This model is supported by observations of the formation of dislocation loops and helices associated with δ' growth (Flower and Gregson, 1987), dimensional contraction in 8090 during natural ageing (Murphy and

Martin, 1986) and most convincingly by direct high resolution TEM observations of the nucleation of S' at the δ'/matrix interface (Radmilovic et al, 1989).

2.3.4 THE T_1 PHASE

The T_1 phase (Al_2LiCu) is partially coherent and forms as thin hexagonal plates (a=4.97Å and c=9.34Å) (Silcock, 1959). Noble and Thompson (1972) found the orientation relation to be

$$(0001)_{T1}//(111)_{Al};\ (10\bar{1}0)_{T1}//(1\bar{1}0)_{Al};\ (1120)_{T1}//(211)_{Al}$$

The mechanism of T_1 nucleation depends upon the degree of supersaturation. For high levels of supersaturation Gunier-Preston zones act as nucleation sites. For low levels of supersaturation, as in 8090 and 8091 alloys, the precipitation of T_1 begins with partial dislocations passing on adjacent planes of atoms (Cassada et al, 1987). More specifically, Noble and Thomson (1972) suggested that 1/2[110] dislocations dissociate into 1/6[211] Shockley partials. These partials bound a region in which there is an intrinsic stacking fault. A thin layer of T_1 precipitates when copper and lithium enrich the fault. The amount of T_1 is significantly increased by stretch as the number of dislocations and the number of dislocation-dislocation interactions is increased. This shortens the time to peak yield strength as the T_1 is already nucleated (Cassada et al, 1987).

2.3.5 OTHER PRECIPITATES

Zirconium is usually added in a composition range of 0.1-0.2% and precipitates, during homogenization, to form coherent Al_3Zr particles (β'). β' particles can act as heterogeneous nucleation sites for δ'. This leads to larger average δ' particle sizes (Gu et al, 1986). However, the primary function of zirconium is to inhibit

recrystallization and grain growth during thermo-mechanical processing. For a recrystallization front to pass through a β' precipitate, β' would have to dissolve or, at least, change from being coherent to semicoherent. The energy required for these processes inhibits recrystallization.

There are also several precipitates that typically form on grain boundaries. The icosahedral I phase ($Al_6Cu(LiMg)_3$) forms snake-like precipitates along grain boundaries and, although not much is known about its properties, appears to reduce fracture toughness (Miller et al, 1987). The high temperatures required for its formation (300°C) reduce its significance for probable heat treatments. Miller et al (1987) suggests, however, that its formation is more favoured in 8091 than 8090. Another phase that forms on the grain boundaries is the tetragonal C phase. It, too, forms at relatively high temperatures and is detrimental to fracture toughness because of influence on the width of the precipitate-free zone (Miller et al, 1987). It has a near icosahedral symmetry (Lapasset and Loiseau, 1987). Finally, intermetallics, containing iron for example, may be formed which are also detrimental to fracture toughness.

2.3.6 PRECIPITATION BEHAVIOUR OF AL-LI-CU-MG-ZR ALLOYS

After solution treatment, the microstructure of Al-Li-Cu-Mg-Zr alloys is free of vacancy loops and dislocation helices due to the high binding energy between lithium and vacancies. The δ' phase precipitates first and is present in the as-quenched condition. As mentioned before, the precipitation of δ' is independent of lattice defects and so is homogeneous. Therefore, the precipitation of δ' is fairly independent of prior processing history (eg solution treatment temperature or prior stretching). During artificial ageing the δ'

coarsens in accordance with Lifshitz-Slyosov-Wagner kinetics.

The precipitation of the S' is, however, highly dependent on the thermo-mechanical treatment prior to artificial ageing. For practical ageing treatments S' precipitates heterogeneously. Thus, post-solution treatment stretching, as discussed before, can dramatically change the speed at which S' appears and its homogeneity. Since S' can also precipitate on vacancy clusters, the precipitation of S' is a function of the vacancy density. An increased number of vacancies can be the result of higher solution treatment temperatures or a natural age (Flower et al, 1986). The higher solution treatment temperature will increase the number of quenched in vacancies. The natural age on the other hand allows time for increased precipitation of δ'. As the δ' is formed, the vacancies originally bound tightly to the lithium are released. Regardless of the source of the vacancies they can coalesce to form nucleation sites for the S'.

The precipitation of T_1 is also dependent on thermo-mechanical history prior to artificial ageing. In particular T_1 has been shown to be sensitive to the degree of stretch (Cassada et al, 1987). Since copper is an ingredient of both T_1 and S', these two precipitates are in competition with each other. The relative amount of each precipitate is a function of the relative concentrations of lithium, copper and magnesium (Miller et al, 1987). For the composition ranges specified for 8090 and 8091, S' is the predominant phase. More T_1 precipitation would be anticipated in the 8091 alloy, which has a higher copper content.

2.4 MECHANICAL BEHAVIOUR

Having discussed the formation and structure of the phases in

Al-Li alloys, their role in determining mechanical behaviour can be discussed. Once again, the discussion will focus on 8090 and 8091 although much of what is said may have been demonstrated with other Al-Li alloys and be true of them in general.

2.4.1 ELASTIC MODULUS

The addition of lithium to aluminium increases the modulus of aluminium by about 2 GPa for each atomic weight percent of lithium added (Agyekum et al, 1986). As the increased stiffness of Al-Li alloys is an important characteristic, several workers have examined the mechanisms responsible. Most of the work has focussed on identification of the phase or phases responsible for the overall increase in stiffness of Al-Li alloys. In all of these studies the moduli of alloys with differing compositions and phase volume fractions were measured. The contributions of individual phases were estimated using a rule-of mixtures approach.

Noble et al (1982) found that the modulus of the solid solution α increased significantly with increasing lithium content. They found that for alloys in commercial composition ranges, the modulus of the solid solution increased from 66 GPa to 79-81 GPa which accounts for most of the modulus change of the overall alloy. They also found that the change in modulus with the addition of lithium did not follow Vegard's Law which predicts linear dependence between atomic volume and concentration of a solute in solid solution. Such a deviation implies that it is a change in the electronic environment around the atoms that is responsible for the change in modulus rather than a change in the strain energy. Fox and Fisher (1988) confirmed that the valence electrons in an Al-Li solid solution alloy are held in a smaller volume than the pure alloy.

This implies a stronger bond between atoms and a higher stiffness.

The influence of various precipitates on the stiffness of Al-Li alloys has also been investigated. The modulus of δ' has been estimated from 96 GPa (Noble et al, 1982) to 106 GPa (Muller et al, 1986). Because of the relatively low volume fraction, however, the high stiffness of δ' has little influence on the overall stiffness of Al-Li alloys. An increase in alloy modulus of 0.1 GPa/vol% δ' has been estimated (O'Dowd et al, 1987). This increase appears to be almost independent of the size and distribution of the δ' precipitates (Broussaud and Thomas, 1986). The T_1 precipitate has the very high modulus of 350 GPa (O'Dowd et al, 1987). The precipitation of T_1 accounts for most of the increase of modulus with ageing time despite low volume fractions. Nevertheless, its effect is also relatively minor compared with that of the solid solution α.

2.4.2 YIELD STRENGTH

The yield strength of any precipitation hardened alloy is dependent on the extent that the precipitate interferes with dislocation motion. In aluminium-lithium alloys the primary strengthening precipitate appears to be the coherent δ'. Four mechanisms by which a coherent precipitate can increase strength are coherency hardening, chemical hardening, modulus hardening, and order hardening. Coherency hardening results from the energy required to move dislocations through the stress fields around particles. Chemical hardening results from the energy required for the new surface area when a particle is sheared by a dislocation. Modulus hardening results from a difference in modulus between the matrix and the precipitate. And finally, order hardening is a result of the energy associated with the formation of an antiphase

boundary within an ordered precipitate when a dislocation passes through.

Coherency hardening and chemical hardening have been shown by Sainfort and Guyot (1986) to be relatively insignificant in aluminium-lithium alloys due to the small lattice mismatch and low interfacial energy of δ' in α. Jensrud (1986) has shown that modulus hardening is also insufficient to account for the strengthening effect of δ' precipitates. He further calculated a theoretical yield strength increase of 87 MPa based on the order strengthening mechanism. This agrees well with experimental results and confirms that order hardening is the primary mechanism by which δ' strengthens Al-Li alloys.

There is some dispute as to the exact role that T_1 plays in the strengthening of Al-Li alloys. Gregson and Flower (1985) have proposed that T_1 particles cannot be a barrier to slip because of their crystallographic relation with the matrix. As the basal plane of T_1 is parallel to the matrix (111) plane, they argue that dislocations could move freely in that plane. The extreme thinness of the T_1 plates, they feel, enables dislocations perpendicular to the basal plane to penetrate without difficulty. In contrast, Sainfort and Guyot (1986) have proposed that T_1 precipitates are unshearable and are important to the strength of Al-Li alloys. In a series of experiments Huang and Ardell (1987) have found that T_1 precipitates do strengthen Al-Li alloys. They proposed that strengthening could occur either through chemical strengthening or Orowan looping.

The formation of S' has several effects which increase the yield strength of Al-Li-Cu-Mg-Zr alloys (Harris et al, 1987). Firstly the S' is effective at dispersion hardening. Secondly, the formation of S' discourages the formation of T_1 which frees more lithium to

form δ'. The formation of δ' will be further enhanced since the addition of the magnesium to form the S' reduces the solubility of lithium. As a useful side effect, the presence of magnesium in solution also increases the amount of solid solution strengthening. S' is also thought to improve the yield strength at elevated temperatures by preventing sub-grain boundaries from acting as dislocation sinks and thus inhibiting dynamic recovery (Pridham et al, 1986).

2.4.3 DUCTILITY AND FRACTURE

The ductility and fracture behaviour of Al-Li alloys is dominated by the tendency in these alloys towards the localization of strain in slip bands (Sanders, 1981). In overaged alloys, strain localization is caused by the formation of precipitate free zones which, being softer than precipitate hardened material, deform more easily. In underaged and peakaged alloys this localization occurs because of the shearing of δ' precipitates by dislocations. When a δ' particle is sheared by a dislocation its effective cross-sectional area is reduced and thus the stress required to move the next dislocation through the δ' precipitate is reduced. This reduces the ability of δ' to act as a barrier to slip resulting in regions of material which are less resistant to deformation and the formation of slip bands. The localization of strain in slip bands results in dislocation pileups and stress concentrations at the grain boundaries leading to fracture of the grain boundaries at low macroscopic strains. Attempts to improve the ductility and fracture toughness of Al-Li alloys have thus focussed on homogenising the slip distribution and improving the cohesiveness of the grain boundaries.

The distribution of slip in Al-Li alloys has been homogenised

by the formation of precipitates and by thermo-mechanical treatment such as stretching. The primary slip homogenising precipitate in 8090 and 8091 has been S'. As a non-shearable precipitate, S' precipitates are looped by dislocations. Thus, the slip plane is hardened and slip homogenised, thereby improving ductility. In fact, the ability of the S' phase to improve ductility and fracture toughness is the primary explanation for its desirability. T_1, if it is indeed a non-shearable precipitate, should also be able to homogenise slip. The volume fraction of T_1 in 8090 and 8091 is, however, probably too low for it to contribute a significant effect. Stretching Al-Li alloys prior to ageing, besides providing nucleation sites for the S' phase, also produces a dislocation cell structure which interferes with the formation of slip bands and thus homogenises slip. Similarly, the addition of grain refiners, such as zirconium, encourage activation of many slip systems through the complexity effect associated with smaller grains.

As mentioned above, the fracture properties of Al-Li alloys may also be improved by improving the cohesiveness of the grain boundary - particularly through control of grain boundary precipitation. Constituent grain boundary precipitates appear to be detrimental to fracture toughness (Owen et al, 1986). Their effects are most effectively reduced by reducing the volume fraction of these precipitates which is achieved by minimizing the trace elements (particularly iron and silicon). Other grain boundary precipitates resulting from the heat treatment practices may also be detrimental to fracture toughness. White and Miller (1987) have studied the effect of various heat treatments on grain boundary morphology. They have found that the rate of quenching from solution treatment is an important factor. Air cooling resulted in precipitation of both

I phase and C phase, both of which are detrimental to fracture toughness. They also found that the growth of precipitate free zones in 3090 is controlled by the rate of lithium diffusion. Consequently, they recommend low ageing temperatures. Finally, the level of precipitation on high angle grain boundaries can be decreased by stretching.

2.4.4 FATIGUE

The fatigue behaviour of Al-Li alloys is also affected by the slip planarity introduced by the shearability of the δ' phase. As will be discussed later in this section, the degree of slip planarity affects levels of closure, slip reversibility, and the crack driving force. In addition, the localization of slip has been observed to change the local microstructure through either dissolution of the δ' precipitates or through enhanced coalescence due to the super-saturation of point defects during fatigue (Brechet and Livet, 1987). The severity of the planar slip has been shown to be a function of the size of the δ' precipitates (Schneider et al, 1987) and dislocation cell structure resulting from a pre-ageing stretch (Di et al, 1987). Other factors that homogenise slip, such as the homogeneous precipitation of S', would also be expected to affect the degree of the planarity of slip. The planarity of slip appears, in addition, to be associated with cyclic instabilities in cyclic stress-strain hysteresis loops (Gentzbittel and Fougere, 1987).

Al-Li alloys generally have improved long crack fatigue resistance as compared with conventional aluminium alloys of the same strength (McDarmaid, 1985). Partially, this improvement in fatigue resistance may be due to the higher stiffness of Al-Li alloys (Coyne et al, 1981). Increased stiffness will decrease crack opening

displacements and thus crack growth rates. The observation that the superiority of 8090 diminishes at high stress ratios indicates, however, that closure, rather than increased stiffness, is primarily responsible for the good fatigue resistance of Al-Li alloys (Peters et al, 1987). This is confirmed by Peacock and Martin's (1989) direct measurement of high closure levels in 8090 and 8091. Others, by removing the effect of closure through an effective ΔK, have been able to account for both the influence of load ratio and texture on fatigue crack growth in Al-Li alloys (Tintillier et al, 1987)

The mechanism of closure appears to be roughness-induced closure. Oxide-induced closure can be discounted since the oxide layer associated with Al-Li alloys is very thin (Vasudevan and Suresh, 1985). Plasticity-induced crack closure tends to be more significant at high ΔK's and under plane stress conditions - neither of which apply to the fatigue work that has been done (eg Peters et al, 1987). On the other hand, the main requirement for roughness-induced crack closure is a tortuous crack path. In Al-Li alloys this requirement is satisfied since the crack path follows crystallographic slip bands. Furthermore, fretting debris, expected with roughness-induced crack closure, has been observed (Peters et al, 1987).

Peters et al (1987) and Peacock and Martin (1989) agreed that the superior fatigue resistance of Al-Li alloys persisted at high stress ratios, although it was much reduced. This indicates that roughness-induced crack closure is not the only significant factor determining the relative fatigue resistance of Al-Li alloys. The planarity of slip also has an effect on slip reversibility. In highly planar slip it is easier for dislocations to reverse their motion as there is less interaction between dislocations. Through this mechanism, damage done at the peak of the loading cycle can be

"undone" when the stress is reversed resulting in lower overall damage ahead of the crack tip and a lower fatigue crack propagation rate. Increased slip reversibility has been cited as significant to the fatigue behaviour of 8090 and 8091 alloys by Peacock and Martin (1989) and in underaged Al-Li-Cu alloys by Jata and Starke (1986). In addition, it has been suggested that the significant crack deflection lowers the crack driving force in Al-Li-Cu alloys (Vasudevan and Suresh, 1985). Specifically, they found that differences in threshold behaviour in these alloys could be linked to reductions in the effective crack driving force due to varying amounts of crack deflection.

Small fatigue cracks in Al-Li alloys propagate significantly more rapidly than do long fatigue cracks under the same nominal ΔK. Largely, this discrepancy appears to be due to the low closure levels typical of small cracks. Venkataswera Rao et al (1986) have suggested that the discrepancy between the low closure levels in small fatigue cracks and the particularly high closure levels in long fatigue cracks results in an especially large difference between long and small fatigue crack growth rates in Al-Li alloys. As confirmation, they showed that small fatigue crack growth rates compared closely with long fatigue crack growth rates when long fatigue crack growth rates were plotted as a function of ΔK_{eff} (effectively subtracting out the contribution of closure to long fatigue crack growth rates). Similarly, James (1987) found that lower closure levels accounted for much of the discrepancy between long and small crack growth rates in 8090.

The limited work on the microstructural effects on small crack growth in Al-Li alloys is somewhat contradictary. Venkatswera Rao et al (1986), working with a number of Al and Al-Li alloys including

8091, found that small crack growth rates were relatively insensitive to ageing time and to composition. Therefore, they suggested that the microstructural effects observed in long cracks were primarily due to the effects of microstructure on closure levels. In small cracks, changes in closure levels would have relatively little effect as closure overall has little influence. James (1987), on the other hand, observed that the small fatigue crack resistance of underaged 8090 was significantly better, possibly linked to sub-surface crack branching.

The S-N behaviour of Al-Li alloys may be divided into two regimes - greater than 100,000 cycles to failure (HCF) and less than 100,000 cycles (LCF). For the latter case, Farcy et al (1987) found that cracks initiated within the first 10% of the total life and so the rate of small crack propagation was the dominant factor in determining LCF lifetimes. Similar small crack propagation rates and similar LCF lifetimes were observed in 2091 T8 and 2024 T351. For the HCF regime, the time to failure was found to be dominated by crack initiation processes. Xiao and Bompard (1987) found that shearing of δ' precipitates caused strain localization in persistent slip bands and stress concentrations at the intersections of these bands with grain boundaries. This led to early crack initiation. They also observed that S' precipitates in 8090 homogenised strain so that several slip systems were activated in the subgrains. Bischler and Martin (1987) invcstigated the effect of slip distribution on the S-N behaviour of 8090. They found that the LCF behaviour of the two alloys was similar but that the stretched material had longer lifetimes in the HCF regime. These observations indicate that the distribution of slip has more effect on crack initiation than on small fatigue crack growth rates.

2.5 THE CURRENT WORK

Among the reasons for selecting 8090 and 8091 for study is that the potential application of these alloys in aircraft makes an understanding of their fatigue behaviour important. As was previously discussed, 8090 and 8091 have very good fatigue resistance in the long crack regime that can, at least partially, be attributed to high closure levels. Since small fatigue crack resistance does not benefit from high closure levels, it is important to characterize small fatigue crack behaviour.

The low closure levels in small cracks may also allow the role of slip reversibility in the fatigue behaviour of these alloys to be determined without confusion with closure effects. 8090 and 8091 are suitable when examining the effect of slip distribution since it is possible to alter the distribution of slip through thermo-mechanical treatment (eg post-solution treatment stretching).

As will be discussed later, the small cracks studied in this work were physically and mechanically small. It is important to note that the fact that they were not microstructurally small does not exclude the possibility of microstructural effects. After all, long cracks, which by definition are not microstructurally small, are affected by microstructure. Nor does the microstructural "largeness" of the small cracks studied imply that they will be affected by microstructure in a similar manner to long cracks. Either large scale plasticity or the lack of closure could alter microstructural effects.

This point is made because it explains the organization of Chapters Four and Five. In Chapter Four the relationship between microstructure and small crack behaviour will be discussed as will

the effects of "physical smallness" on the role of microstructure in small fatigue crack behaviour. The influence on microstructural effects of the "mechanical smallness" of the cracks will be discussed in Chapter Five along with the alternative viewpoint on small crack behaviour provided by low cycle fatigue.

Having reviewed work related to aluminium-lithium alloys and to the fatigue of small cracks, it remains to describe the objectives of this work. The overall goal of this work is to define the role of microstructure on the behaviour of small fatigue cracks in 8090 and 8091. This overall goal can be broken down into the following objectives.

1. Define the relation between the behaviour of small fatigue cracks and the size and distribution of precipitates. Particular emphasis will be placed on the distribution of slip and on the role of slip reversibility on small fatigue crack behaviour.

2. Compare the behaviour of small fatigue cracks in 8090 and 8091. Explain differences in small fatigue crack behaviour based on the differences in grain size, texture and copper content between the two alloys.

3. Examine the suitability of using ΔK as a correlating parameter when investigating microstructural effects on small cracks. This will include examining the method of calculating ΔK and determining whether the use of ΔK for physically and mechanically small cracks obscures microstructural effects.

4. Compare long and small fatigue crack growth rates under nominally the same ΔK. Determine the causes of any differences in behaviour and if any other correlating parameters (eg ΔJ) are more effective when comparing long and small fatigue crack growth behaviour.

5. Examine the interplay between the physical "smallness", mechanical "smallness" and the effect of the microstructure on small fatigue crack behaviour.

6. Examine the relationship between low cycle fatigue, cyclic stress-strain behaviour, and small fatigue crack behaviour for microstructural implications.

7. Examine the mechanism of small crack growth, the implications for general fatigue mechanisms and any implications for alloy development where small fatigue crack growth is a concern.

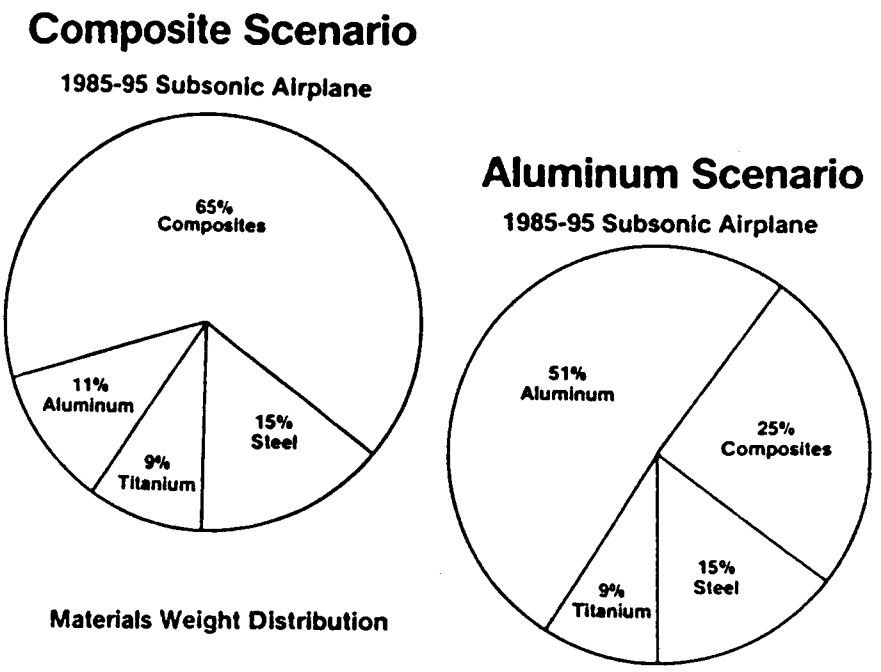

Figure 2.1 Composite versus aluminium scenarios for future aircraft composition (after Quist et al, 1984).

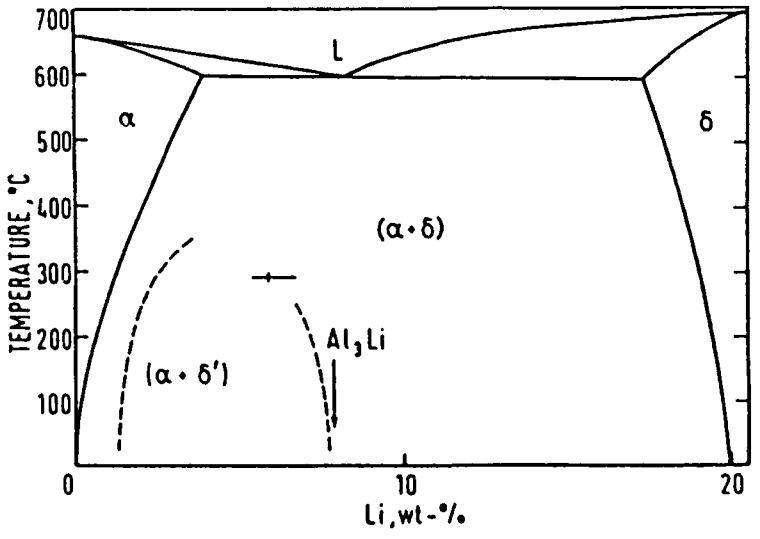

Figure 2.2 Al-Li binary phase diagram (after Mcalister, 1982)

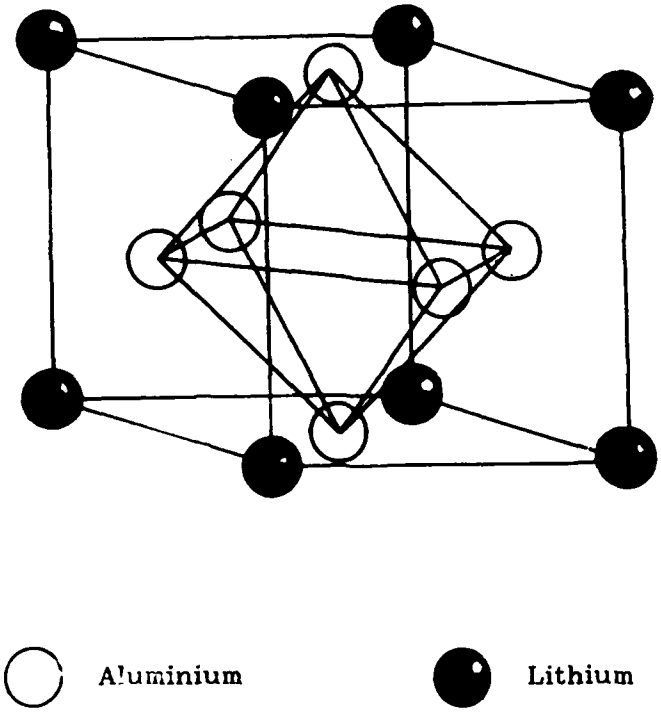

Figure 2.3 The $L1_2$ superlattice

CHAPTER 3

MATERIALS AND EXPERIMENTAL PROCEDURES

3.1 MATERIALS

3.1.1 CONDITION WHEN RECEIVED

Two 45 mm thick plates of 8090 and one 50 mm thick plate of 8091 were supplied by the Materials and Structures Department at the Royal Aircraft Establishment, Farnborough. The material was manufactured using standard commercial practice by Alcan International Ltd. Both plates had been stretched by 6%. The 8090 plates had been hot cross-rolled and then aged for 32 hours at 170°C whereas the 8091 had only been unidirectionally rolled and was in the naturally aged condition. Their chemical compositions, as determined by RAE Farnborough, are given below. The major difference between the two alloys is that the 8091 has more copper.

Chemical compositions in wt %

Alloy	Li	Cu	Mg	Zr	Fe	Si	Al
8090	2.29	1.10	0.63	0.13	0.06	0.03	Bal.
8091	2.26	1.57	0.61	0.15	0.05	0.04	Bal.

Comparison with the alloy specifications given below shows that these are weak alloys with respect to lithium, copper and magnesium. In fact, the 8091 alloy could be classed as an 8090 alloy based on a copper content just below 1.6%. The alloy was, however, supplied as 8091 and will be referred to as such for the remainder of this thesis.

Nominal compositions in wt %

Alloy	Li	Cu	Mg	Zr	Al
8090	2.2-2.7	1.0-1.6	0.6-1.3	0.04-0.16	Bal.
8091	2.4-2.8	1.6-2.2	0.5-1.2	0.08-0.16	Bal.

Optical micrographs of both materials are shown in Figure 3.1. The grain sizes, in the L, T and S directions respectively were 216, 176 and 26 microns for 8090 and 281, 71 and 14 microns for 8091 as measured by the mean linear intercept method. At least 200 grains were used so that the 95% confidence interval is $\pm$5%. Both materials had pancake shaped grains but the grains in 8091 were more elongated in the L direction than the grains in 8090. This is attributed to the fact that the 8090 was cross-rolled while the 8091 was not.

For pole figure analysis, 25.4 mm diameter disks, approximately 1.5 mm thick were cut from the plates with the flat face normal to the S direction. For each alloy, one disk was cut from the surface of the plate and one from the centre. The disks were abraded using 1200 grit silicon carbide paper and Selvyt cloths successively impregnated with 6 micron, 3 micron and 1 micron diamond pastes. Pole figure construction was performed courtesy of Dr Rawlings at the Imperial College of Science and Technology using a Phillips PW1078 texture goniometer interfaced to a BBC micro-computer. The <111> pole figures generated (see Figures 3.2 and 3.3) showed that the surface is more isotropic than the centre. For this reason, test specimens were never taken from the outer 5 mm of the plate. The texture of 8091 was determined to be {110}/<112>. The texture for 8090, was determined to be a mixture of {110}/<112> and {110}/<111>.

3.1.2 THERMO-MECHANICAL TREATMENT

Variation of the distribution of slip was an important part of this work. As was discussed in section 2.3.3, this can be accomplished by controlling the distribution of heterogeneous precipitation sites for the slip homogenising δ' phase. A uniform

distribution of nucleation sites can be the result of either stretching the material to form dislocations or through naturally ageing the material to form vacancy clusters (Flower and Gregson, 1987). Previous work had shown that the distribution of the S' phase is non-uniform in unstretched Al-Li-Cu-Mg-Zr alloys with no natural pre-age (Bischler and Martin, 1987).

Three heat treatments were used in this work to vary the S' phase distribution. One heat treatment was to artificially age the 6% stretched material at 170°C for 32 hours. A second heat treatment began with solution treatment at 540°C for 30 minutes followed by a 24 hour natural age to allow the formation of vacancy clusters. The material was then artificial aged at 170°C for 48 hours. Both of these heat treatments were expected to result in a homogeneous distribution of S' precipitates. The final heat treatment, expected to result in a non-uniform distribution of S' precipitates, was a solution treatment at 540°C for 30 minutes immediately followed by artificial ageing at 170°C for 100 hours. These heat treatments will be referred to throughout the rest of the text as stretched, duplex aged unstretched, and ~~duplex aged~~ unstretched respectively.

The artificial ageing times were chosen to result in peak hardness as indicated by measurements of hardness and tensile properties as a function of ageing time. Vickers Hardness Number is plotted for all the heat treatments and alloys as a function of ageing time in Figure 3.4. Yield strength and tensile strength are plotted as functions of ageing time in Figures 3.5 and 3.6. It should be noted that, as the 8090 was received peak-aged, it was necessary to re-solution treat and re-stretch a bar of this material to determine the ageing behaviour of the 6% stretched material. The stretching was done in a screw-driven Instron machine on bars that had been

slightly waisted so that they would not fail at the grips.

The hardness specimens were wet abraded after heat treatment using successive grades of silicon carbide paper up to 1200 grade. Using established techniques the hardness number was measured under a load of 10 kg with a Vickers Hardness Machine. Three measurements were taken for each hardness value.

Tensile testing was performed in accordance with ASTM specification E 8M (ASTM, 1987). A drawing of the two tensile specimens used is shown in Figure 3.7. The longer of the two specimens was used when measurement of the elongation was desired. This specimen satisfies the ASTM requirement that the gauge length be at least five times the diameter of the specimen.

Tensile specimens were machined from bars of 8090 and 8091 so that the axis of the specimen coincided with the L or the T direction. The tensile tests were performed using an Instron fitted with a 50 kN load cell. The Instron was calibrated before each series of tests by hanging weights from the load cell and adjusting the chart recorder to the correct reading. Specimens were gripped by specially built holders locked together by a ring and a 9 mm stainless steel pin. All tests were performed at a constant crosshead speed of 1 mm/min. This translates to an initial strain rate of 9.3×10^{-4}. Load extension curves were plotted on a built-in recorder running at a speed of 50 mm/min. In some cases, elongation was measured using an Instron extensometer.

Specimens were solution treated at 540°C in a Carbolite furnace for 30 minutes. An unknown reaction was observed between the specimens and the supporting stainless steel tray during the solution treatment. To prevent this, a saturated solution of Borax in ethanol was poured onto the tray and allowed to dry into a thin

ceramic layer. Each specimen was quenched separately in still water since variations in quench rate caused mechanical behaviour anomalies when multiple specimens were quenched simultaneously.

Specimens were artificially aged in a silicone oil bath. The temperature of the bath was controlled by a contact thermometer that used the mercury level within the thermometer as a switch. The oil within the bath was constantly stirred with an electric impeller. For ageing times less than 3 hours, only a few specimens were added to the bath at a time to avoid a significant drop in bath temperature. Aged specimens were quenched in still oil at room temperature. When natural ageing was not part of the thermo-mechanical treatment, artificial ageing was begun within 15 minutes of solution treatment.

Overaged and underaged 8091 were also examined in this work. The overaged 8091 was artificially aged for 96 hours at 190°C. Only the stretched material was overaged. After 96 hours the VHN was 158, 18 less than the peak of 176. Both stretched and unstretched 8091 were underaged. In both cases, artificial ageing lasted five hours at 170°C.

3.2 CRACK GROWTH CHARACTERIZATION

In basic terms, the fatigue growth of small cracks was characterized by applying a cyclic stress to a specimen and measuring the change in crack length as a function of the number of applied load cycles. The use of artificial crack initiators was avoided as artificially initiated cracks may not be equivalent to cracks that form naturally. For example, a small crack that is created by machining away most of the length of a long crack may have a plastic wake that is significantly different from a naturally

initiated small crack.

An Avery plane bender was used to apply and measure the cyclic stress. The crack length was measured from photographs taken of cellulose acetate replicates of the specimen surface and the number of cycles measured with a specially designed counter. The equipment and associated procedures are described in more detail in the following sections.

3.2.1 THE AVERY PLANE BENDER

The Avery plane bender applies a bending moment to a sheet specimen. One end of the specimen is attached with two bolts to the loading arm which moves vertically. As the loading arm moves it applies a force to the end of the specimen. The other end of the specimen is pinned and, beyond the pin, attached to a measuring arm which is mounted on a dynamometer spring. The force that the loading arm exerts is reacted by the pin and the dynamometer spring as the spring deflects.

The loading arm is attached to a 0.5 horsepower electric motor that rotates at a nominal 1420 RPM. The loading arm moves vertically as the motor rotates since the arm is eccentrically mounted on the rotating spindle of the motor. The amplitude of the vertical displacement can be changed by adjusting the double eccentric mounting of the loading arm on the motor. Furthermore, the entire motor can be moved up or down to define a mean position about which the arm oscillates.

A fixed fraction of the force applied to the specimen by the loading arm must be reacted by the dynamometer spring. The bending moment applied to the specimen is inferred from measurement of the motion of the measuring arm as it moves with

the deflection of the dynamometer spring. From the applied bending moment and the dimensions of the specimen (given in Figure 3.7) the stress applied to the specimen can be calculated using the strength of materials equation $\sigma = My/I$. This equation can also be expressed as $\sigma = 6M/bt^2$ where b and t are the specimen width and thickness respectively.

3.2.2 EXPERIMENTAL PROCEDURES

Specimen preparation began with milling specimens to the correct dimensions but one or two mm thicker than required. After heat treatment the sides of the specimen waist were wet abraded with 1200 grit sandpaper until the discolouration of the surface was removed. The abrading motion was always parallel to the length of the specimen. Both sides of the specimen were then milled to reduce the specimen thickness to 4.05 mm $\pm$ .03 mm. This operation removed the lithium-depleted zone at the surface due to solution treating. The specimen was then further abraded with 1200 grit silicon carbide paper until 4.00 mm thick. Successive Selvyt cloths, impregnated with 6 micron, 3 micron and 1 micron diamond pastes were then used for final polishing. All abrading and polishing operations were along the length of the specimen to avoid introducing stress concentrations. As a check of the heat treatment, the hardness of all specimens was measured before testing.

Prior to mounting a specimen, the Avery plane bender was zeroed. This was done by swinging the dial micrometer so that it was in contact with the measuring arm and then turning the dial of the micrometer to zero. In addition, the mounting of the loading arm was set for zero eccentricity.

Mounting of the test specimen began with selection of an

appropriate shim thickness. The purpose of the shim is to bring the neutral axis of the specimen in line with the midpoint of the loading arm oscillation. In units of millimeters the required thickness of the shim is given by $t = 7.14 - h/2$ where h is the thickness of the specimen. For this work, the specimens were 4 mm thick and so shims 5.14 mm thick were used. Prior to putting the shims in place, the mounting surface of the plane bender and the surface of the shims were inspected for dirt and cleaned if necessary. The specimen was then placed on top of the shims and the retaining nuts tightened to hold the specimen in place. The motor was moved so that the dial micrometers again showed zero deflection and then the tightness of the retaining nuts was rechecked.

The next step was to set the mean and maximum applied stresses. All tests were run so that the maximum stress was either 85% or 70% of the yield stress as determined from the tensile tests. The mean stress and stress amplitude were set with iterative adjustments to the position of the motor and the eccentricity of the loading arm mounting.

To begin the test the dial micrometer was swung out of contact with the measuring arm, the cycle counter was switched on, the reset button depressed and the motor started. Periodically, the motor was stopped so that cellulose acetate replicates could be made of the specimen surface. The blocks of cellulose acetate used were approximately 25 mm square and 6 mm thick. For tests at 85% of the yield strength replicates were made every 1,000 cycles. For tests at 70% of the yield strength, they were made every 5,000 cycles. Before replicating the specimen surface the loading arm was manually moved and wedged in place so that the maximum load was applied to the specimen and that any crack present would be fully open.

Then, a little acetone was squirted on the specimen surface followed by the placement of the cellulose acetate block. Finger pressure was kept on the block for between 30 and 60 seconds and it was allowed to dry for five minutes. A wooden lever was used to prise off the replica to avoid scratching the specimen surface. An optical microscope was used to inspect the replica for cracks. If a crack was found then the frequency of inspection was increased so that crack growth increments were approximately 20 microns. The replicates were stored to form a permanent record of the crack growth and later photographed so that crack length could be measured.

3.2.3 MEASURES TAKEN TO REDUCE OR ESTIMATE ERROR

As there is typically considerable scatter in experimental small fatigue crack growth data, it was considered especially important to reduce random errors so that changes in behaviour due to microstructure were not masked. For possible comparison to the work of other researchers it is also important to minimize systematic errors. In these experiments, the measured quantities are the crack length, the number of cycles, and the applied stress (which is directly inferred from the deflection of the measuring arm). Estimates of the errors made in measuring these quantities will now be discussed.

Crack length was measured from photographs of the cellulose acetate replicates. Accuracy in locating the crack tip was significantly improved by placing the replicates on the Avery specimen when the specimen was fully loaded and the crack fully open. Although chemical attack of the fully open crack tip by the acetone was possible, the improved accuracy in locating the crack

tip justified this technique. The smallest consistently measurable distance was less than 2 microns. Attempts to improve resolution through the Nomarski interference technique proved unsuccessful.

Assuming a resolution of two microns, the error in measuring cracks between 50 and 500 microns in length is insignificant. The errors in measuring an increment of crack growth would be larger as shorter lengths are involved. In this work, all increments of crack growth were at least 20 microns so that the errors would be less than 10%.

In 1000 cycles small cracks were found to grow between 10 and 100 microns. Thus, measurements of crack length were desired every 500-1000 cycles. Unfortunately, the cycle counter supplied with the Avery plane bender was marked in increments of 1000 cycles and so lacked the necessary resolution. Therefore, a new counter was built that was able to resolve single cycles by detecting motion of the loading arm. The cycle counter emitted infrared light that was reflected by the loading arm when the arm was at its maximum height. Detection of the reflected light caused a signal to be sent to a counter. Thus, a signal was sent to the counter once per cycle whenever the loading arm reached its maximum height. The circuit diagram for the counter is given in Figure 3.8.

There are several factors that affect the calculation of the applied stress. These include the accuracy of the calibration between the deflection of the loading arm and the applied moment, the consistency of the moment applied by the Avery plane bender, and factors associated with the effect of the geometry of the specimen on the distribution of stresses. Measurements of the deflection of the measuring arm and the dimensions of the specimen are unlikely to contribute greatly to errors since the measured

quantities are much larger than the accuracy of the micrometers used. The deflection of the measuring arm was periodically checked during experimentation and the moment applied to the specimen was found to vary randomly by up to 4%. This was judged acceptable.

Probably of more importance is the relation between the deflection of the measuring arm and the applied moment. To determine this relationship, a strain-gauged dummy specimen was prepared. The accuracy of the strain gauge was checked by pulling the dummy specimen in tension with a calibrated Instron machine. The strain output from the strain gauge was within 5% of the strain calculated from the applied load and the modulus of the material. This difference was probably due to a small error in strain gauge placement or a deviation in the gauge factor. In any case, the error is relatively small. The dummy specimen was placed in the Avery plane bender and the strains for various displacements of the measuring arm were recorded. Based on these experiments the applied moment was found to be linearly related to the deflection of the measuring arm with a proportionality constant of 9.12 N-m/mm. This conclusion differed from the calibration curve supplied by the manufacturer by 50%. This discrepancy may have been due to modifications that were made to the measuring arm prior to this work.

As the test specimen was waisted and loaded as a cantilever beam, the stresses were not uniform throughout the specimen. A mild stress concentration factor is introduced by the waist. This was, however, found to be negligible for more severe radii (Peterson, 1974) and so it was neglected. On the other hand, the change in moment along the length of the specimen and the change in cross-sectional area were not negligible. The variation of stress as a

function of the distance from the centre of the specimen is depicted in Figure 3.9. Not surprisingly, most cracks appeared where the stresses were greatest. In that region the stress level is relatively independent of position. Nevertheless, the position of the crack was factored into all calculations of stress. The cracks were too small for there to be significant variations of stress for different parts of the crack.

The mechanical polishing operations could have introduced residual stresses into the specimens. Residual stresses can significantly affect small fatigue crack growth rates. Therefore, in examining sources for error, it was important to assess the effect of residual stresses for the specimens used in this work.

This was done by annealing a specimen of 6% stretched 8091 for one hour at 170°C after the mechanical polishing. The resulting small crack growth rates of annealed and unannealed specimens are shown in Figure 3.10. As there was no significant difference between the two, it was concluded that the residual stresses introduced by mechanical polishing had a negligible effect on the rate of small crack growth. Also, the small fatigue crack growth rates observed in this work were comparable with those measured by other workers (eg Venkateswera Rao et al, 1986).

So far the measurements of stress, crack length, and the number of stress cycles have been discussed. These measurements can be combined to form a crack driving force and a crack growth rate. The crack growth rate can be calculated by dividing the change in crack length by the number of elapsed cycles. There are, however, a number of crack driving force parameters. Most of these, however, can be related to ΔK. Therefore, the method of calculating ΔK will now be discussed.

3.3 CALCULATION OF K

There is no exact method of calculating K for small cracks because of their complex and variable shape. The crack shape must be simplified to match one for which a K solution has been developed. In addition, a choice must be made from among the several K solutions that may exist for a given shape of crack. The selection of a good approach for calculating ΔK is important when studying small fatigue cracks because each specimen tested contained a differently shaped crack. A poor approach could potentially distort comparisons of small fatigue crack growth in different materials.

In this work the basic approach to calculating K was to model the crack as being semi-elliptical, to calculate a nominal K on that basis, and then to adjust this value of K to account for crack inclination, changes in crack direction and crack branching. This analysis will now be described in more detail along with a short discussion of how K as a driving force and Δa, the increment of crack growth, were defined.

3.3.1 K FOR A SEMI-ELLIPTICAL CRACK

The basic shape of small surface cracks was assumed to be semi-elliptical. This assumption agrees with observations of sectioned cracks made in this work. Furthermore, as this assumption is widely used, comparison with other work is facilitated.

It is worthwhile mentioning that some of the cracks studied in this work initiated from a corner of the specimen and so were actually quarter-elliptical. Because solutions for K by different authors for semi-elliptical cracks were found to vary widely (Scott

and Thorpe, 1981), it was felt that for consistency only a single worker's solutions based on a single approach could be used. Unfortunately, this has not been done for quarter and semi-elliptical cracks under pure bending. Since the difference between the solutions for quarter and semi-elliptical cracks under pure tension was only 6% (Murakami, 1987), it was decided that the solution for semi-elliptical cracks under bending would also be used for quarter-elliptical cracks.

A number of solutions for K of a semi-elliptical crack have been published. The Newman-Raju semi-empirical solution (Newman and Raju, 1981) was selected primarily because it has been found to be the most accurate (Mahmoud and Hosseini, 1986). In addition, it was valid for the range of expected geometries without interpolation for constants and has been used for other work on small fatigue cracks. The Newman-Raju solution for bending is given below.

$$K_I = H\sigma \left(\frac{\pi a}{Q} \right)^{1/2} F(a/t, a/c, c/b,)$$

where

$$H = 1 - 0.34(a/t) - 0.11(a/t)(a/c)$$

$$Q = 1 + (a/c)^{1.65}$$

$$F = [M_1 + M_2(a/t)^2 + M_3(a/t)^4][1.1 + 0.35(a/t)^2](a/c)^{1/2} f_w$$

$$M_1 = 1.13 - 0.09(a/c)$$

$$M_2 = -0.54 + \frac{0.89}{0.2 + (a/c)}$$

$$M_3 = 0.5 - \frac{1.0}{0.65 + (a/c)} + 14[1.0 - (a/c)]^{24}$$

$$f_w = \sec \frac{\pi c}{2b} (a/t)^{1/2}$$

These equations have been simplified and are valid only for the points where the crack intersects the surface of the specimen. Although, as can be seen from Figure 3.11, the variations of K around the crack perimeter are relatively small, the issue of where

on the perimeter of a 3-D, semi-elliptical crack ΔK should be calculated is raised. In this work, ΔK was calculated at the point of intersection of the crack with the surface of the specimen because the crack growth measurements were taken at the specimen surface and because it was only at the surface that angles of crack inclination were known.

As Figure 3.12 shows, the calculation of K using the Newman-Raju equation is dependent on the crack depth to crack length ratio (a/c). To determine this ratio, small cracks were grown, their lengths measured and then they were sectioned so that their depth could be measured. Actual determination of a/c is complicated by the fact that the crack path was found to be inclined into the surface of the specimen (as shown in Figure 3.13). This raises the issue of whether the length a should be defined as the actual length or the length of the crack projected on to the plane normal to the load. This issue is further discussed in section 3.3.4. Values of a/c using both of these definitions of a are given below.

c (um)	a_{act} (um)	a_{act}/c	a_{proj} (um)	a_{proj}/c
541	403	.74	231	.43
310	208	.67	133	.43
159	117	.73	70	.44
234	153	.65	82	.35

Taking a as the actual length, the average value of a/c was taken to be 0.7. Taking a as the projected length, the average value of a/c was taken to be 0.4. Values that have been reported in the literature for Al-Li alloys range from 0.8 (Venkatswera Rao et al, 1986) to 0.35 (James, 1987).

As the specimen was loaded in bending, shear stresses are produced toward the neutral axis of the specimen. These shear stresses could result in either Mode II or Mode III loading depending on position around the crack perimeter. The relative

magnitudes of these stresses as compared with the normal stresses were calculated using strength-of-materials equations. These calculations showed that the magnitude of the shear stresses was less than 0.3% of the normal stresses. Therefore, the shear stresses due to bending were neglected in further calculations of K.

3.3.2 CALCULATION OF K FOR KINKED AND BRANCHED CRACKS

The basic variables in crack shape that could affect the calculation of K are changes in crack direction (crack kinking), crack branching, and crack inclination. Many researchers (eg Venkateswera Rao et al, 1986) considered only the projection of the crack on to the plane perpendicular to the loading axis. Crack kinking, crack branching and crack inclination were not considered. If this approach is taken then the equations given in the previous section are sufficient to calculate ΔK.

Suresh (1983) has pointed out, however, that crack kinking, crack branching and crack inclination may significantly affect the crack driving force. If so, then neglecting these variables could contribute significantly to the scatter normally present in small crack data. In addition, these factors could have a systematic effect on small crack growth data. To study the effect of including crack inclination, both approaches were used in this work. That is, the data were reduced both with the equations given in the previous section (which do not include crack shape) and with the approach described in the following paragraphs. In this section it will be shown that kinked and branched cracks can be treated as inclined cracks.

There have been several solutions for K of a kinked crack. Some focussed on an infinitesimal kink. These were irrelevant as

the smallest increment of crack growth measured in this work was 20 microns and so was not infinitesimal. Vasudevan and Suresh (1985) have suggested the following equation for K_I of a kinked crack where ΔK is the apparent driving force, Δk is the driving force for a straight crack, θ is the angle of the kink, D is the length of the deflection, and S is the length of the straight portion of the crack.

$$\Delta K_I = \frac{D + S}{D \cos^2(\theta/2) + S} \Delta k$$

This equation was not used as it is based on a 2-D approach and would not be able to include the effects of inclination perpendicular to the specimen surface.

As the length of the kink increases, the value of K approaches that for an inclined crack with the same projected length (Suresh and Shih, 1986). Therefore, in this work, a kinked crack was modelled as an inclined crack with the same projected length and with the same angle of inclination as the kink to the applied load. From Suresh and Shih (1986), this approach is accurate as long as the length of the kink is at least 10% of the total length. This approach required that ΔK be calculated separately for each end of a kinked crack as the angle of inclination was often different for each end of a kinked crack. This requirement may be appropriate since the environment of each end of the crack could also be different - a different grain, for example.

When branching occurred, K was calculated for the major crack and the branches were assumed to have a negligible effect. This assumption is necessary because no currently available solution can handle the possible number of permutations of relative branch lengths and angles between branches. Fortunately, the assumption that the branches have a negligible effect is reasonable. Suresh and Shih (1986), for example, have found that K is similar for a

crack with a kink at 45° to the main crack direction and a branched crack where the two equal branches are each at 45° to the main crack direction. It is not unreasonable, therefore, that K for branched crack in general will be similar to K for the major crack without the branch. In this work, no differences in the crack growth rates of branched cracks and unbranched cracks were observed.

3.3.3 CALCULATION OF K FOR AN INCLINED CRACK

Inclination of the crack with respect to the load axis means that there will be a mixed mode of loading on the crack. There are two axes about which the crack may be inclined to the load as illustrated in Figure 3.13. In general $K_I=Y\sigma_I(a)^{1/2}$, $K_{II}=Y\tau_{II}(a)^{1/2}$, $K_{III}= Y\tau_{III}(a)^{1/2}$. Therefore, in order to calculate K_I, K_{II}, and K_{III}, σ_I, τ_{II}, and τ_{III} must be calculated as functions of σ. This can be accomplished by calculating the force applied in the appropriate direction and the area that it is applied upon and then using the relation $\sigma=P/A$. These quantities are illustrated in Figure 3.14. As can be seen the area is the same in each case and given by $A'=A/\cos\phi$. The loads giving rise to the Mode I, II and III components of K respectively are given by

$$P_I = P\cos\phi$$
$$P_{II} = P\sin\theta$$
$$P_{III} = P\sin\alpha$$

Therefore,

$$\sigma_I = P_I/A' = \sigma\cos^2\phi$$
$$\tau_{II} = P_{II}/A' = \sigma\sin\theta\cos\phi$$
$$\tau_{III} = P_{III}/A' = \sigma\sin\alpha\cos\phi$$

$\cos\phi$ must now be found in terms of θ and α. The crack plane is shown in terms of the direction cosines l, m, and n in Figure 3.14. Note that $\cos\alpha=n$. Now, $l^2+m^2+n^2=1$ or, dividing both sides of this

equation by n^2,

$$\frac{l^2}{n^2} + \frac{m^2}{n^2} + 1 = \frac{1}{n^2}$$

From Figure 3.14 it can be seen that $l/n=\tan\theta$ and $m/n=\tan\alpha$. Substituting these expressions in the above expression results in

$$\tan^2\theta+\tan^2\alpha+1 = 1/n^2 = 1/\cos^2\phi$$

Therefore, K_I,K_{II},and K_{III} are given by the following equations where θ and α are illustrated in Figure 3.13 and k_I is the value of K based on a crack with the same length as the inclined crack but perpendicular to the applied stress.

$$K_I = k_I/B^2$$
$$K_{II} = k_I\sin\theta/B$$
$$K_{III} = k_I\sin\alpha/B$$

where $B = (\tan^2\theta+\tan^2\alpha+1)^{1/2}$

To calculate the K's in these equations, the applied stress, the crack length c, the inclination of the crack on the surface θ, and the inclination of the crack into the interior of the specimen must be measured or estimated. This is only a problem for the angle α because it can only be measured by sectioning the specimen. This was undesirable as this procedure would destroy the specimens preventing later examination using the TEM or the SEM. Therefore, a method of estimating α was sought.

As will be shown in Chapter Four, the small cracks studied were found to grow crystallographically on {111} planes. Al-Li alloys have been found to have a <112>/{110} texture (Yoder et al, 1988) and, as mentioned earlier, this texture was found in the plates of material studied in this work. This implies that certain angles of α would be favoured. From Figure 3.15 it can be seen that one of the four {111} planes is parallel to the <112> loading direction. No crack could, therefore, propagate on this plane. It can also be seen that the angle between the $[1\bar{1}0]$ direction and the intersection of the

remaining {111} planes with the (111) plane is α. This angle was calculated to be -60°, 60, and 0° for the remaining three {111} planes. Although slip is possible on the {111} plane with the α of 0°, it is more likely on the planes more inclined with respect to the load axis.

These assumptions were fairly well supported by measurement of α on selected cracks. The angle α was measured for five cracks as 60°, 55°, 55°, 55°, and 50°. This averages to an angle of 55° with a fairly narrow distribution. It, therefore, seemed reasonable to assume the theoretical value for α of 60° for all specimens.

3.3.4 DEFINING ΔK AND CRACK GROWTH INCREMENT

Two definitions of ΔK and crack growth increment were used in this work depending on whether or not crack inclination, branching, and kinking were considered. When not considered, ΔK was calculated based on the projection of the crack on a plane normal to the load. For consistency, the crack growth increment was similarly projected on to the plane normal to the load. Similarly, the projected value of a was used to calculate a/c.

On the other hand, when the effects of crack inclination, branching, and kinking were included then the mode of loading was usually mixed Mode I, Mode II and Mode III. This raises the question of whether the driving force for crack extension is K_I, K_{II}, K_{III} or some combination thereof. Socie et al (1987) suggested that the driving force of a crack under mixed loading conditions could be expressed with the following equation.

$$K_{eq} = (K_I^2 + K_{II}^2 + (1+\nu)K_{III}^2)^{1/2}.$$

This equation is based on strain energy release rate theory and is for plane stress conditions. It was used to calculate the effective

driving force in this work when crack inclinations were taken into account.

For an inclined crack, there is also a choice as to whether the increment of crack growth should be defined as the actual increase of crack length or as the increase in projected crack length perpendicular to the direction of loading. Based on the concept that K is related to G and the energy required to create new surfaces, the decision was made to define the increment of crack growth as the actual change in crack length. Also, the value of a used to calculate a/c was now taken as the actual value of a rather than its projected length.

A drawing of the orientation of the specimens with relation to the plate of material is shown in Figure 3.16. By convention the crack length along the specimen surface is denoted as c and the crack length perpendicular to the crack surface is denoted as a. As the crack lengths and crack growth increments measured in this work were along the surface they will henceforth be referred to as c and dc/dN respectively.

3.4 GENERATION OF CYCLIC STRESS-STRAIN DATA

The generation of cyclic stress-strain data was performed in accordance with ASTM specification E 606 (ASTM, 1987) with the exception that the specimen was 5 mm in diameter rather than the recommended 6.35 mm. The specimen was a threaded dumb-bell (see Figure 3.7) machined with the longitudinal axis in either the L or the T direction. To avoid stress concentrations, wet grinding with 1200 grade silicon carbide paper was followed by successively polishing with 6, 3 and 1μm diamond impregnated Selvyt cloths.

The stress ratio for all tests was -1. Over a period of time

(normally about 20 cycles) the response of the specimen stabilized and the plastic strain was recorded. The test was repeated at a higher stress and a new plastic strain recorded until failure of the specimen. By plotting these stress-strain points a cyclic stress-strain curve can be constructed. A description of the equipment and specific procedures follows.

The specimen was retained in a Mand servohydraulic test machine using a Woods metal grip to ensure axiality and alignment of loading. To eliminate backlash within the system at zero load, all joints in the load train were compressively loaded with spiral wedges. After mounting the specimen the LVDT's were attached to the gauge length of the specimen. The LVDT's were held in place by springs which maintained tension on knife edges gripping the circumference of the specimen. If cyclic life data had been desired the damage done to the specimen surface by the knife edges would have been of concern. In this case, however, only the relation between the cyclic stress and the cyclic plastic strain was desired. The outputs from the two LVDT's were averaged and recorded on an X-Y recorder. The other input to the X-Y recorder was the applied load.

Initially, it had been planned to characterize the cyclic stress-strain response of 8090 and 8091 with constant plastic strain amplitude tests. For this purpose a custom-built Electro Servo-Hydraulic (ESH) unit was connected to LVDT's mounted on the specimen. The purpose of the ESH unit was to electronically subtract the elastic portion of the strain signal so that plastic strain could be fed back to the servohydraulic system for control purposes. When an experiment was performed in this manner, it became apparent that the ESH unit lacked the resolution required to

measure the plastic strains at stresses comparable to those used to grow small cracks. For that reason the remaining cyclic stress-strain experiments were conducted at constant stress rather than constant plastic strain.

When constant stress experiments are performed on materials that cyclically harden, there is a relatively large amount of deformation on the first cycle as compared with constant strain experiments. This can lead to differences in cyclic stress-strain behaviour measured under constant stress versus constant strain conditions (Starke and Lutjering, 1978). In this work, only a small amount of cyclic hardening was observed. Nevertheless, sets of data obtained under constant plastic strain and constant stress were compared (see Figure 3.17) to see if there was a significant difference in the resulting cyclic stress-strain data. No significant difference was observed.

3.5 MICROSCOPY

3.5.1 OPTICAL METALLOGRAPHY

Specimens for grain size determination were first mounted in a block of thermosetting polymer for ease of handling. The mounted specimens were then successively wet ground on 220, 320, 600, and 1200 silicon carbide abrasive papers. Between each grinding they were washed in water to remove the abrasive. After washing in soap, water and methanol they were succesively polished on Selvyt cloth impregnated with 6 micron, 3 micron and 1 micron diamond paste. Between each stage the specimens were washed in soap, water and methanol. A modified Keller's etchant was used to etch the specimens. The composition of this etchant, which was prepared

fresh prior to use, was 2 ml hydrofluoric acid, 3 ml hydrochloric acid, 20 ml nitric acid and 175 ml water. Etching of the grain boundaries took approximately 30 secconds. All photographs were taken with a Zeiss Ultraphot II microscope.

For lineal roughness measurements, micrographs were taken of cellulose acetate replicates at 140X. The length of the actual crack was measured with a MOP-AMOS 2 digitizer. The actual length was then divided by the projected length to give R_L, the lineal roughness parameter.

3.5.2 GENERATION OF ELECTRON CHANNELLING PATTERNS

All specimens to be examined using selected area electron channelling patterns (SACP's) were cut into blocks approximately 10 mm in length, 4 mm in width and 1 mm in depth. To avoid plastic deformation and provide for a more controlled cut, spark erosion was used to cut the specimens. In general, SACP's were generated on Avery plane bend specimens that had already been polished with one micron diamond paste. Other specimens had to first receive this amount of polish. To further improve the level of polish the specimens were electropolished. Electropolishing was performed in 25% solution of nitric acid in methanol at -35°C for 8090 and -40°C for 8091. The solution was stirred with a magnetic stirrer during electropolishing. The applied voltages and times for 8090 and 8091 respectively were 20V/10 seconds and 15V/7 seconds. The specimens were then mounted on copper boats using silver dag.

All SACP work was performed using a JEOL 100C electron microscope with an EM-ASID-40 scanning attachment. SACP's were used to map the plastic zone and to determine the orientation of grains around the crack. The technique used to determine the

plastic zone size was to observe the degradation in the SACP associated with plastic deformation. The specific procedures to map plastic zones with this equipment have been discussed in detail elsewhere (Tekin and Martin, 1989). Plastic deformation was said to begin with the disappearance of the fourth order {111} line. This is illustrated in Figure 3.18. Plastic zone size measurements were taken in a direction normal to the applied stress from the crack tip.

Determination of grain orientation was achieved through comparison of the SACP's with a Kikuchi map for FCC crystals. This comparison made possible identification of the crystallographic normal to the plane of the specimen and of crystallographic directions within the plane. Determination of the latter was affected by rotation of the image by the lenses. Therefore, a superalloy single crystal with known crystallographic orientation was electropolished and examined in the beam rocking and image mode of the microscope. The SACP and the image were compared to determine angles of image rotation at various rocking angles and magnifications. Because the zone axis was <100> an ambiguity of 90° still existed. To resolve this, image movements resulting from specimen rotation in the rocking mode and specimen translation in the image mode were compared. Based on this work, a rotation of 67° counter-clockwise from image to channelling pattern was determined over the magnification range of interest (standard magnification 300-1500X) and for all rocking angles.

A special application of the orientation of grains was to identify the crystallographic planes favoured for small crack growth. As pictures of the specimen surface only showed the intersection of the plane of crack growth with the plane of the specimen surface a unique plane of crack propagation could not be identified. A unique

plane of crack propagation could have been identified if the crack had been sectioned perpendicularly to the surface as the angle of crack inclination into the specimen would have been determined. This, however, would have destroyed the specimens and they could not have been used for further study. In addition, there were experimental uncertainties in polishing the specimen to desired locations. Therefore, it was assumed that crack propagation was likely to occur on either {111}, {110}, or {100} planes. Having made this assumption, standard stereographic projections were used to identify which of these planes was compatible with a given direction of the intersection of the crack propagation plane with the specimen surface. The results of these calculations are tabulated below.

Zone axis	Index of plane parallel to crack	Possible crack propagation planes
<100>	{100}	{100} or {110}
"	{110}	{110} or {111}
<110>	{100}	{100} or {111}
"	{110}	{100} or {110}
"	{111}	{111}
<111>	{110}	None
<112>	{111}	{100}, {110}, or {111}

3.5.3 TRANSMISSION ELECTRON MICROSCOPY

Specimens to be examined by TEM were first machined into 3 mm diameter rods. Discs 1-2 mm in thickness were cut from the rod using a jewelers saw. The discs were manually wet ground on 1200 grade silicon carbide paper to between 0.16 and 0.20 mm in thickness. The specimens were dished and polished using a Fishioni electropolisher. The electropolishing bath was a solution of 25% nitric acid in methanol at -30°C. Dishing and polishing were automatically stopped as soon as the foil was perforated. The foil was then immediately washed in alternating baths of methanol and ethanol to remove the oxide layer. Foils were stored in methanol to

inhibit oxidation before examination. Nevertheless, for the best results the foils had to be examined within 24 hours of preparation.

Several diffraction conditions could be used to image S', T_1, and δ' precipitates. The δ' precipitates could be seen as round particles in almost any zone axis in bright field (BF) or by putting the objective aperture on a superlattice spot in dark field (DF) conditions. As the only round precipitate it was easily identified. In imaging the T_1, S' and δ' precipitates, the best results were obtained using a zone axis of <100>. The resulting diffraction pattern and precipitate spots are shown in Figure 3.19. It was not always possible to differentiate between the S' and T_1 phases on the basis of morphology alone. Instead the direction of the long axis of the precipitate was used. For a zone axis of <100>, the long axis of the S' precipitates is parallel to the <100> direction which can be found from the diffraction pattern. The long axis of the T_1 phase is at 45° to the S' phase. For this technique to work, any rotation between the image and the diffraction pattern must be known. Such rotations were determined through forming images and diffraction patterns of molybdenum trioxide crystals at various magnifications and camera lengths. As the long axis of the molybdenum trioxide crystals and the <100> direction should be parallel, any apparent rotation would be due to the lenses. The measured rotation angles are given below. The angles are from the image to the diffraction pattern and are in the clockwise direction.

Magnification (x 1000)	Camera length (cm)	θ (degrees)
26	76	70
33	"	65
50	"	60
66	"	34
26	120	75
33	"	70
50	"	65
66	"	39

Foils were also prepared for examination of the dislocation structure associated with small cracks. In these cases, the foils were dished and polished electrochemically, as previously described, until perforation occurred. Then, the foil was ion beam thinned using an Edwards IBMA 2 Ion Beam Thinner until the material adjacent to the crack tip and in the plastic zone was thinned. The voltage, current, and incident angle used for ion beam thinning were 6kV, 60μA, and 25° respectively. Although the foil was ion beam thinned from both sides, ion beam thinning typically took 50-100 hours.

3.5.4 FRACTOGRAPHY

Spark erosion was used to cut the material containing the crack out of the specimen before examination. This facilitated breaking a crack open. The fracture surface were then examined using an Hitachi 530 SEM with an accelerating voltage of 25kV.

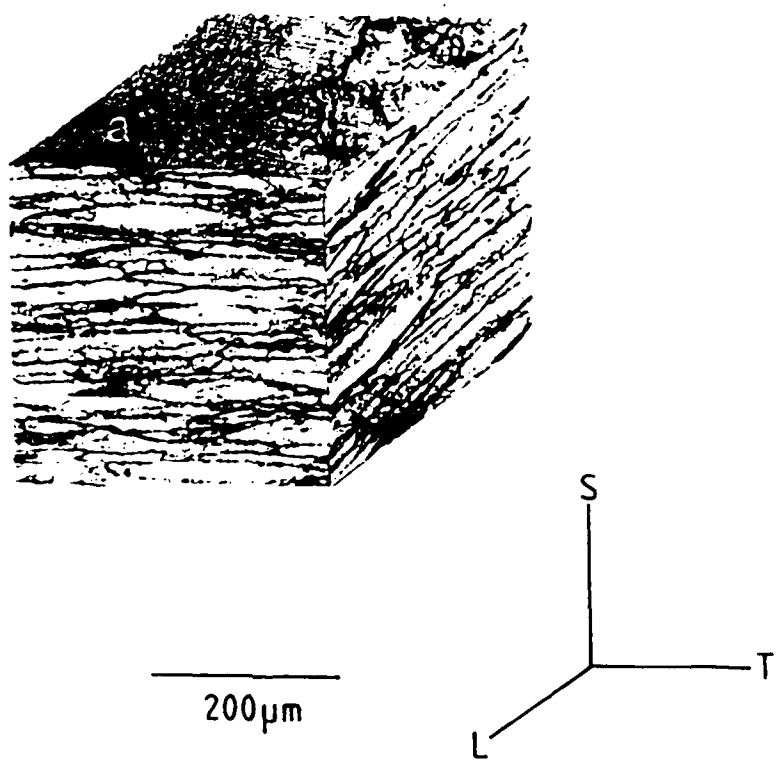

Figure 3.1 Optical micrographs showing the grain structures of a) 8090 and b) 8091.

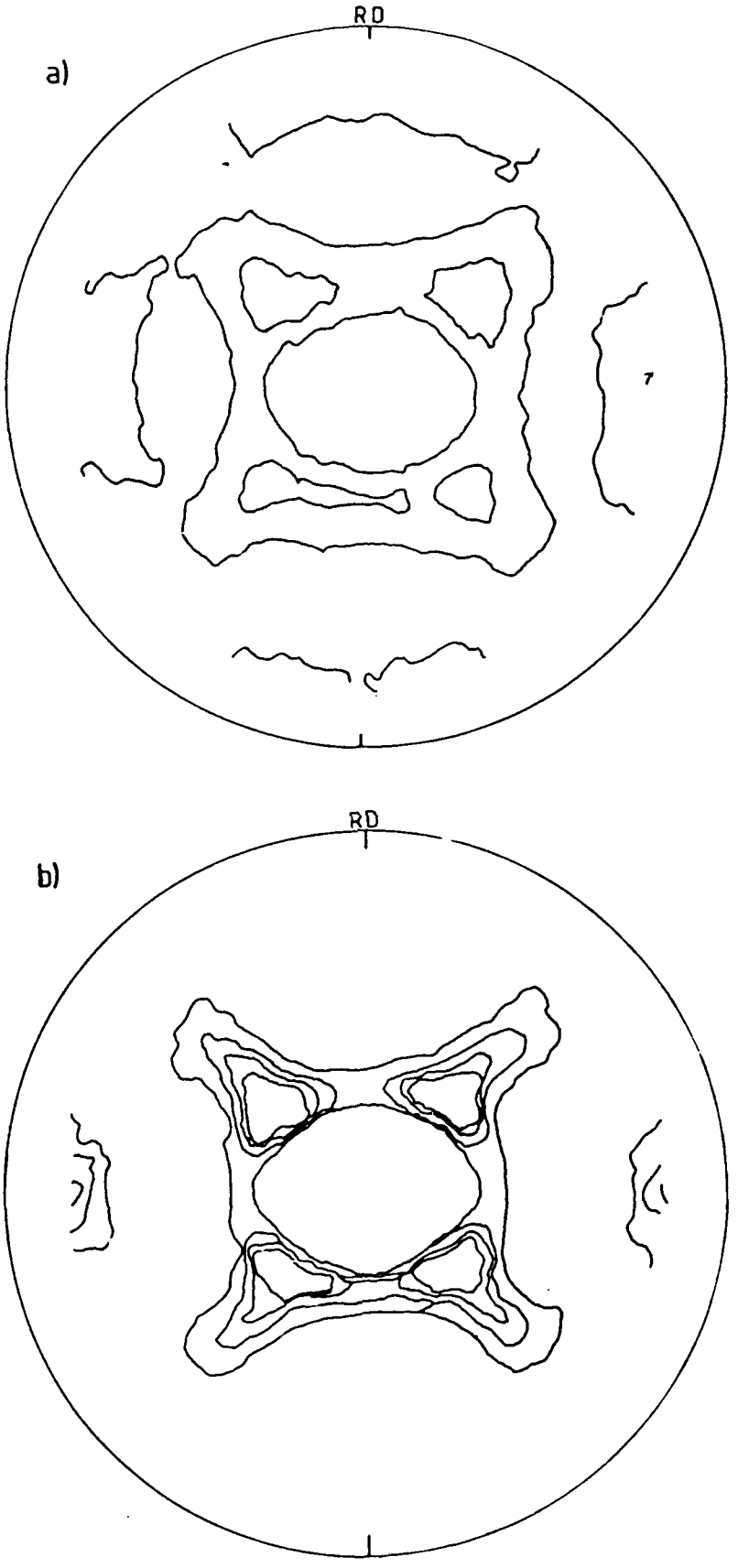

Figure 3.2 <111> pole figures for 8090 from a) the surface of plate and b) the centre of plate.

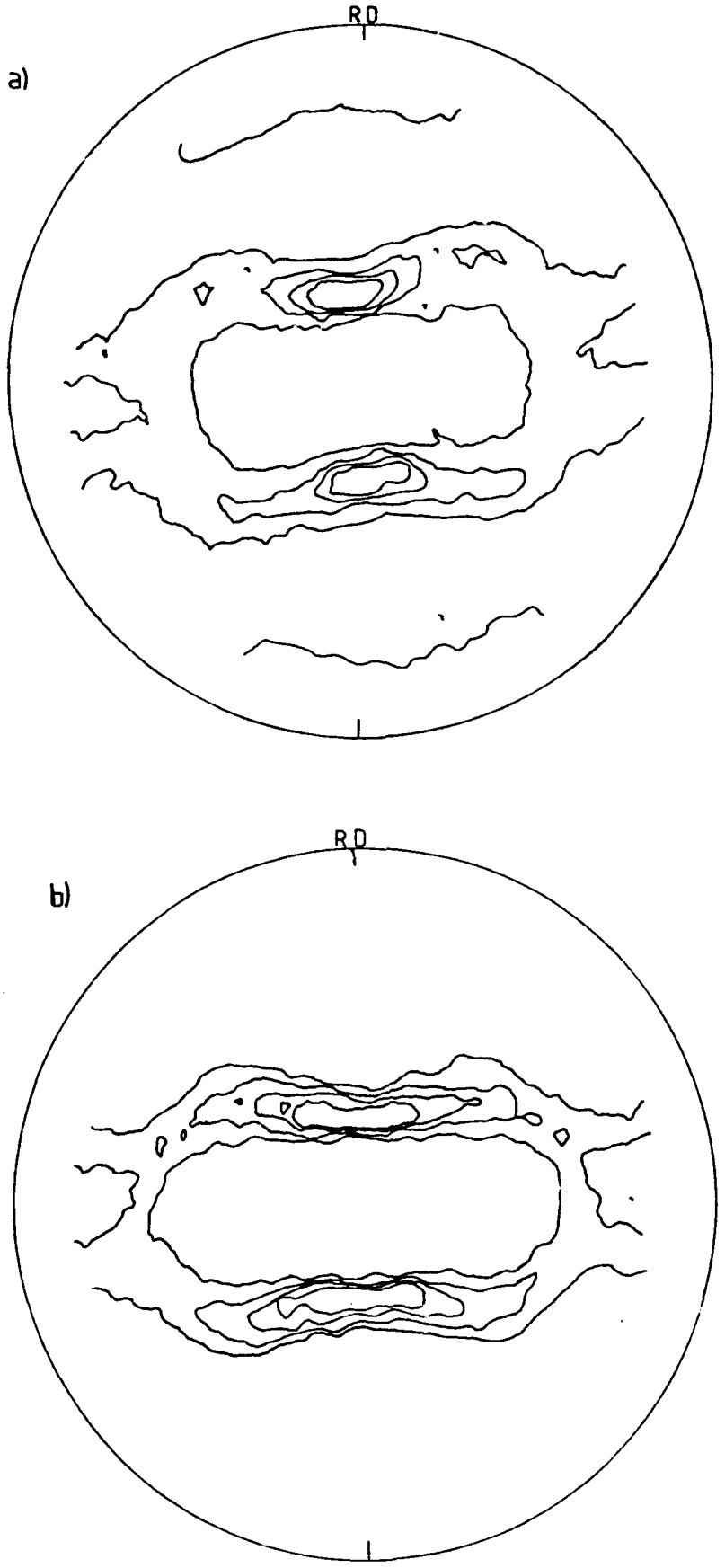

Figure 3.3 <111> pole figures for 8091 from a) the surface of plate and b) the centre of plate.

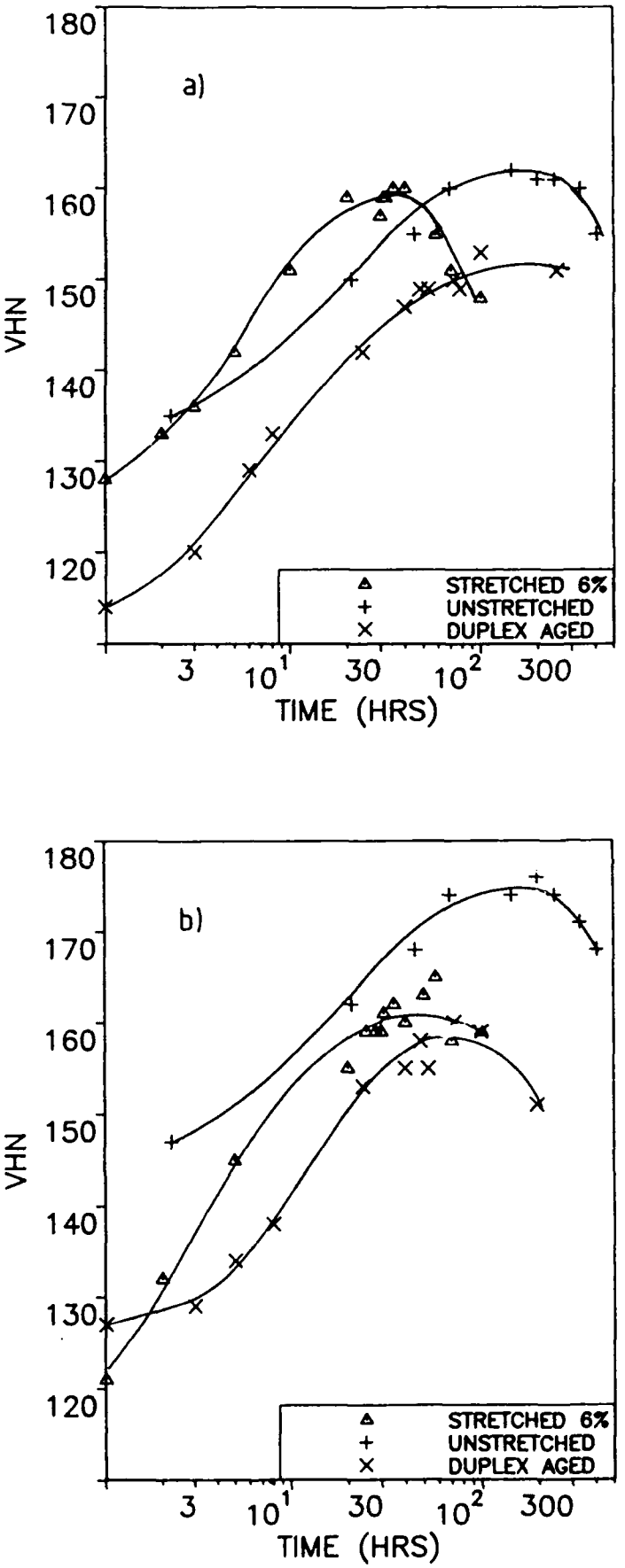

Figure 3.4 Vickers hardness as a function of ageing time at 170°C for a) 8090 and b) 8091.

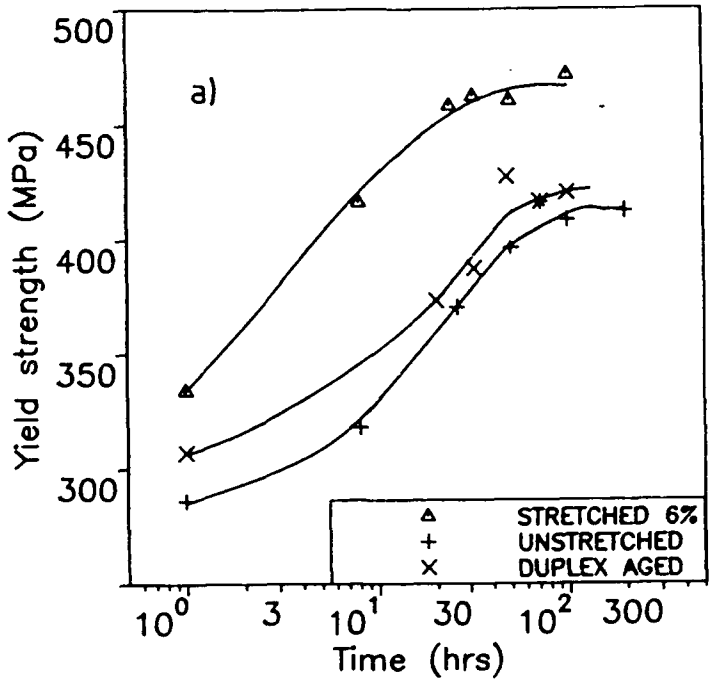

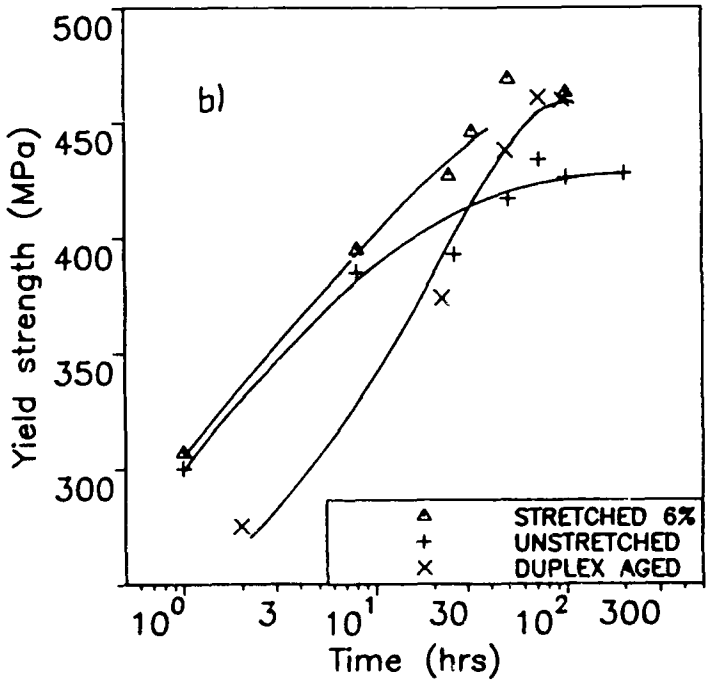

Figure 3.5 Yield strength (0.2% offset) as a function of ageing time for a) 8090 and b) 8091.

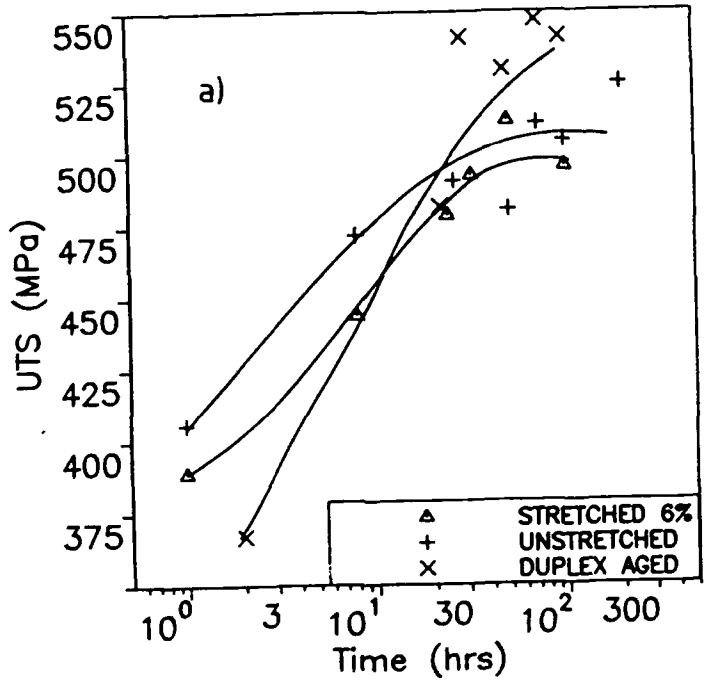

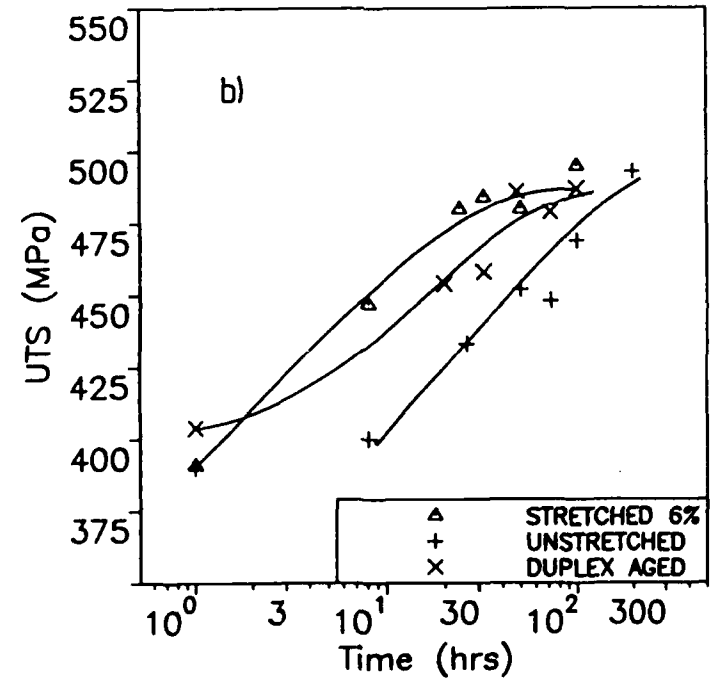

Figure 3.6 Ultimate tensile strength as a function of ageing time for a) 8090 and b) 8091.

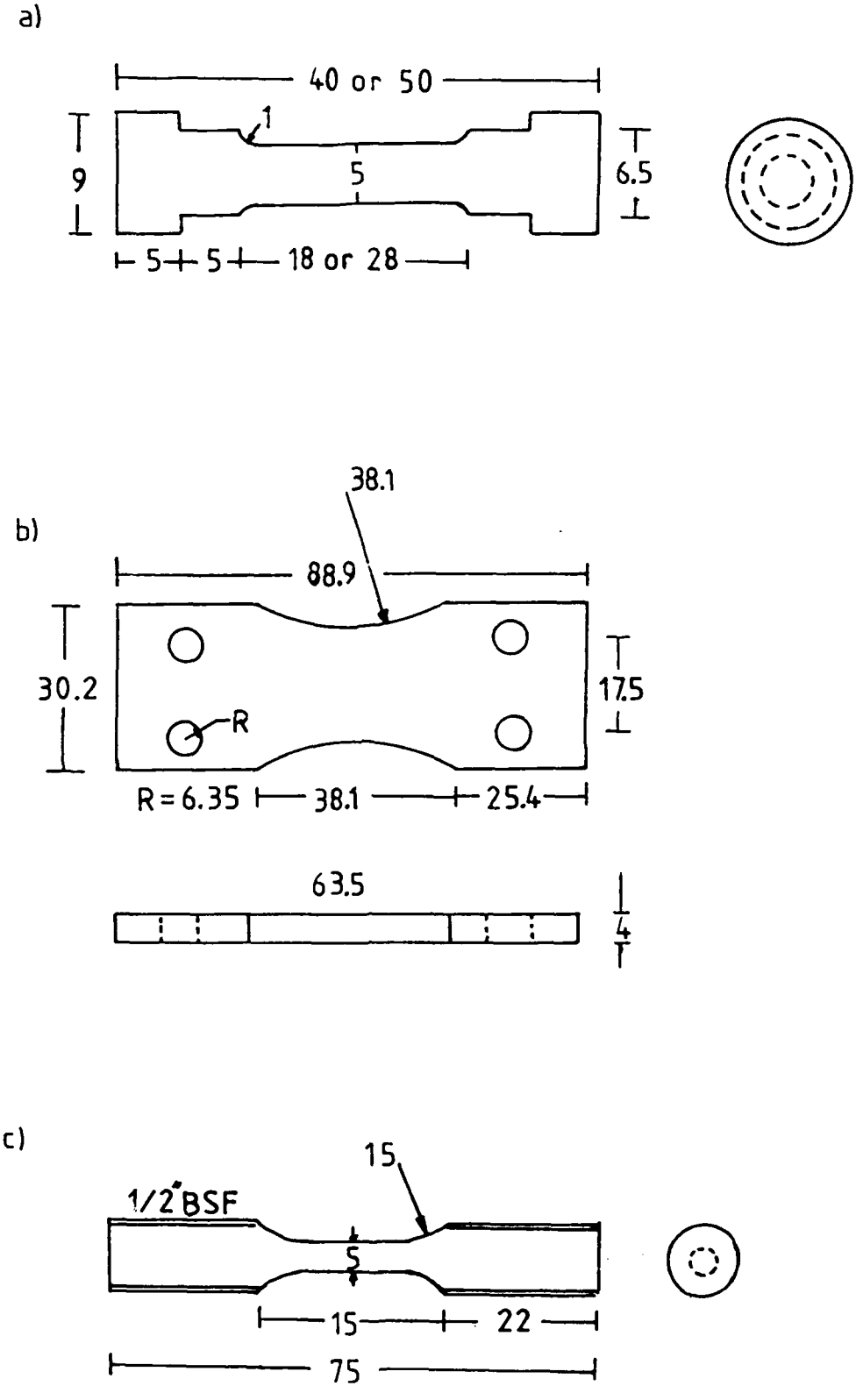

Figure 3.7 Test specimen dimensions in mm for a) tensile specimens, b) Avery plane bend specimens and c) cyclic stress-strain specimens.

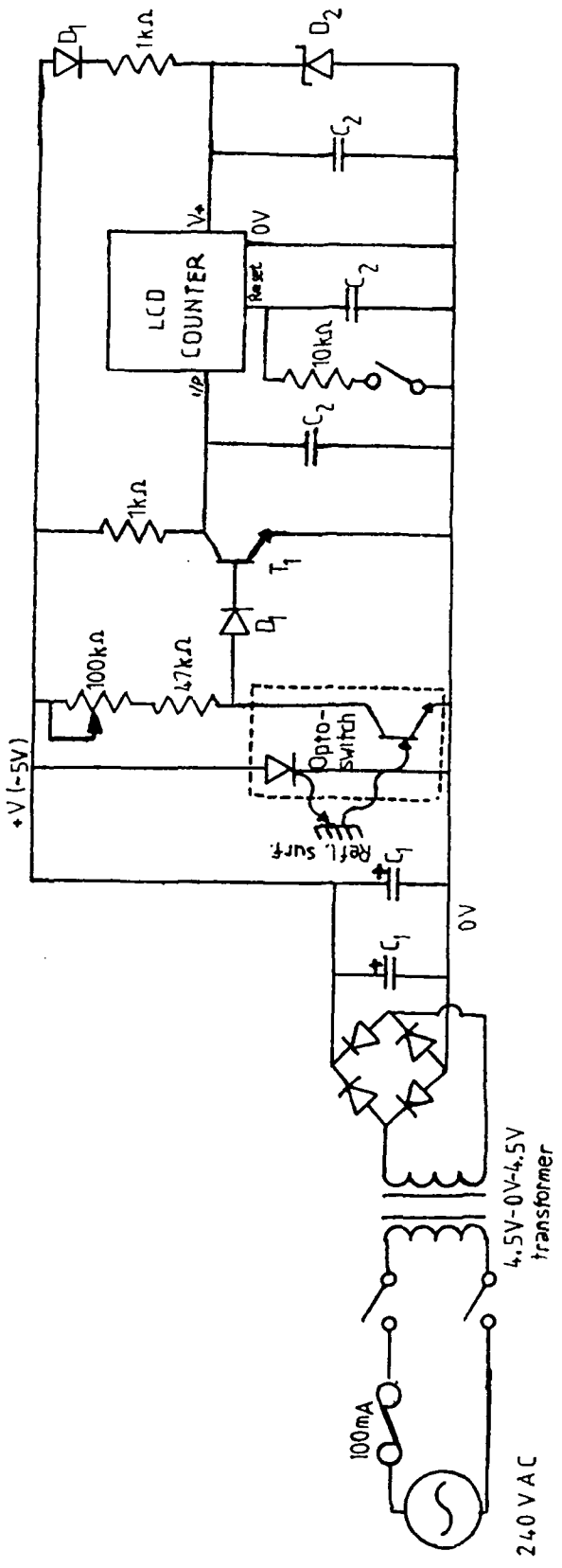

C_1 = 1000µF Opto-switch supplied by R.S. Stock # 307-913

C_2 = 100µF LCD counter supplied by R.S. Stock # 343-442

T_1 = BC184 Transformer supplied by R.S. Stock # 196-381

D_1 = 1N418 silicon diode

D_2 = 3V zener diode

Figure 3.8 Circuit diagram for cycle counter.

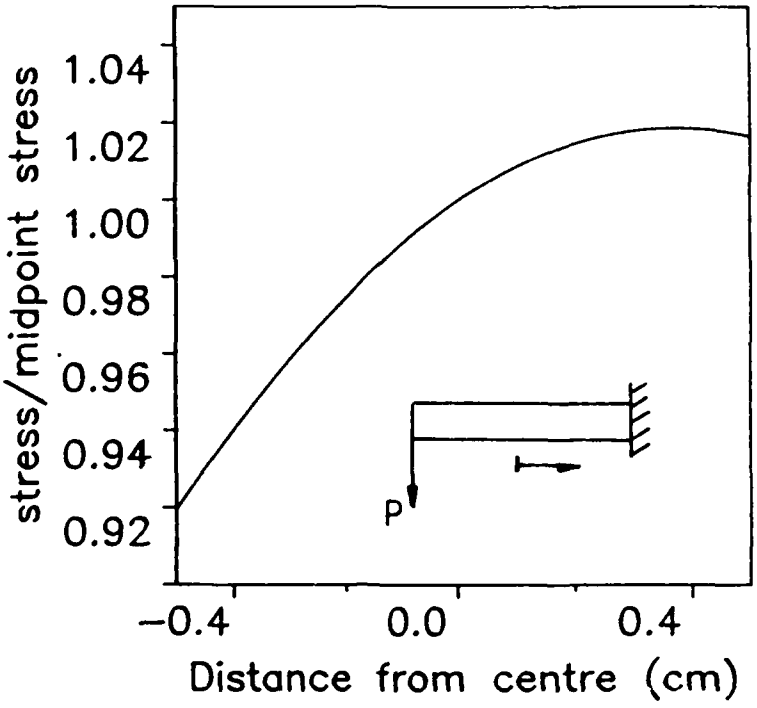

Figure 3.9 Stress variation with crack position along length of specimen (midpoint of specimen at 0.0).

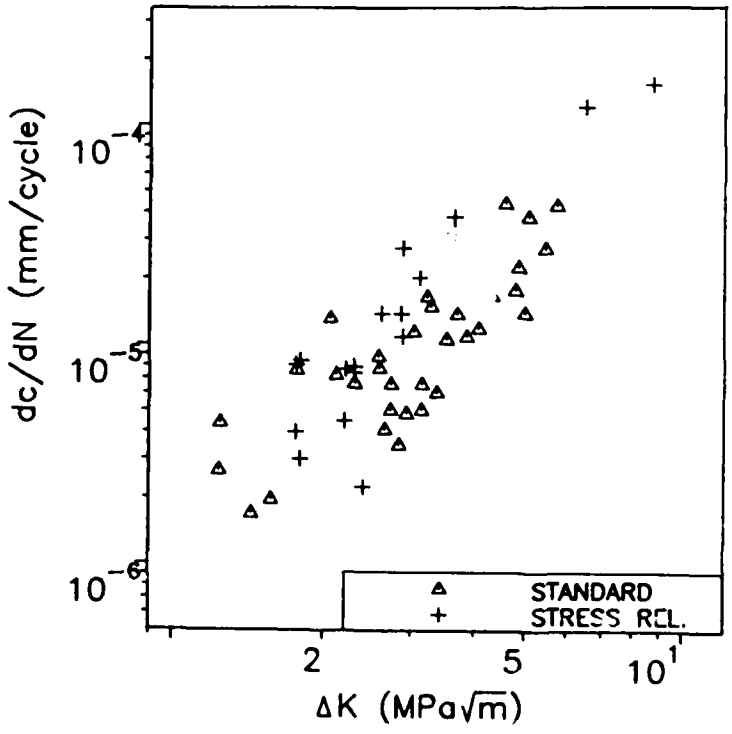

Figure 3.10 Comparison of crack growth rates for annealed and unannealed 8091 (6% stretched 8091).

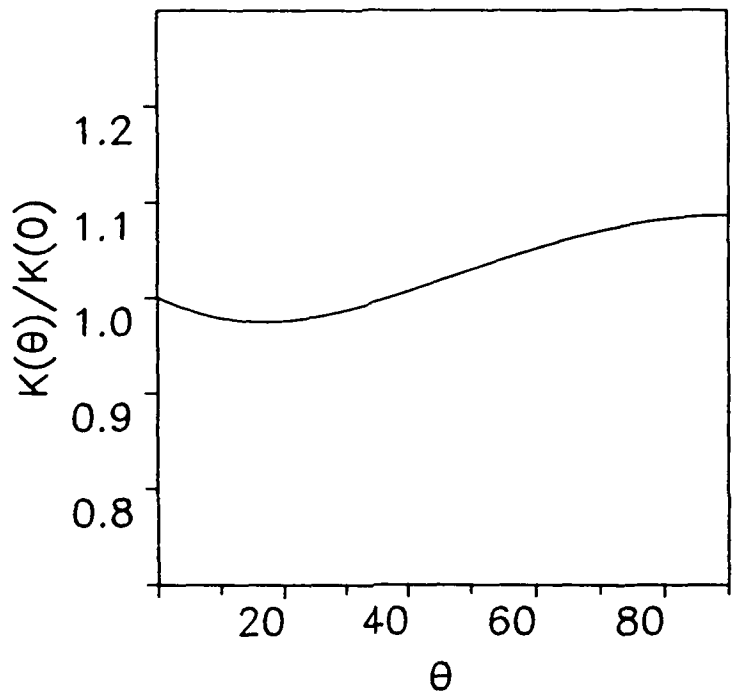

Figure 3.11 Variation of K as a function of position on crack perimeter (θ=0 at crack surface).

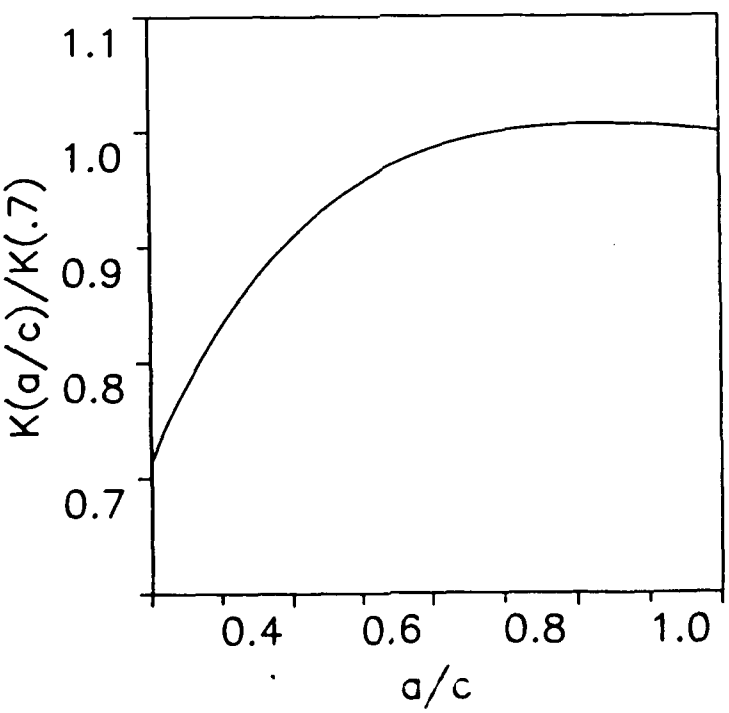

Figure 3.12 Variation of K with crack depth to length ratio (a/c).

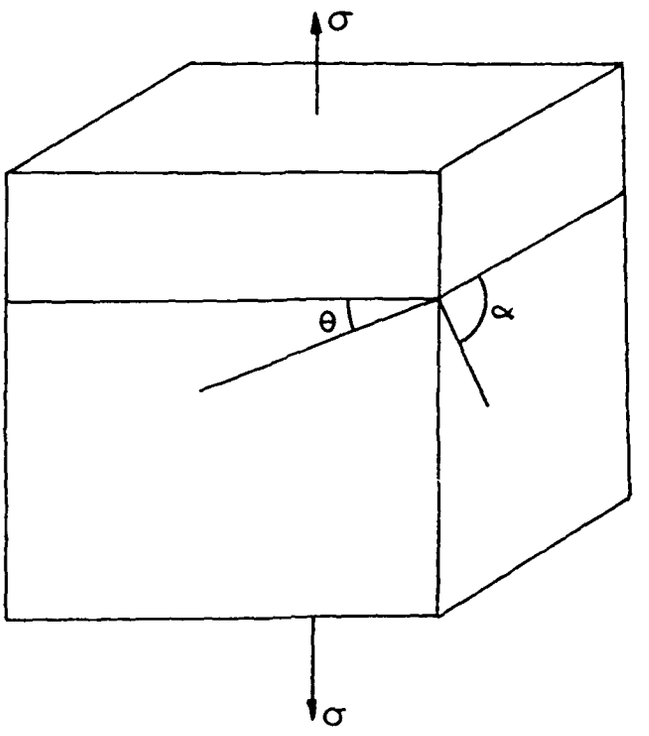

Figure 3.13 Depiction of crack inclined about two axes.

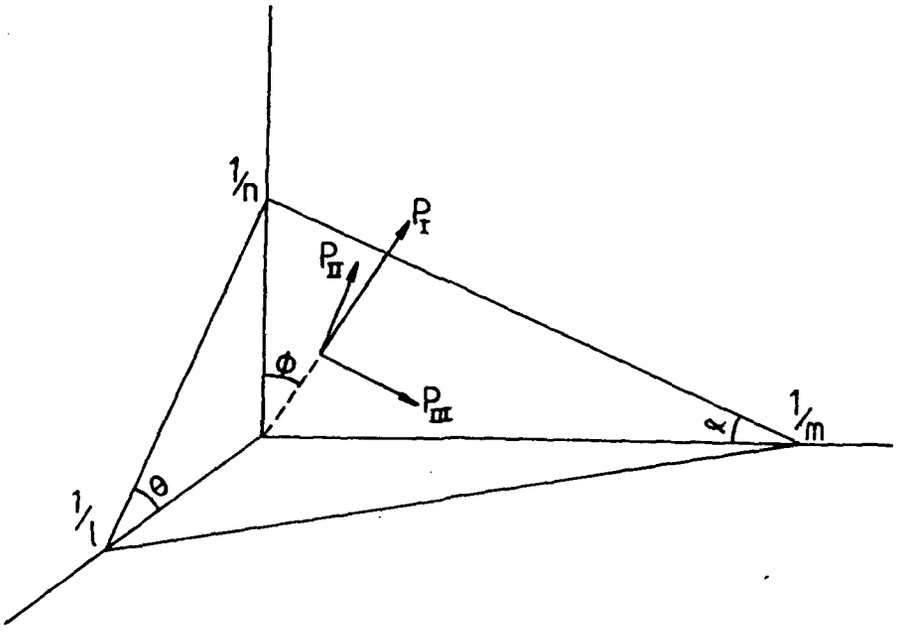

Figure 3.14 Illustration of geometry used to calculate K_I, K_{II} and K_{III}.

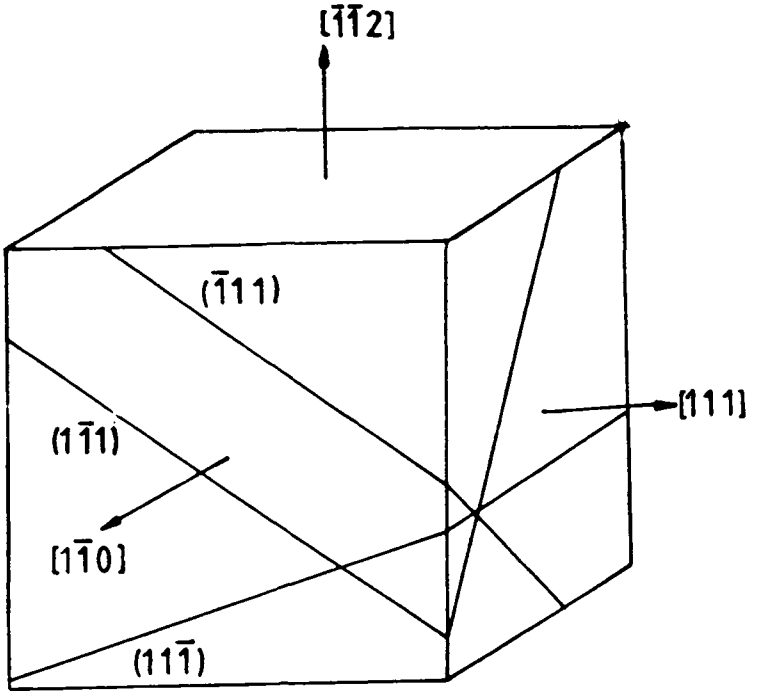

Figure 3.15 {111} planes depicted on block with <112>, {110} texture.

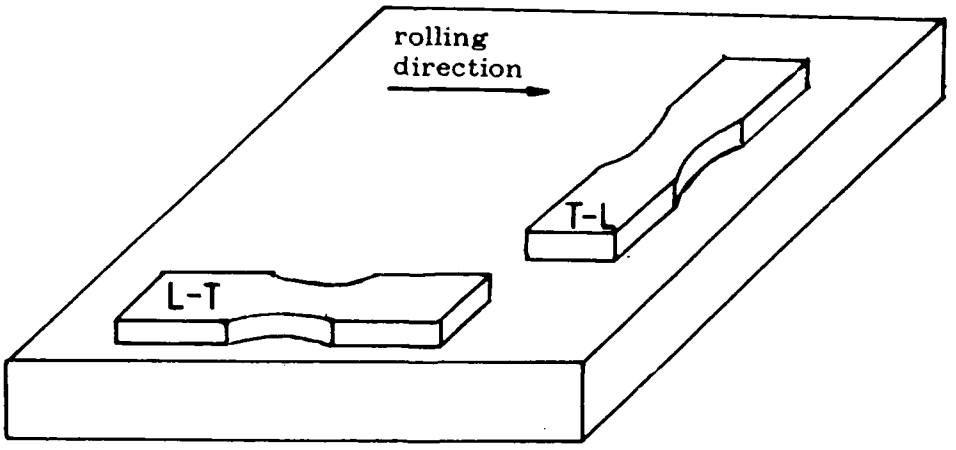

Figure 3.16 Orientation of specimens with relation to rolling direction.

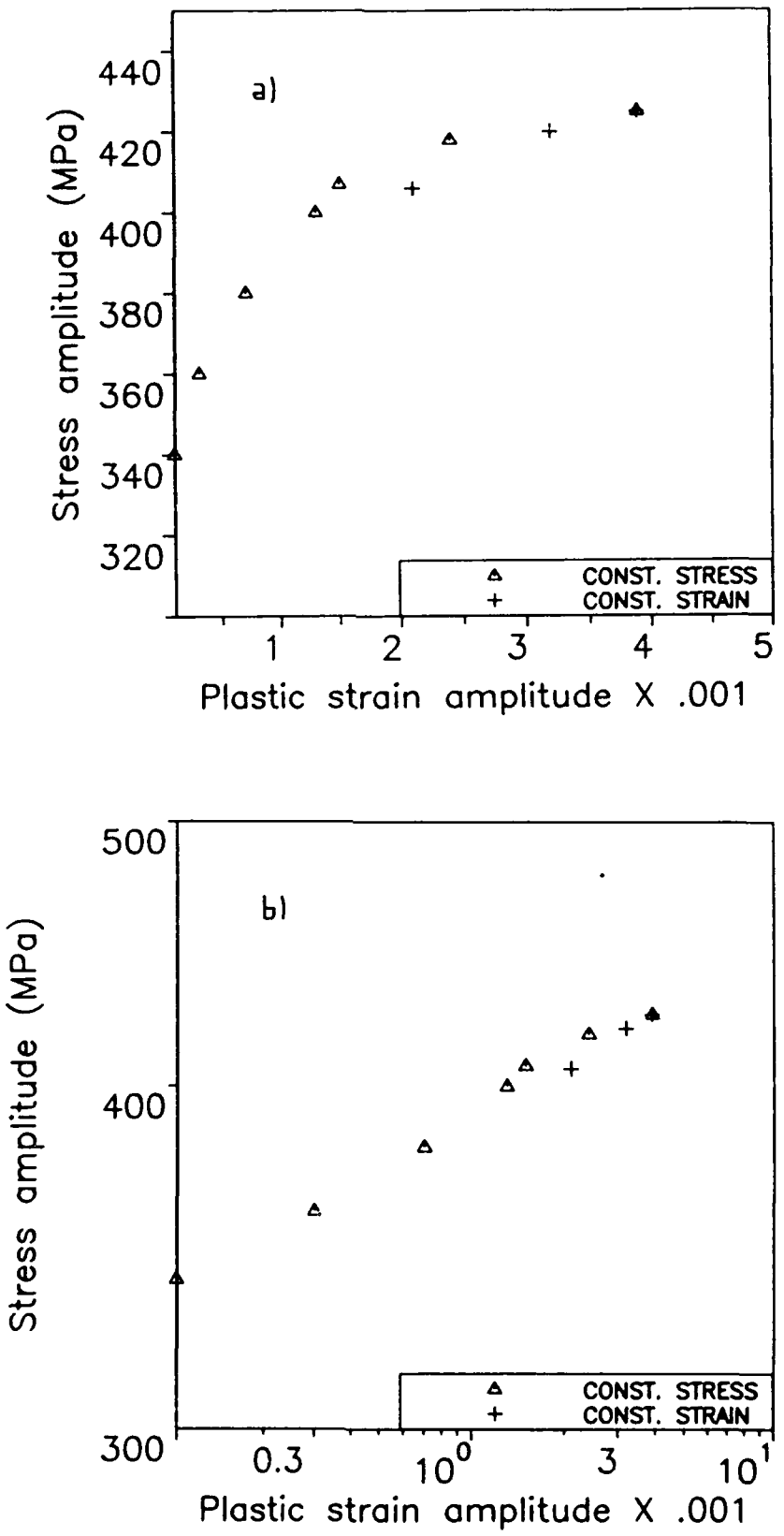

Figure 3.17 Comparison of cyclic stress-strain data obtained under constant strain and under constant stress a) on a linear scale and b) on a logarithmic scale.

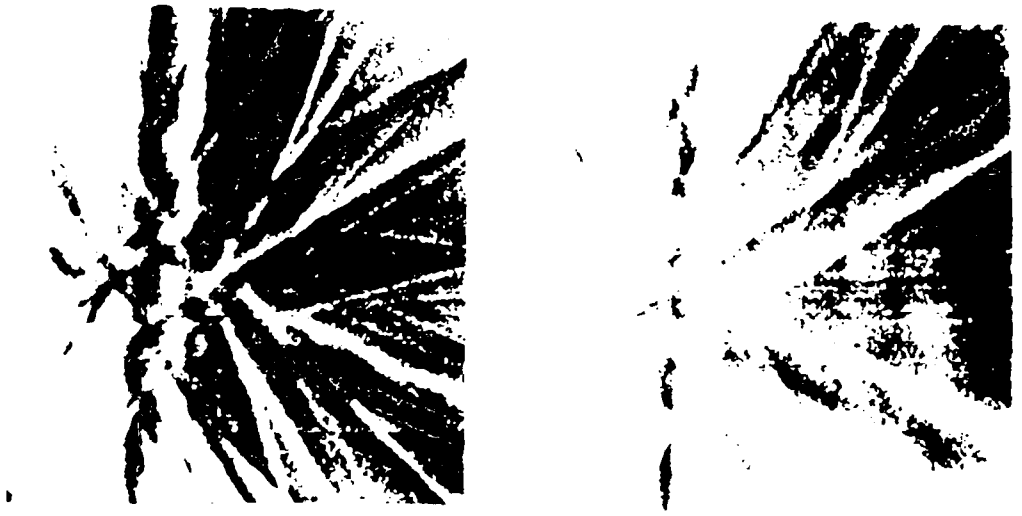

Figure 3.18 Illustration of disappearance of fourth order {111} line with plastic deformation for a) material just outside plastic zone and b) material just inside plastic zone.

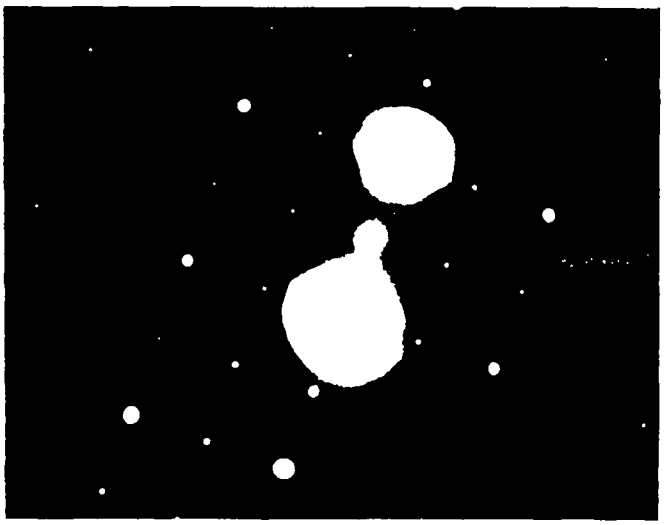

Figure 3.19 Diffraction spot pattern showing S' precipitate streaks, Z=<100>.

CHAPTER 4

THE EFFECT OF MICROSTRUCTURE ON SMALL CRACK GROWTH

4.1 INTRODUCTION

The principal aim of this work was to relate the microstructure, with particular emphasis on the resulting slip distribution, to the growth of small fatigue cracks in the two Al-Li-Cu-Mg-Zr alloys 8090 and 8091. Supporting that goal, this chapter begins with a discussion of the precipitate size and distribution in the various peakaged alloys. Mechanical and physical data are presented to show that the slip distribution was significantly altered through thermo-mechanical treatment. This is followed by a description of the effects of slip distribution, texture, and grain size on the growth rate of small fatigue cracks in 8090 and 8091. The discussion will then turn to non-peakaged materials and the effects of ageing time on small crack growth, cyclic stress-strain response and monotonic stress-strain response. Finally, because small cracks fail to satisfy assumptions implicitly made when using ΔK, the effectiveness of ΔK as a correlating parameter when examining microstructural effects is discussed.

4.2 THE DISTRIBUTION OF S' AND SLIP

Thin foils of 8090 and 8091 in the stretched, unstretched, and duplex aged conditions were examined in the TEM. Representative photographs showing the distribution of S' are given in Figure 4.1. The δ' precipitates were small, spherical and uniform in distribution for all the alloys (see Figure 4.2). No δ precipitation was observed. Due to the increased concentration of copper in 8091, very small amounts of T_1 were occasionally observed as thin trapezoidal plates.

Since the amount of T_1 precipitation was very small and their overall mechanical effect would be similar to that from the S' phase, T_1 would be unlikely to have a distinct effect on properties. When present, δ', δ and T_1 were unaffected by thermo-mechanical treatment. So, any change in slip behaviour as a function of thermo-mechanical treatment must be related to the distribution/size of the S' precipitates.

The distribution of S' was significantly affected by thermo-mechanical treatment. In the unstretched materials precipitation of S' was very heavy on the grain and sub-grain boundaries but light elsewhere. This is the expected distribution as S' nucleation sites in the grain interior (such as dislocations and vacancy clusters) were uncommon. In contrast, the distribution of the S' in the stretched materials was much more homogeneous because of the homogeneous distribution of dislocations which act as nucleation sites. In the duplex aged materials, where the vacancies had been liberated from the lithium and allowed to coalesce, the S' was distributed throughout the grain in clumps. On the basis of the S' distribution, the distribution of slip would be expected to be relatively homogeneous in the stretched and duplex aged alloys as compared with the unstretched alloys.

As tabulated below, however, the size of the S' precipitates was also affected by the thermo-mechanical treatment. Notably, the S' precipitates resulting from the duplex age treatment were significantly smaller than in the unstretched and stretched alloys.

Alloy and heat treatment	S' rod diameter (nm)
8090 stretched 6%	6
" unstretched	4
" duplex aged @ 170°C	2
8091 stretched 6%	6
" unstretched	5
" duplex aged @ 170°C	3

The diameter of the S' precipitates determines whether they are sheared or looped by dislocations. Precipitates that are looped would be effective slip homogenisers with successive dislocations being hindered by the passage of the first dislocation. Shearable precipitates would be less able to homogenise slip regardless of the distribution. In the following section the diameter of S' particles required for Orowan looping is estimated.

4.2.1 CALCULATION OF S' PRECIPITATE DIAMETER REQUIRED FOR OROWAN LOOPING

Based on Xia and Martin's (1989) work, the precipitates were assumed to be circular in cross-section. In order to calculate the precipitate diameter where shearing gives way to Orowan looping, the geometry shown in Figure 4.3 was used. From equilibrium of forces, $F=2T\cos\theta$ where F is the force on the precipitate and T is the dislocation line tension. At the transition from Orowan looping to particle cutting $\theta=0$. According to Huang and Ardell (1988), the dislocations that control plastic flow in aged Al-Li alloys are initially screw in character. However, when the dislocations are bowed around particles they become edge dislocations in character. So, taking T as approximately given by $T=Gb^2/2$, the force required for Orowan looping becomes $F=Gb^2$. G is the shear modulus of the matrix and b is the Burger's vector.

The particle will be cut when the shear stress equals the shear strength of the particle (τ_c). The area on which the shear stress acts is $A=1.732\pi d^2/4$ where the factor of 1.732 reflects the increase in cross-sectional area due to the angle at which the S' precipitates are cut by the {111} planes. The shear stress applied to the particle is $\tau=F/A$ which, when rearranged to solve for the

force required to cut the particle, becomes $F=1.36\tau_c d^2$. At the transition from looping to cutting the force required for looping must equal the force required for cutting. Rearrangement of that equality to solve for the critical precipitate diameter results in

$$d_c = \left(\frac{1.36Gb^2}{\tau_c} \right)^{1/2}$$

G is the shear modulus of the matrix solid solution which, as discussed by Noble et al (1982) would be very similar to the shear modulus of the overall alloy. The Young's modulus of the overall alloy was 78.9 GPa so G (approximately 0.4E) is approximately 32 GPa. The Burger's vector is given by the average distance between atoms in the solid solution α, i.e. 0.286nm (Fox and Fisher, 1988). Unfortunately, the shear strength τ_c of the S' precipitates is not known. Its magnitude can, however, be bounded.

When magnesium is added to a 2.5% stretched Al-Li-Cu-Zr alloy of similar composition to the alloys studied in this work, the yield strength rises (Harris et al, 1987). As discussed in section 2.4.2, the addition of magnesium strengthens the alloys through several mechanisms including the dispersion hardening effect of the S' phase. It is reasonable, therefore, to take the yield strength of an alloy containing 0% magnesium as the lower bound of the strength of the S' phase. From Harris et al (1984) the tensile yield strength of such an alloy is 380 MPa. This value must be divided by two since τ_c is the yield strength of the S' phase in shear. This results in a lower bound estimate for τ_c of 190 MPa.

The theoretical yield strength can be used as an upper bound. This is commonly considered to be $\tau_{theor}=G/10$. The modulus of intermetallic compounds can be approximately estimated by the rule of mixtures (Gulliet and LeRoux, 1967). This results in an estimate

of 26.8 GPa for the shear modulus of S'. Therefore the upper bound to the shear strength of S' is 2.68 Gpa. With these bounds to the shear strength of S', the diameter at which dislocations shear S' precipitates rather than loop them must be between 0.8 and 3.1 nm.

This calculation of the transition diameter is, of course, only an estimate. The strength of S' was estimated and it is assumed that precipitates only interact with single dislocations. In reality, the build up of dislocations in the vicinity of a precipitate will cause a local stress concentration that may cause shearing of particles with larger diameters than calculated above (Khireddine et al, 1989). Nevertheless, quite conservative bounds were used for the strength of S'. Also, the tendency of single dislocations to loop precipitates larger than 3.1 nm must influence slip distribution even if the precipitates are ultimately sheared when the stress concentration is sufficiently high. Therefore, the estimate in the preceeding paragraph for the critical diameter is felt to be relevant to predicting whether, based on their diameters, the S' precipitates are likely to homogenise slip.

Referring to the precipitate diameters given previously, it is apparent that looping is likely for the stretched and unstretched materials and that the S' precipitates resulting from the duplex heat treatments are likely to be sheared. Thus, despite the homogeneous distribution of S' in the duplex aged alloys, the individual precipitates will be easily sheared and the S' will be less effective at homogenising slip.

4.2.2 MECHANICAL BEHAVIOUR AS A FUNCTION OF S' DISTRIBUTION

In this section the microstructural observations made in the preceeding section will be related to the mechanical behaviour of

these alloys. Monotonic and cyclic stress-strain tests were performed using an extensometer to measure the behaviour at the small plastic strains typical of the tests later used to characterize small crack growth.

The monotonic tensile data are plotted in Figure 4.4. As expected, the stretched materials strained the least for a given stress. The duplex aged materials strained the most for a given stress in spite of the more uniform distribution of S' previously described. The unstretched materials were intermediate in response between the stretched and the duplex aged materials. On the whole, the 8091 materials were less affected by thermo-mechanical treatment than the 8090 materials - probably due to the enhancement of S' precipitation by the higher copper content. The strain hardening exponent was 0.05 for all of these heat treatments and both alloys.

Cyclic stress-strain curves for the stretched, unstretched and duplex aged 8090 and 8091 alloys (all generated at R = -1) are shown in Figure 4.5. The trends for the cyclic stress-strain data are exactly similar to those observed in the tensile tests with the slightly higher average work hardening exponent of 0.09.

The trends from these monotonic and cyclic stress-strain results are also found in Peacock and Martin's (1989) work on long crack fatigue performed with identical materials and heat treatments. They found that long fatigue crack threshold ΔK's were lowest in the stretched materials, intermediate in the unstretched materials and highest in the duplex aged materials. These differences in threshold behaviour were attributed to increased planarity of slip in the unstretched and duplex aged alloys. Planar slip, as was discussed in Chapter Two leads to more reversible slip and higher levels of crack closure - both of which reduce the rate of crack

growth.

The planarity of slip observed in the duplex aged alloys indicates that the S' phase in the duplex aged alloys is ineffective at homogenising slip. As was stated earlier, the S' precipitates in the duplex aged materials were small in diameter and might be expected to be sheared rather than looped by dislocations. It is reasonable that precipitates that are sheared rather than looped would be ineffective at homogenising slip.

This is not to say that all duplex ageing heat treatments result in an inhomogeneous distribution of slip. The effectiveness of the duplex ageing treatment will be determined by the diameter of the S' precipitates which is a function of the temperatures used for each portion of the duplex ageing treatment. Increasing the artificial ageing temperature by 20°C to 190°C, for example, also increases the diameter of the S' precipitates at peak hardness as shown below.

Alloy and heat treatment	S' rod diameter (nm)
8090 duplex aged @ 170°C	2
" duplex aged @ 190°C	4
8091 duplex aged @ 170°C	3
" duplex aged @ 190°C	4

The model described in the previous section predicts that the S' precipitates resulting from a 190°C artificial age would be more likely to be looped by dislocations and, therefore, better slip homogenisers. Certainly, as can be seen in Figures 4.6 and 4.7, increasing the artificial ageing temperature increases the resistance of the alloys to both monotonic and cyclic deformation. Most previous studies of duplex aged 8090 or 8091 appear to have used 190°C as the artificial ageing temperature.

Another point to consider is that, although the tensile, cyclic, and long crack behaviour all indicate that slip character was varied

by the thermo-mechanical treatment used, it was not certain that the slip character would be different in the vicinity of a small crack. After all, the large scale yielding associated with small fatigue cracks would encourage cross-slip and so tend to homogenise slip and decrease slip reversibility. Attempts were made to use a TEM to observe directly the distribution of slip in the plastic zone around a small crack. Although, slip bands were occasionally observed (see Figure 4.8), the volume of material interrogated in the thin portion of the foil was too small for significant conclusions to be drawn.

An alternative measure of the planarity of slip associated with a crack is to measure, the lineal roughness parameter (R_L). As described in section 3.5.1, this parameter is the ratio of the actual length of the crack to the length of the crack projected normal to the load. Increasing slip planarity will result in higher values of R_L. R_L values for the small cracks studied in this work are given in full in Table 4.1 and summarized below.

Material	Average R_L
8090 stretched	1.19
" unstretched	1.40
" duplex aged	1.38
8091 stretched	1.19
" unstretched	1.28
" duplex aged	1.36

The R_L values for the stretched materials are significantly lower than for the unstretched or for the duplex aged materials. In addition, much less scatter was observed in the values of R_L for the stretched alloys. This confirms that the slip character associated with small cracks is, as in long cracks, more planar for the unstretched and duplex aged materials than for the stretched materials.

In summary, then, both stretching and duplex ageing resulted

in a more homogeneous distribution of S' precipitates than the unstretched material. However, the precipitates produced by the duplex ageing treatment were thin and so more easily sheared by dislocations. These factors led to planar slip in the unstretched and duplex aged alloys and relatively homogeneous slip in the stretched alloys. These conclusions are confirmed by cyclic and monotonic stress-strain behaviour, long crack behaviour, and, most importantly, the lineal roughness parameters of the small cracks studied in this work.

4.3 SMALL CRACK GROWTH BEHAVIOUR

The small cracks studied in this work were likely to be mechanically small. To prevent the effects of plasticity obscuring microstructural effects, the stresses used to propagate small crack were chosen to be particular fractions of the yield stress (0.85 and 0.7). As will be further discussed in Chapter Five, if σ/σ_{ys} is constant then the ratio of plastic zone size to crack length should also be constant. Therefore, the effect of plasticity can be reasonably expected to be the same in each case.

In the crack propagation data that follow, crack propagation rate is plotted versus a ΔK_I that is calculated form the projection of the crack onto the plane perpendicular to the applied load. For consistency, dc/dN is also projected perpendicular to the applied load. In section 4.4, this approach will be compared to the calculation of ΔK_{eq} which included the effects of crack deflection and tilt.

4.3.1 MODE OF CRACK PROPAGATION

The number of cycles required for crack initiation depended

on the stress applied. At the highest stress levels less than 10,000 cycles were required and at the lowest up to 600,000. Multiple cracks in the same specimen were sometimes observed - particularly at the higher stresses. In such cases, data were still recorded as long as the cracks were at least 4 crack lengths apart. Crack initiation was not associated with grain boundaries, defects on the specimen surface or inclusion particles. From the crystallographic growth of newly initiated cracks, it appeared that they were initiated and contained in slip bands.

SACP's (Selected area channelling patterns) were used to determine the orientation of grains that the crack passed through and, thus, the plane of crack propagation. Identification of the grain orientation was not always possible. Sometimes, the proximity of the crack to a grain boundary impeded identification of the grain orientation, although the straightness of the crack path suggested that the crack was crystallographic and contained within a single grain. At other times, the deformation close to the crack made the SACP too blurred to interpret. In addition, the small sub-grains in 8090 and 8091 often caused multiple SACP patterns to appear on the screen. These patterns were identical to each other but were rotated through a small angle. These multiple images degraded the pattern slightly. These factors were especially significant when measuring plastic zone size.

It was possible to determine the orientation of the grain containing the crack for sixteen cases. As discussed in section 3.5.2, there are an indefinite number of planes with the same direction of intersection with a surface. Therefore, the assumption was made that the crack propagation plane was either {100}, {110} or {111}. In eight cases, the crack path was compatible only with the

{111} plane. In the other eight cases, the crack growth path was compatible with at least one other plane in addition to the {111} plane. In no case, was the crack path incompatible with growth on a {111} plane. It is, therefore, concluded that small cracks in 8090 and 8091 propagate on {111} planes. This conclusion is confirmed by numerous observations of crack growth parallel to slip bands (which must be on {111} planes). It is also consistent with observations of SACP's generated from mildly electropolished fracture surfaces (Newman and Beevers, 1986).

Crack growth rates were irregular which led to considerable scatter in the crack growth data. The reductions in crack growth rate were associated with grain boundaries or changes in crack growth direction. As the cracks grew, some intergranular growth was observed and, for cracks longer than about 350 microns, the path generally tended to become more perpendicular to the applied load. That is to say, there was an apparent transition from Stage I to Stage II crack growth. Even when the overall crack path was perpendicular to the applied load, however, the crack path was still made up of short crystallographic jogs. The tortuosity of the crack, as measured by R_L was not a function of crack length. Slip bands were often observed for all crack lengths.

SEM photographs taken near the crack initiation site and further into the depth of the specimen are shown in Figures 4.9 and 4.10. All fracture surfaces were crystallographic as might be expected for a Stage I crack. The ridged pattern of lamellae that change direction at grain boundaries is typical of Stage I crack growth with slip alternating between two {111} planes (Plumbridge and Ryder, 1969). No fractographic differences between 8090 and 8091 were observed.

4.3.2 THE EFFECT OF SLIP DISTRIBUTION

Initially, small cracks were propagated with σ/σ_{ys} equal to 0.85. This figure was chosen because it seemed fairly typical of other researchers' work and because cracks initiated relatively quickly (within 20,000 cycles). Small crack growth data for 8090 and 8091 at σ/σ_{ys}= 0.85 are shown in Figure 4.11. No effect of slip distribution on the growth of small cracks is apparent for either 8090 or 8091.

The lack of an effect of slip distribution on small crack growth rates was initially thought to be due to the high stresses employed to grow the cracks. Bischler and Martin's (1987) S-N curves had shown that the effect of slip distribution in 8090 was more pronounced at lower stresses. Furthermore, the effect of the shearability of precipitates is thought to be lessened at high stresses due to the presence of enough mechanical energy to activate multiple slip systems which implicitly homogenise slip (Laird, 1978).

Therefore, a second series of experiments was performed at σ/σ_{ys} equal to 0.7. This ratio was chosen because it was the lowest experimentally practical ratio. The experimental problem that emerges for lower σ/σ_{ys} ratios is that a great number of cycles are required for crack initiation. This makes it impractical to find the crack before it has grown more than 100 or so microns. Even at σ/σ_{ys} equal to 0.7, up to 600,000 cycles were sometimes required for crack initiation. Despite the lower stresses, the rate of small crack growth was still independent of slip distribution (see Figure 4.12). This result is perhaps not surprising when it is noted that the lineal roughness parameter, a measure of slip distribution, was

unaffected by the reduction in stress. Therefore, small fatigue crack growth is concluded to be independent of slip distribution.

This behaviour of small cracks contrasts with the observed effect of slip distribution on long fatigue crack growth (Peacock and Martin, 1989). In the long fatigue cracks that they studied, the effect of slip distribution was partially attributed to changes in closure levels associated with changes in crack path tortuosity. Changes in crack path tortuosity were observed for small cracks in this work as indicated by the varying values of the lineal roughness parameter. In small cracks, however, changes in roughness induced closure would be unlikely to have a significant effect on the crack driving force as, in any case, the closure levels are relatively low for small fatigue cracks.

Peacock and Martin (1989) also found that the increased slip reversibility, associated with increased slip planarity, contributed to the effect of slip distribution on long cracks. To assess the effect of slip reversibility on small crack growth, the proximity of small cracks to the surface must be considered. In small cracks a free surface is accessible to a large fraction of the plastic zone. Edge dislocations emerging on a free surface would create steps upon which oxygen could be adsorbed (Mughrabi et al, 1983). Such dislocations could not re-enter the grain during the reverse cycle of stress and the associated slip would be irreversible. Therefore, slip associated with small cracks would be expected to be less reversible than the slip associated with long cracks where the bulk of the plastic zone is remote from a free surface. Microstructural changes that influence the slip reversibility for long cracks would be expected to have less effect for small cracks. This conclusion is further supported by work in which small fatigue cracks were

observed to grow faster in an air environment than an argon environment (Wagner and Lutjering, 1987). As closure is relatively insignificant in the growth of small cracks, it is likely that this difference is due to increased slip reversibility in vacuum where no oxygen adsorption on to steps can occur.

The lack of an effect of slip distribution on small crack growth also seems to contradict the observed effect of slip distribution on S-N curves generated on 8090 (Bischler and Martin, 1987). Some similarity might be expected as cracks in S-N specimens are small cracks for the majority of the time that they are present. However, the life of an S-N specimen is composed of the time required to initiate a crack as well as the time required to grow a crack to failure. As the effect of slip distribution in S-N specimens was more apparent at low stresses (where initiation time dominates), it seems reasonable to ascribe the effects to crack initiation rather than crack growth.

The lack of a relation between slip distribution and small crack growth has some support from the literature. Gungor and Edwards (1989) examined the effect of varying slip distribution on the behavior of small cracks in an Al-Mg-Si alloy. Slip distribution was varied by dispersoid phases and, as in the present work, no effect on small fatigue crack growth was found. In comparing their small crack data to S-N data, they also concluded that slip distribution affects the time to initiate a crack rather than small crack growth rates.

4.3.3 SMALL CRACK GROWTH RATES IN 8090 VERSUS 8091

A comparison of the dc/dN versus ΔK curves for 8090 and 8091 (see Figure 4.13) revealed that the small cracks in 8091 grew

about a factor of two slower than in 8090. The similarity of the fracture surfaces, crack propagation on {111} planes for both alloys, and similar lineal roughness parameters indicated that the mechanism of crack growth was the same for both alloys. The higher copper content in 8091 increased the precipitation of S'. However, the effect of this on the mechanical behaviour was less than stretching and so the difference in copper content is unlikely to have a significant effect on small crack growth rates. A major difference between the two alloys was that the 8091 had not been cross-rolled during the manufacture of the plate. As a result, 8091 consisted of more elongated, smaller grains and the texture for 8091 was {110}/<112> as opposed to 8090 where the texture was a mixture of {110}/<112> and {110}/<111>. Therefore, efforts to explain the slower growth rates in 8090 focussed on the differences in texture and grain shape.

There are three ways in which the crystallography of texture could influence small crack growth. The first applies to cracks contained within one or two grains. Chan (1987) has suggested the use of a modification to ΔK that uses the Taylor factor to incorporate the effect of locally lower yield stresses in favourably oriented grains. However, the small cracks studied in this work intersected about 160 grains (in the case of 8091) by the time the half crack length, a, was 100 microns. Therefore, it is unlikely in this case that this microstructural modification to ΔK is justified.

A second way that texture could affect the rate of small crack growth is by altering the barrier to crack growth posed by grain boundaries. In highly textured materials less deflection of the crack would be required to follow a new slip system and, so, higher growth rates would be expected. This does not explain the faster

crack growth in 8090 since it was not more highly textured.

Finally, the overall texture could imply a more favourable average orientation of the grains to crack growth. To examine this last possibility some 8091 specimens were prepared and tested in the T-L orientation rather than the L-T. As can be seen from Figure 4.14, no difference in growth rates was found as a function of specimen orientation. This indicates that the crack growth rate is relatively insensitive to overall texture. One might also expect that if the crack propagation planes were less favourably oriented on average in 8090 than in 8091, there would be qualitative differences in the observed angles of crack propagation or a quantitative difference in the measured lineal roughness parameters. No differences in the angles of crack propagation were observed and the lineal roughness parameter for T-L specimens averaged 1.17 which is very similar to the value of 1.19 previously reported in section 4.2.2.

Grain size, however, is an additional factor known to affect small crack growth (Brown and King, 1986). Small crack growth in planar-slip materials has been observed to be slower in materials with small grains where there are more grain boundaries to retard crack growth and slip line lengths are smaller. Such an effect might have been expected as a function of the orientation of the 8091 specimens as the average distance between grain boundaries in the L direction was 281 microns versus 71 microns in the T direction. However, as previously mentioned no such effect was observed.

The grain size differences in the S direction must, however, also be considered. 8090 grains are almost twice as big as 8091 grains in the S direction (26 vs 14μm). As the grain size for both

alloys is so much smaller in the S direction than in the L or T directions, more grain boundaries are crossed for crack growth in the S direction. Consider, for example, one half of a semicircular crack with a=300μm. The difference between 8091 and 8090 in the number of grain boundaries encountered in the L direction is approximately 2 (4 for 8091 and 2 for 8090). On the other hand, the difference in the S direction is approximately 14 (29 for 8091 and 15 for 8090). It is concluded, therefore, that the differences in crack growth rate between 8090 and 8091 is due primarily to the difference in grain size in the S direction.

4.3.4 THE EFFECT OF AGEING TIME

Peak and overaged alloys show poorer resistance to long crack propagation than underaged alloys. Hornbogen and Zum Gahr (1976) related this observation in a γ'-Fe-Ni-Al alloy to the distribution of slip. They observed that in underaged materials slip was localised into intense slip bands with little opportunity for cross-slip. As has been previously discussed, this should increase the reversibility of slip and closure levels thereby decreasing the fatigue crack propagation rate. Jata and Starke (1986) also used this concept to explain improved long crack fatigue resistance in an Al-Li-Cu alloy. On the other hand, Suresh et al (1984) have suggested that cracks are deflected more in the underaged alloys. Increased crack deflection, they argued, decreases the crack driving force and thus the crack propagation rate. This could also be a result of slip planarity.

The effects of ageing time on both long and small cracks in the aluminium alloy 7010 have been examined by Bolingbroke and King (1986). Consistent with the previous work cited, they observed

improved crack propagation resistance in long cracks. Based on the persistence of the improved crack propagation resistance for high stress ratios (R=0.8), they concluded that the improved crack propagation resistance was due to the material's inherent resistance to fatigue rather than a mechanical effect like roughness induced closure. They observed superior crack propagation resistance in underaged alloys for small cracks as well, which they attributed to slip reversibility. The effect of increased crack deflection was discounted as the crack path was similar for all the alloys studied.

The effects of underageing on small crack growth and the explanations for them are, however, inconsistent. As just mentioned Bolingbroke and King observed an effect. Similarly, James (1987) found that small crack propagation resistance was enhanced in underaged 8090. He attributed this to sub-surface crack branching associated with the short distance between grain boundaries in the S direction. Venkatswera Rao et al (1986), however, did not find any effect of ageing on small crack propagation behaviour in Al-Li alloys. Wagner and Lutjering (1987), working with an Al-Zn-Mg-Cu alloy with an equiaxed microstructure, found that grain size determined whether underageing had an effect on small crack growth rates.

This brief discussion demonstrates that the long crack propagation resistance observed in underaged alloys appears to be associated with the planarity of slip, although there is not complete agreement as to whether the exact mechanism is slip reversibility or deflections in the crack propagation path. This explanation has also been used to explain slower small crack propagation rates in underaged alloys, although small cracks do not always appear to be affected. As the effects of slip planarity on small crack growth have already been examined in the stretched, unstretched and

duplex aged versions of 8090 and 8091, it was relevant to investigate the effects of ageing. Further aspects of the effect of ageing will also be discussed in Chapter Five.

The effect of ageing time was only determined for 8091. 6% stretched material was examined in both the overaged and underaged conditions while unstretched material was examined in the underaged condition only. The tensile and cyclic stress-strain properties of peakaged, overaged, and underaged materials are given in Chapter Five where they will be discussed further. Small crack fatigue tests were conducted at σ/σ_{ys}=0.85.

Figures 4.15 and 4.16 compare small crack growth rates as a function of ageing. The effect of ageing appears to be negligible for all conditions. Accepting, for the moment, that the effect of underageing is to increase the planarity of slip, this observation is consistent with the previous data showing that altering the distribution of slip through stretching and duplex ageing also had no effect on small crack growth rates. To further examine the distribution of slip in the underaged and overaged alloys, measurements of the lineal roughness parameters were taken. The data is summarized below.

Material	Average R_L
8091 stretched, peakaged	1.19
" , underaged	1.17
" , overaged	1.17
8091 unstretched, peakaged	1.28
" , underaged	1.46

The lineal roughness parameters in the underaged materials show the same trends that were observed in the peakaged materials. That is, the R_L values for the stretched materials are significantly lower than for the unstretched materials. Overall, the amount of ageing appears to have relatively little effect on the extent of slip

planarity. Therefore, slip planarity does not appear to be a factor for these underaged alloys.

The observed lack of an effect of ageing on small crack growth is consistent with work on the Al-Li alloys 2090, 2091 and 8091 (Venkataswera Rao et al, 1986). It disagrees, however, with James' (1987) work where small crack growth rates in underaged 8090 was shown to be significantly higher than in peakaged 8090. It is apparent from Figure 4.17, where James' data are compared to the data generated for this thesis that the correlation between the crack growth rates observed for the peakaged samples is quite good. James, however, shows much more rapid growth for the underaged samples than were seen in this work. Nor was the considerable sub-surface cracking that James observed in underaged 8090 seen in this work. The reason for these discrepancies is not known.

4.4 THE VALIDITY OF ΔK AS A CORRELATING PARAMETER

The discussions in this chapter of the influence of microstructure on small fatigue crack growth rates have all been based on ΔK as a correlating parameter. From the data generated in this work, it appears that small fatigue crack growth rates are related to ΔK^2 as has been reported for small fatigue cracks in general (Wojcik et al, 1988). Doubts as to the validity of ΔK as a correlating parameter only emerge because, as discussed in Chapter One, ΔK fails to correlate small and long fatigue crack growth rates. In Figure 4.18, where the small fatigue crack growth rates observed in this work are compared to long fatigue crack data generated on the same materials, the failure of ΔK to correlate long and small fatigue crack growth data is confirmed. This failure raises the question of whether the use of ΔK is likely to bias the conclusions made earlier

in the chapter as to the effects of microstructure on small fatigue crack growth by either creating apparent effects or obscuring genuine effects.

To settle this issue, the reasons for the discrepancy between long and small fatigue crack growth rates must be examined for possible influences on ΔK when comparing different materials. As discussed in Chapter One, small cracks have been classed as physically small, microstructurally small and mechanically small - the explanation for their crack growth behaviour depending upon the type of crack. In addition, the geometry of small fatigue cracks is significantly different from that of long fatigue cracks. In this section, the validity of ΔK will be discussed in the context of the influence of microstructure, crack geometry and low closure levels. The impact of mechanical "smallness" on the validity of ΔK as a correlating parameter will be discussed in the next chapter which is devoted to the effects of plasticity on small fatigue crack growth.

4.4.1 THE INFLUENCE OF MICROSTRUCTURE

According to the literature, a microstructurally small crack must be similar in size to the grains of the material so that it is contained within a few grains (Lankford and Davidson, 1987). Because of the relatively small grain size in the S direction, this condition was not generally satisfied for the materials studied in this work. A semi-elliptical crack with a=100 μm in 8091, for example, would intersect about 160 grains. The crystallographic path of the small fatigue cracks in this work is seen in long cracks as well (Yoder et al, 1988) and so is not associated with microstructural "smallness". The primary effect of the grains, grain boundaries and perhaps other obstacles to small crack growth appears to be to

increase the amount of scatter rather than alter the average growth rate.

It is worth noting that such microstructural barriers are likely to also affect long fatigue crack growth rates. Data, however, are collected less frequently for long fatigue cracks than for small fatigue cracks. For long fatigue crack studies, ASTM Standard E647 recommends a crack growth increment of 254 microns between data points. The small cracks in this work, however, were monitored about ten times as often. As Kendall and King (1988) have pointed out, the interval used between data collection points can have a significant effect on the amount of scatter observed in small fatigue crack growth data. Furthermore, small fatigue cracks are monitored using different methods from those used to monitor long fatigue cracks. When studying long fatigue crack behaviour, techniques such as changes in compliance or potential drop are used. These tend to average out crack growth rates along the entire crack front. On the other hand, the growth rate of small fatigue cracks is generally only measured at one point, the surface. Therefore, no averaging of crack growth rate along the crack front occurs.

The small size of the cracks studied combined with microstructural features such as grain boundaries and texture does affect the shape of the crack. The small fatigue cracks in this work were typically inclined or kinked which led to higher lineal roughness parameters (1.2-1.4 for the small fatigue cracks in this work versus the values of 1.1-1.2 for long fatigue cracks in the same materials (Peacock and Martin, 1989)). In addition, as discussed in Chapter Three, the small fatigue cracks in this work were also typically inclined by 60° into the interior of the specimen. So, while the small fatigue cracks studied were not microstructurally small, the

angles of crack inclination and changes in crack direction are related to microstructural features. Thus, the geometry of the small fatigue cracks studied in this work was significantly different from the crack geometry associated with long fatigue cracks.

To assess the influence of crack shape on the validity of the ΔK for examining the effects of microstructure on small fatigue crack growth, two approaches were taken to calculate ΔK. The first, which was used throughout this chapter to characterize microstructural effects, was to calculate ΔK_I for the projection of the crack on to the plane perpendicular to the applied load. For consistency, the increments of crack growth used to calculate dc/dN were similarly projected. The second approach was conceived to account for the effects of crack inclination and tilting on the crack driving force. Using the procedures described in Chapter Three, Mode I, II and III components of K were calculated. These were then combined into a single term using the following expression (Socie et al, 1987).

$$\Delta K_{eq} = (\Delta K_I^2 + \Delta K_{II}^2 + (1+\nu)\Delta K_{III}^2)^{1/2}.$$

The crack growth increment was now taken to be the actual crack growth increment in the direction of crack growth. Considering the differences observed in the lineal roughness parameters, crack deflections might well influence the crack driving force. It was hoped that this approach might reduce the scatter in the data due to changes in crack direction as well as provide a basis for judging the effect of crack shape on the validity of ΔK.

In Figure 4.19 a representative sample of crack growth data, previously calculated as a function of ΔK_I, is compared with K_{eq}. As can be seen, the data scatter is, if anything, worse for the data employing ΔK_{eq}. To examine the suprising persistence of the data scatter, the calculation of K_{eq} was examined more closely. As

discussed in section 3.3.3, the angle of crack inclination into the depth of the specimen (α in Figure 3.13) was taken as 60° based on experimental observations. In Figure 4.20, ΔK_{eq} is plotted as a function of the angle of crack of crack inclination (θ) in the plane of the specimen surface for α=60°. At this large value for α, the angle of the crack deviation in the plane of the specimen can be seen in Figure 4.20 to have little effect. That is, the value of ΔK_{eq} is relatively insensitive to θ. Since a constant value of α was assumed this means that ΔK_{eq} would essentially differ from ΔK_I by a constant. Thus, the described calculation of ΔK_{eq} would have no effect on reducing data scatter. Any reduction in scatter would have to come from the difference between taking the projected length of dc/dN and the actual length of dc/dN. This, however, apparently makes little difference.

If the inclination and kinking of small fatigue cracks were to invalidate the use of ΔK when comparing long and small fatigue crack growth data, then the relationship between crack growth rate and ΔK should depend on whether the method used to calculate ΔK takes into account for crack kinking and inclination. In addition, differences in small crack growth behaviour might have been expected as a function of thermo-mechanical treatments since the different thermo-mechanical treatments resulted in different amounts of crack path tortuosity as measured by the lineal roughness parameters. Figure 4.19 shows that the relationship between crack growth rate and ΔK is very similar whether K_I for the projection of the crack on to the plane normal to the load or K_{eq} which includes the effects of crack kinking and crack inclination is used. In addition, no differences were observed in crack growth rate as a function of thermo-mechanical treatment. Therefore, it appears that

the crack driving force for the small fatigue cracks in this work was not highly dependent upon crack geometry. This may have been due to lack of an effect of crack inclination (θ) on the value of ΔK because of the aforementioned steep angle of crack inclination into the interior of the specimen (α). In any case, it is unlikely that the approach taken to calculate ΔK has biased the data to conceal microstructural effects.

4.4.2 THE INFLUENCE OF LOW CLOSURE LEVELS

Since the significantly different lineal roughness parameters observed for the duplex aged, unstretched and stretched alloys had no effect on small crack growth, it appears that closure levels were low and that the cracks studied in this work were physically small. This is reasonable, as the general criterion for physical "smallness" is that the crack be less than 0.5 mm (Suresh and Ritchie, 1984) which was true for all the small cracks studied. It is, therefore, appropriate to compare small fatigue crack data to long fatigue crack data generated at an R=0.7 where long fatigue crack closure levels are small. As can be seen in Figure 4.18, the correlation between long and small fatigue crack growth rates is greatly improved although the discrepancy is not entirely eliminated.

The effect of the reduction of closure in small cracks is to make microstructurally influenced crack path tortuosity irrelevant to the crack driving force. In essence, the apparent ΔK for small cracks is close to what has been called the effective ΔK in long cracks. In this respect, the apparent ΔK for small cracks is a more accurate representation of the crack driving force than is the apparent ΔK for long cracks. Reduced closure levels for small cracks does decrease the influence of the microstructure on small

crack growth rates. Larsen (1987) has shown examples in titanium alloys where, although the closure levels associated with long fatigue cracks differed, the closure levels associated with small cracks were indistiguishable. There is no reason, however, to believe that the validity of ΔK is affected by the reduction of closure or that real microstructural effects on small crack growth have been masked by the use of ΔK.

4.4.3 CONCLUSION

The measurement of the growth rate of small cracks as a function of ΔK was expected to fulfil the following goals: to confirm the failure of ΔK to correlate the growth rate of small cracks and long cracks; to explore the ability of ΔK to reveal microstructural effects; and finally, to serve as a baseline against which other correlating parameters, which included the effects of plasticity, could be compared. The failure of ΔK to correlate long and small crack growth rates has been demonstrated. This failure appears to be due, in part, to a failure to account properly for the lack of closure. Closure levels were not measured in this work, but other studies have shown that closure levels are typically much lower in small cracks due to the lack of a wake. This work has shown that significant differences in crack path tortuosity did not have an effect on crack propagation rate which supports the claim of low closure levels.

Thus far, ΔK appears to be a suitable parameter to determine the effect of microstructure on small fatigue crack growth. Neither, the lack of closure nor the geometry of small fatigue cracks are likely to affect the use of ΔK. As was mentioned earlier, however, the small cracks studied in this work were mechanically small and so

the influence of large scale yielding is likely to be important. This will be discussed in the next chapter along with other approaches for characterizing the crack driving force, small crack growth mechanisms, the relation between small fatigue crack behaviour and low cycle fatigue behaviour and the mechanisms of small fatigue crack growth.

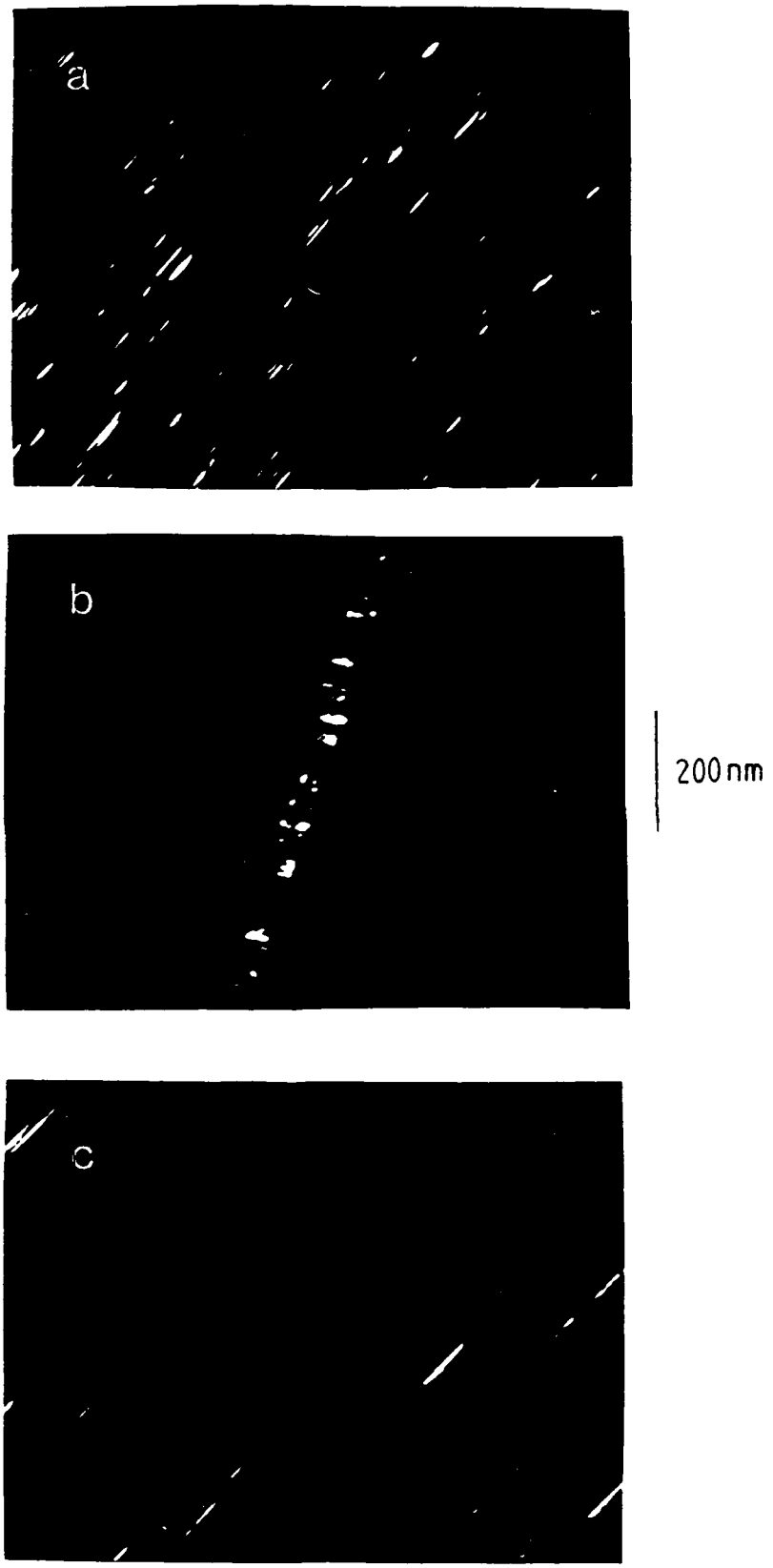

Figure 4.1 Darkfield TEM photographs, Z=100, showing distribution of S' in a) 8090 stretched 6% b) 8090 unstretched c) 8090 duplex aged (continued next page).

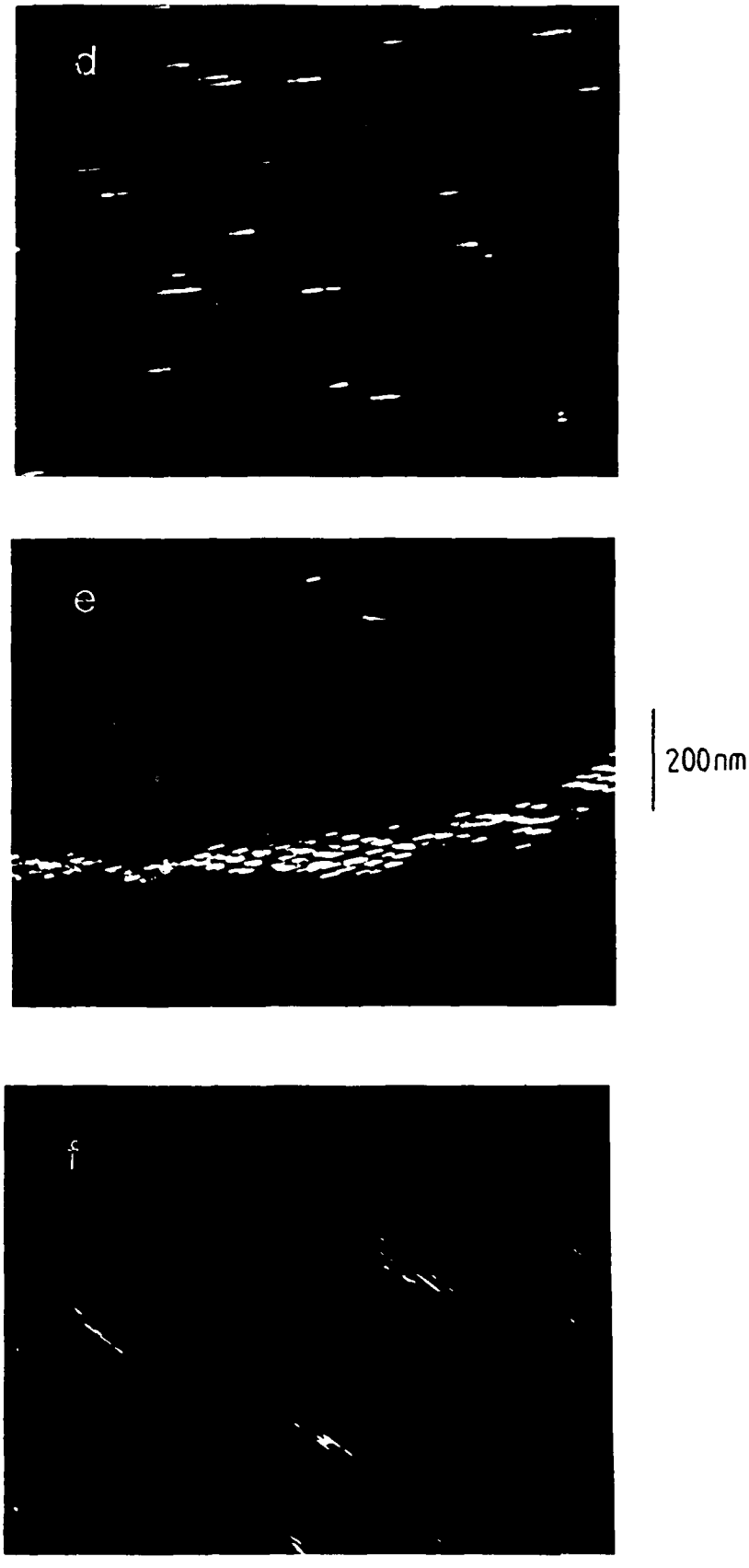

Figure 4.1 cont'd Darkfield TEM photographs, Z=100, showing distribution of S' in d) 8091 stretched 6% e) 8091 unstretched f) 8091 duplex aged.

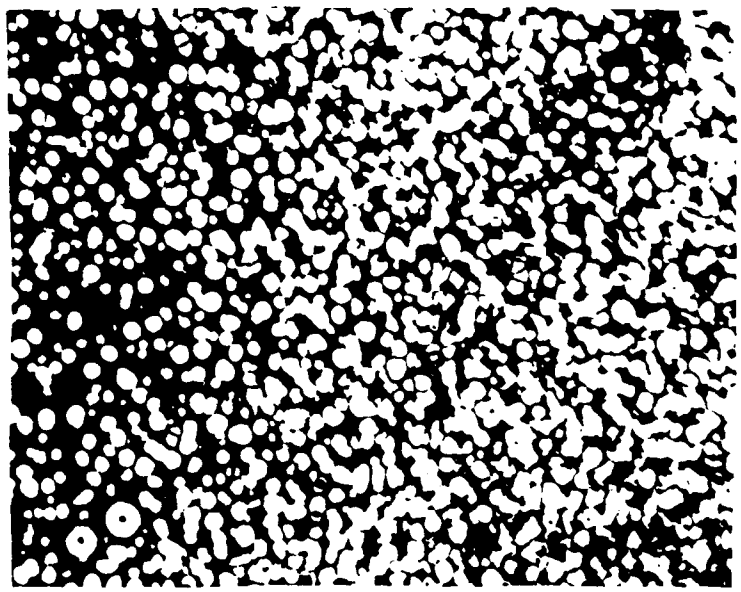

Figure 4.2 Darkfield TEM photograph of δ', aperture over *superlattice spot.*

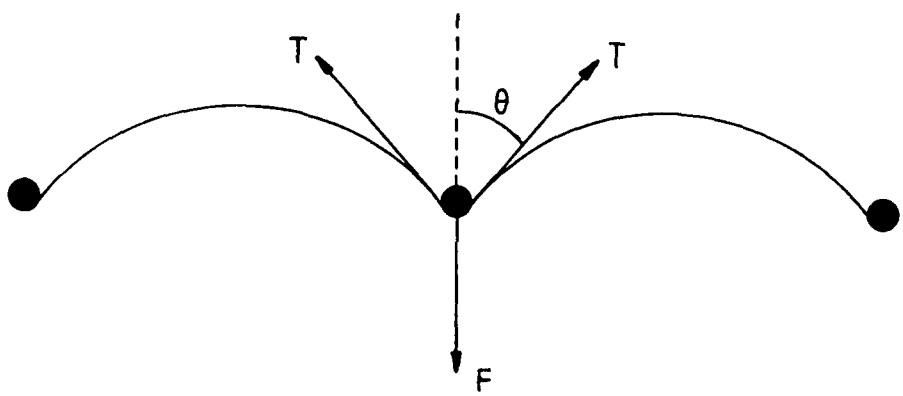

Figure 4.3 Schematic of a dislocation held up at precipitate particles (adapted from Martin, 1980).

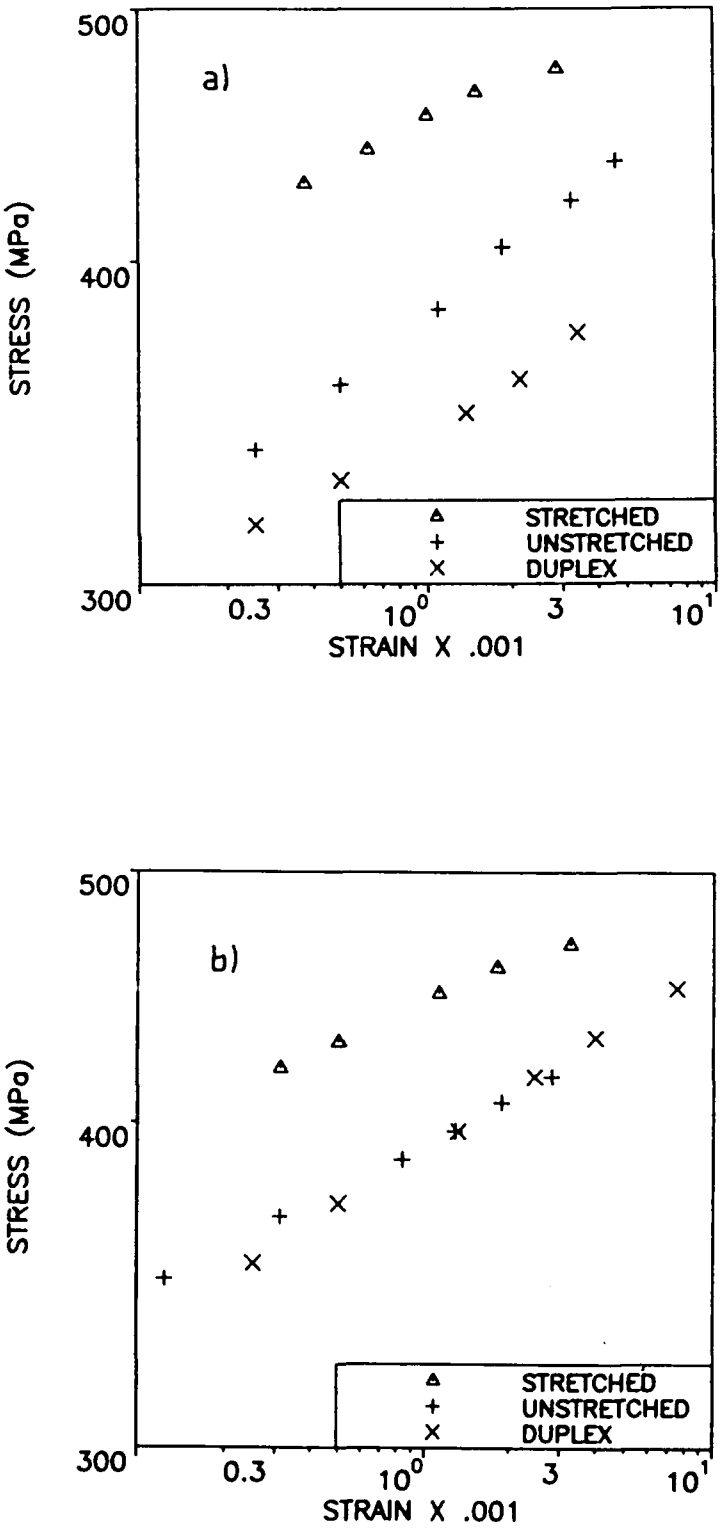

Figure 4.4 Tensile data for a) peak aged 8090 and b) peak aged 8091.

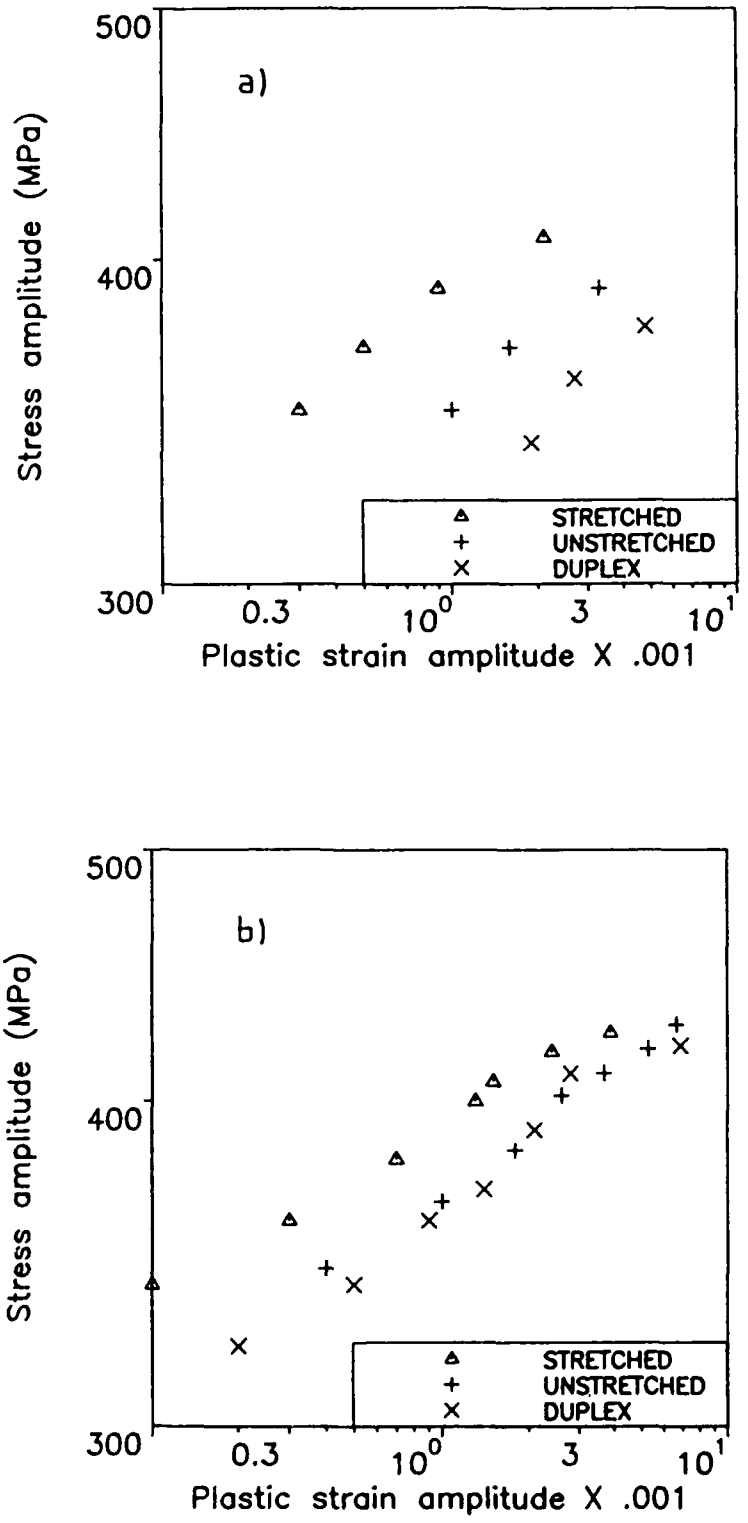

Figure 4.5 Cyclic stress-strain data for a) peakaged 8090 and b) peak aged 8091.

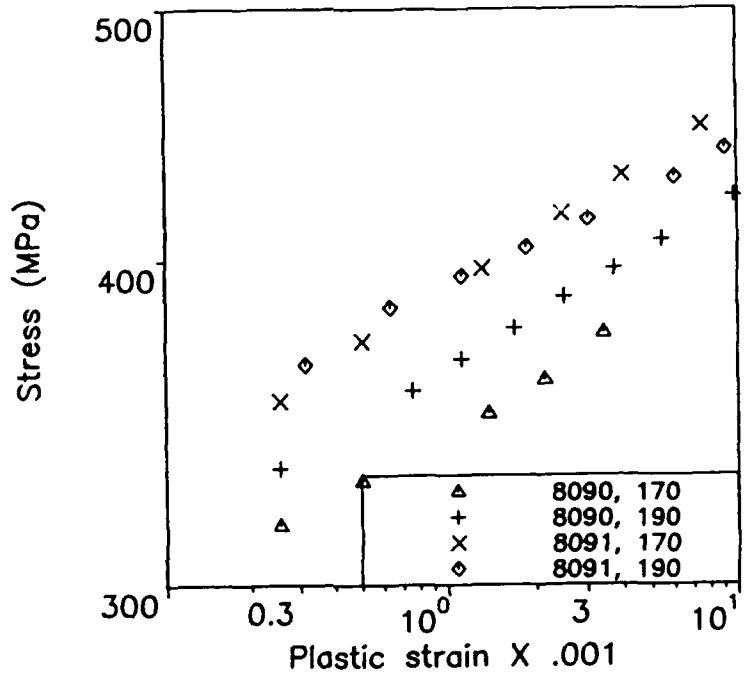

Figure 4.6 Comparison of monotonic tensile behaviour for alloys duplex aged at 190°C versus 170°C.

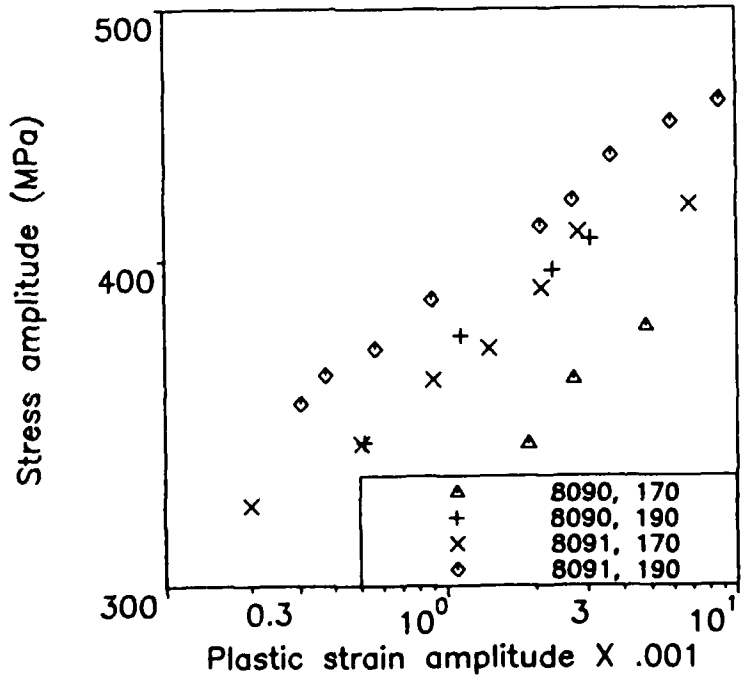

Figure 4.7 Comparison of cyclic stress-strain behaviour for alloys duplex aged at 190°C versus 170°C.

Figure 4.8 Bright field TEM, Z=100, showing isolated slip band in unstretched 8090.

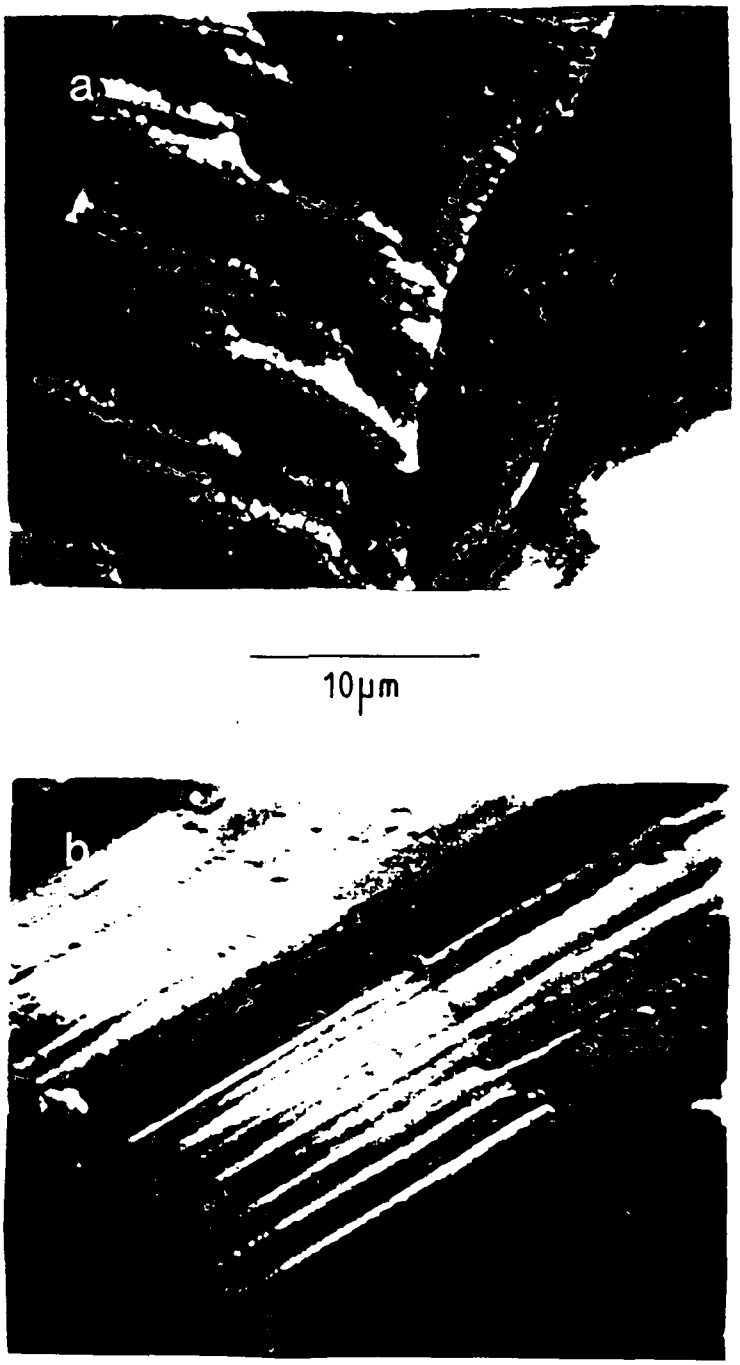

Figure 4.9 SEM photographs of 8090 fracture surface a) near crack initiation site b) about 100 microns from crack initiation site.

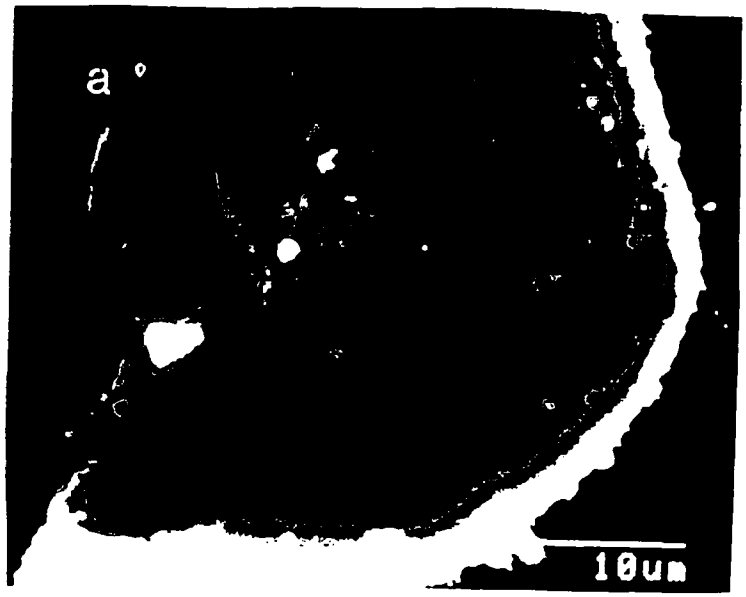

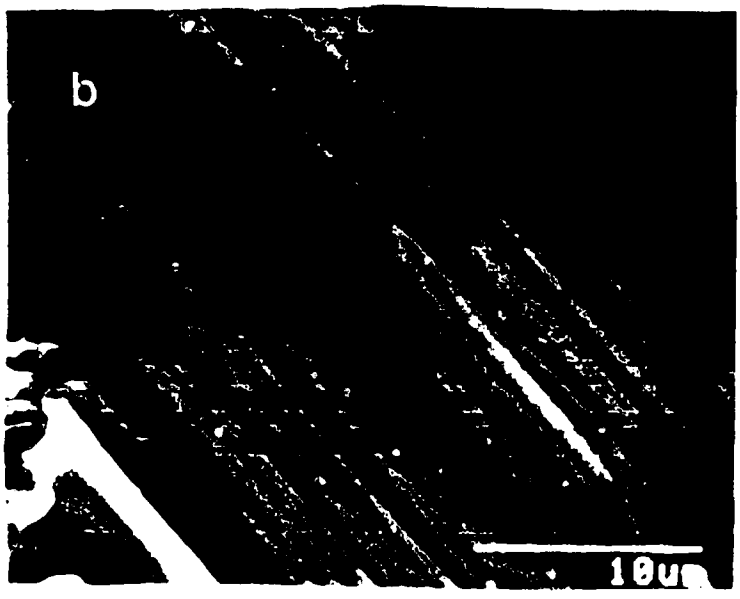

Figure 4.10 SEM photographs of 8091 fracture surface a) near crack initiation site b) about 100 microns from crack initiation site.

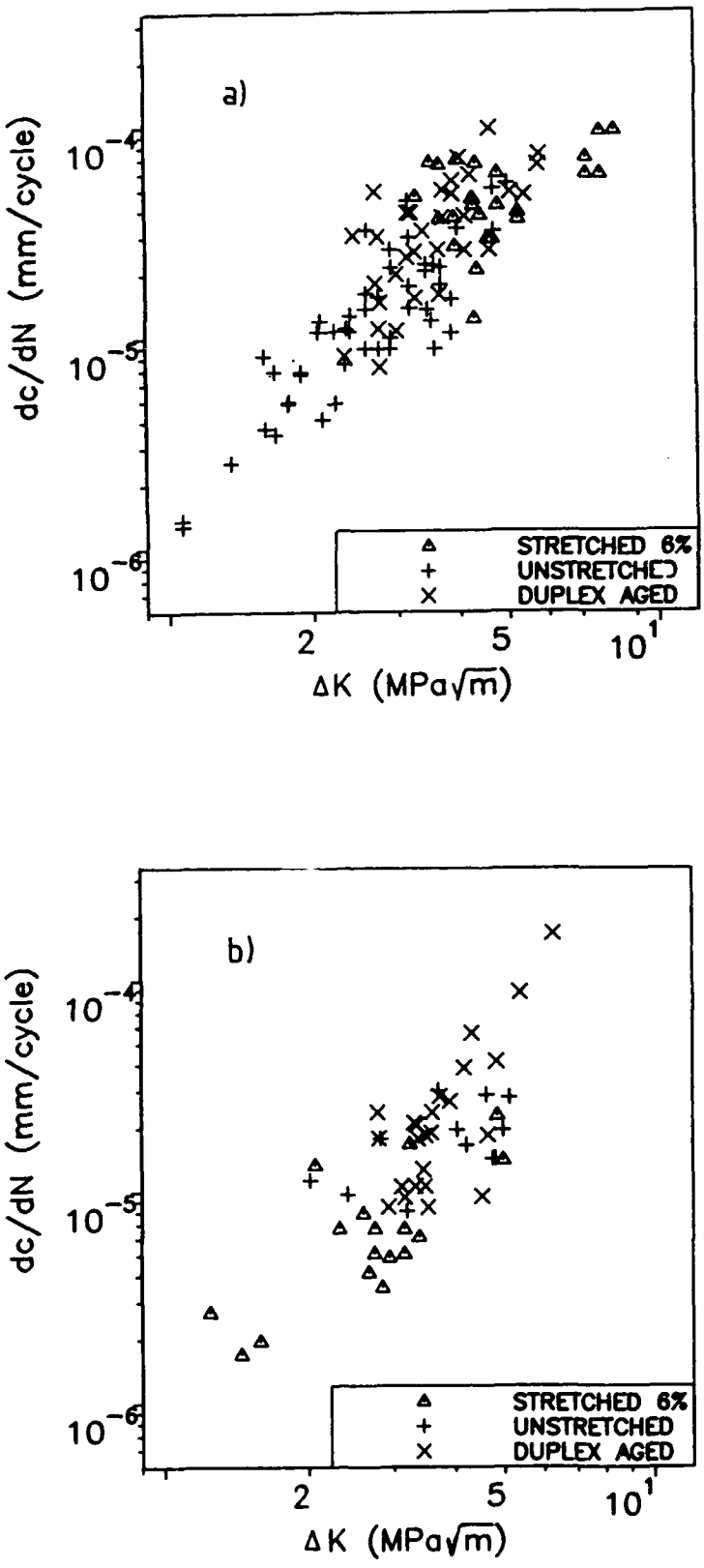

Figure 4.11 Crack growth rate as a function of ΔK (σ/σ_{ys}=.85) for a) 8090 b) 8091.

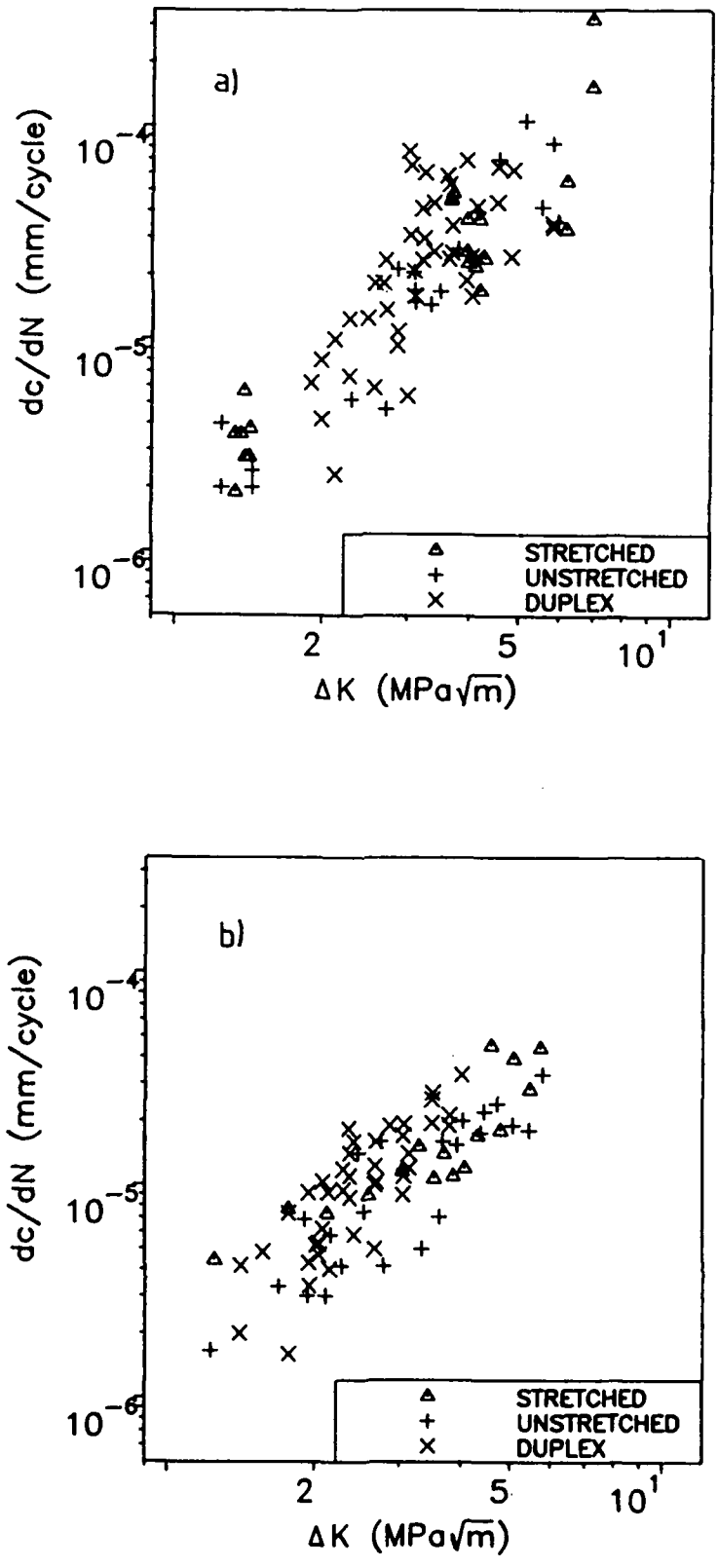

Figure 4.12 Crack growth rate as a function of ΔK (σ/σ_{ys}=.7) for a) 8090 b) 8091.

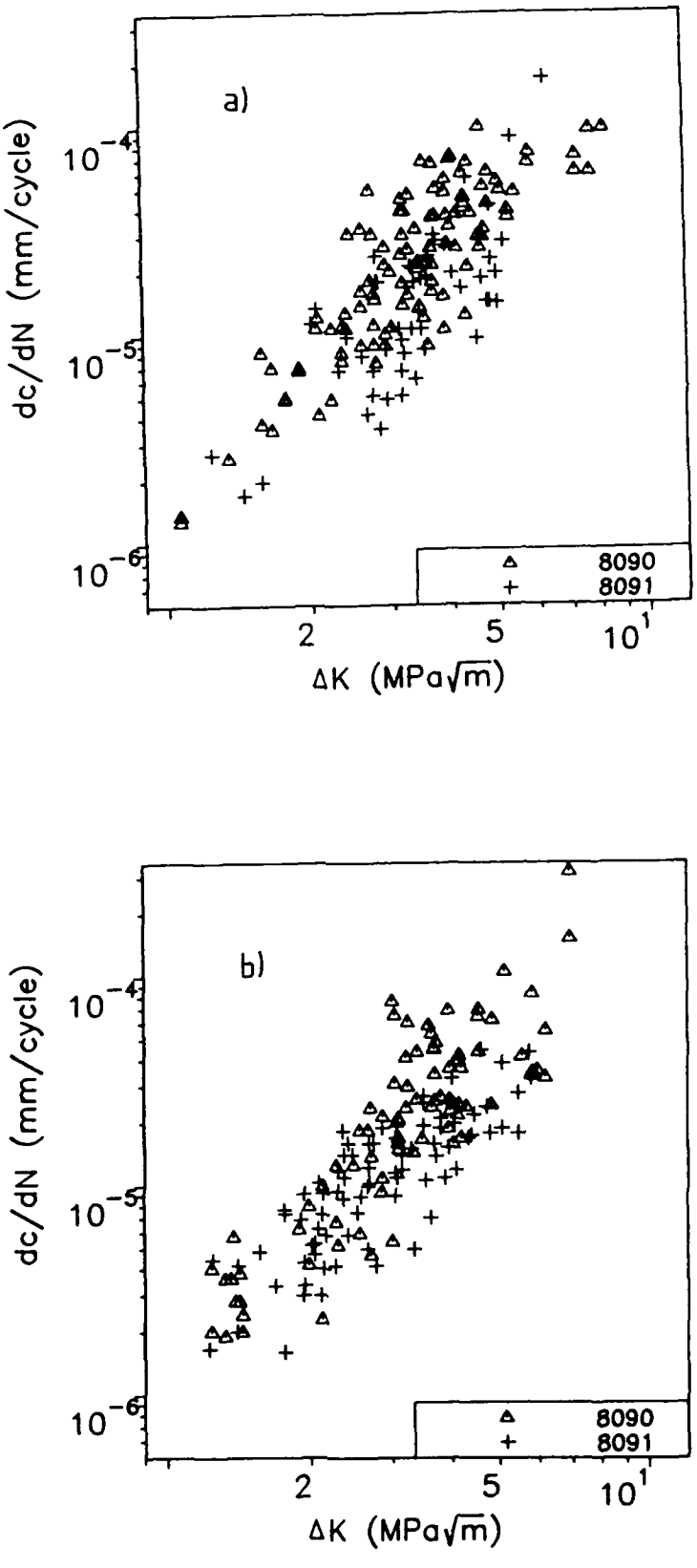

Figure 4.13 Comparison of crack growth rates for 8090 and 8091 a) σ/σ_{ys}=.85 b) σ/σ_{ys}=.7.

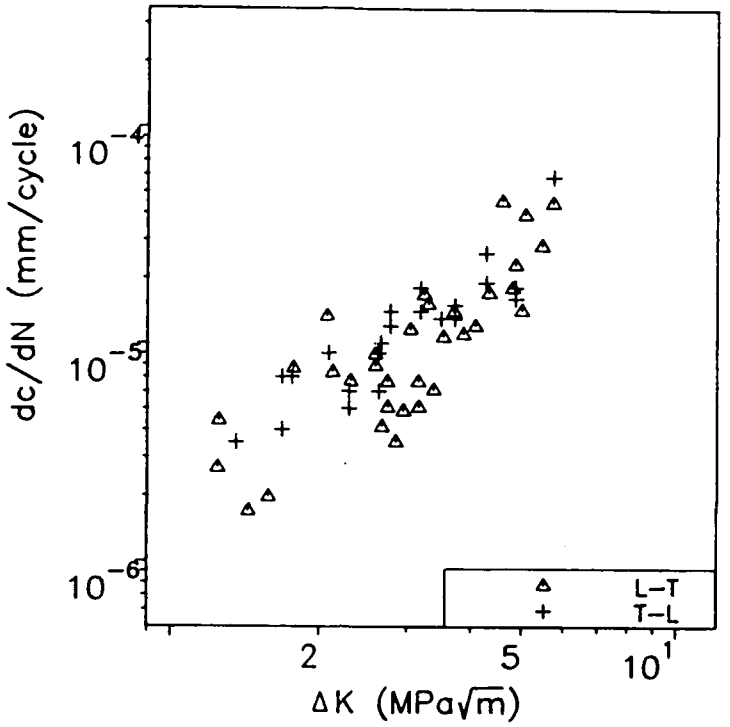

Figure 4.14 Comparison of crack growth rates in 8091 as a function of specimen orientation (σ/σ_{ys}=.85).

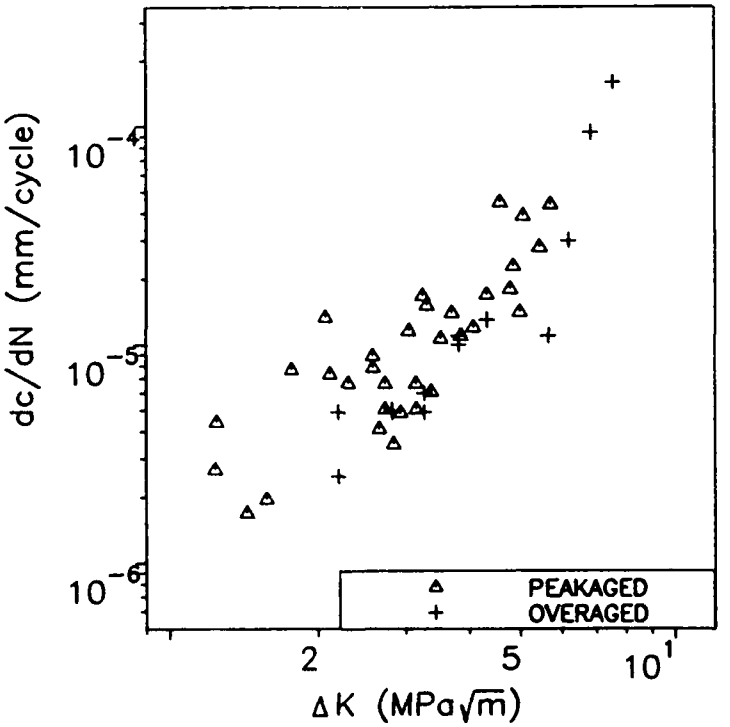

Figure 4.15 Small crack growth rates of peakaged versus overaged 8091 (both materials 6% stretched).

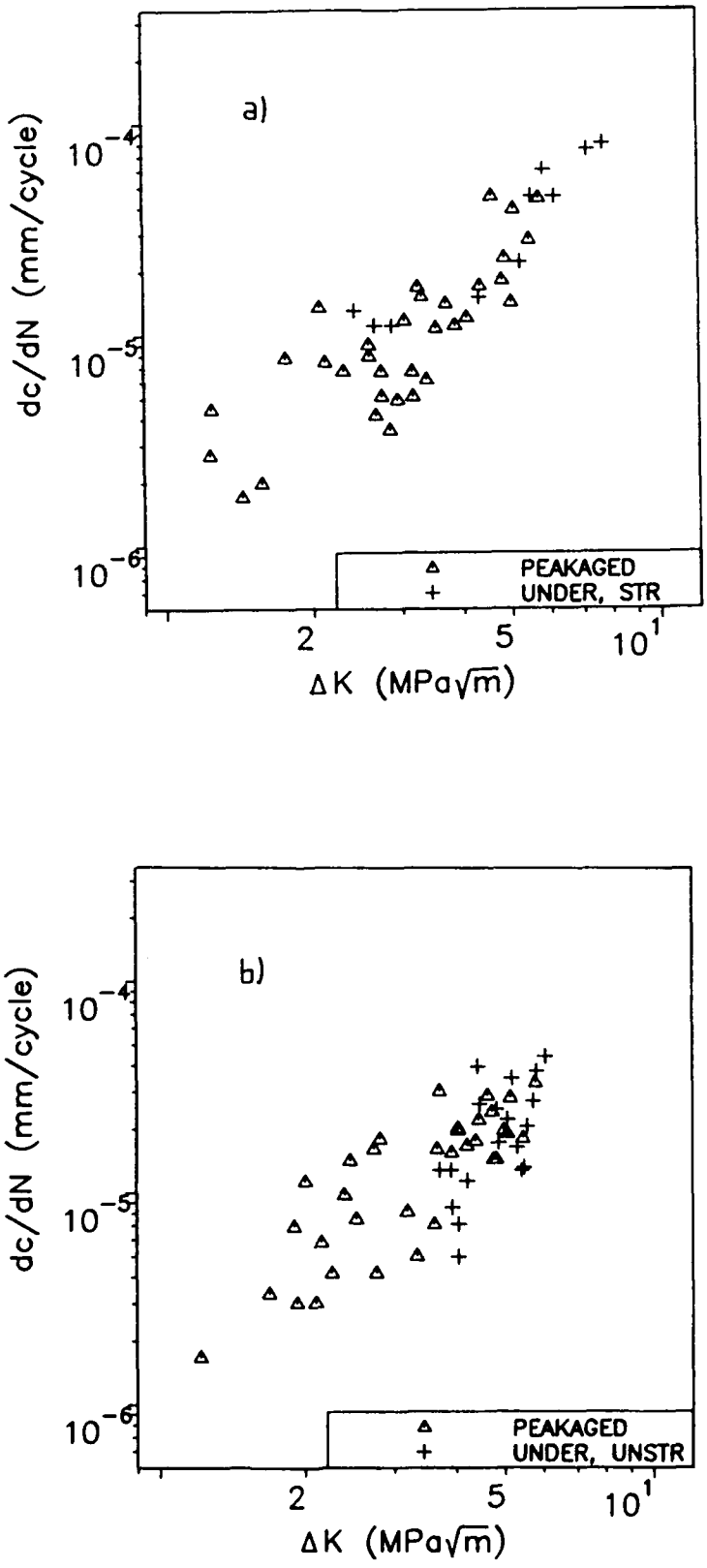

Figure 4.16 Small crack growth rates of peakaged versus underaged 8091 a) 6% stretched b) unstretched.

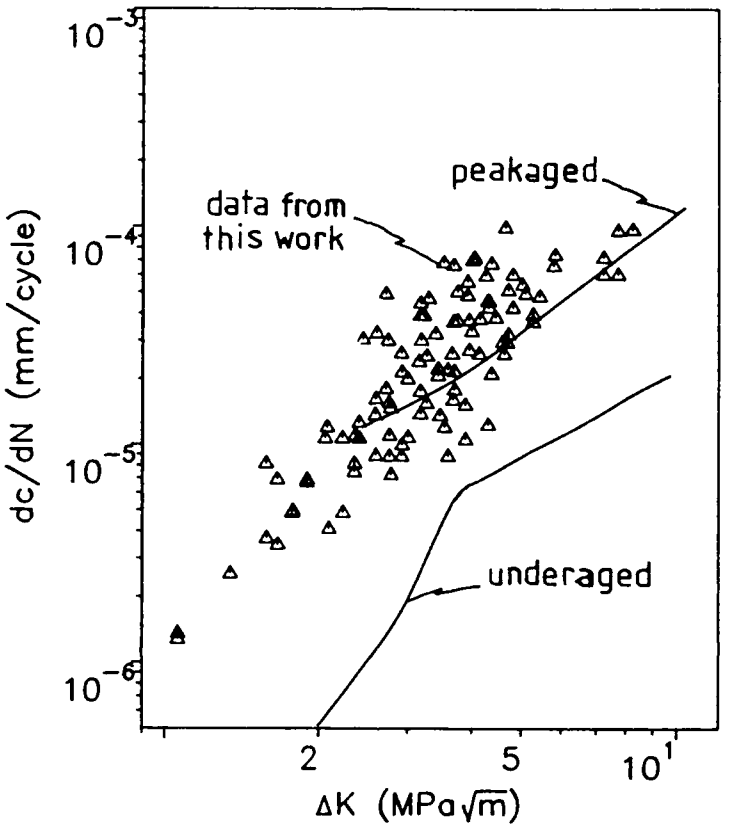

Figure 4.17 Comparison of small crack growth data generated on 8090 in this work with data on peakaged and underaged 8090 generated by James (1987).

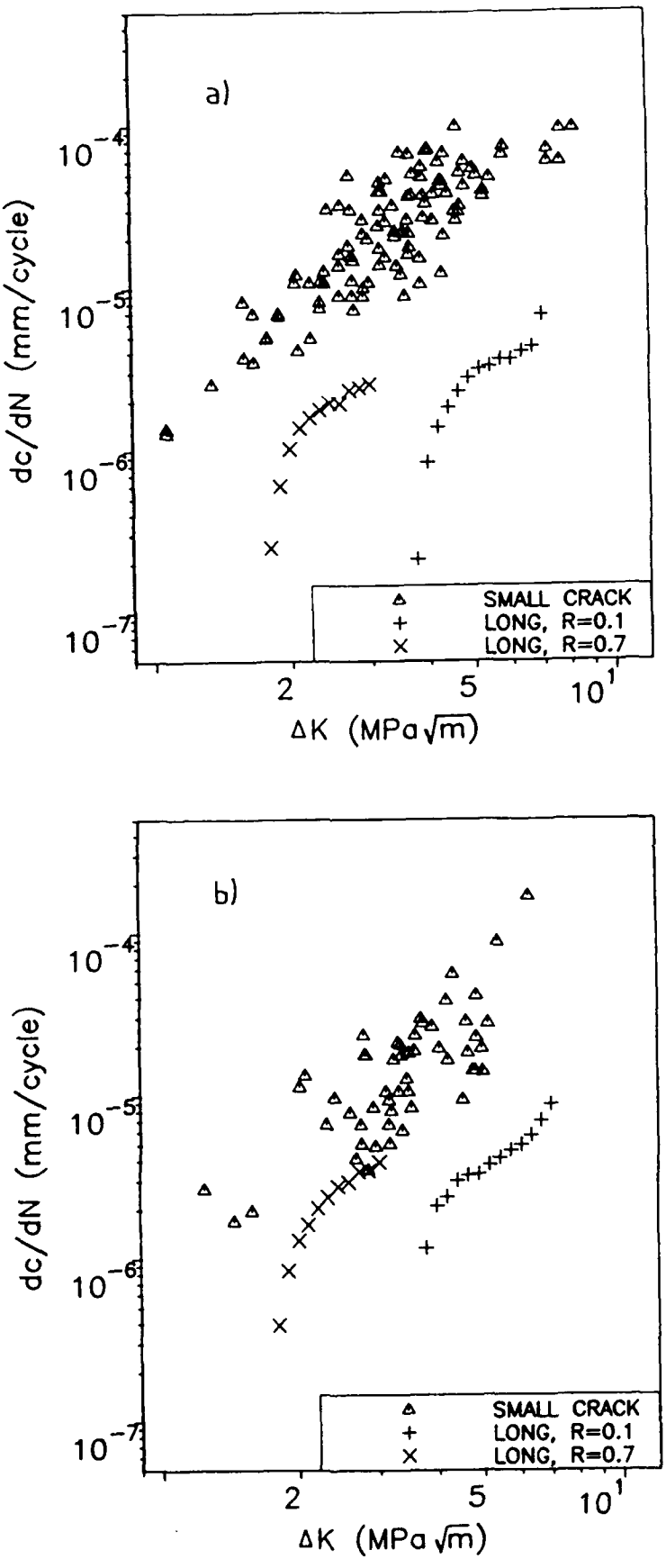

Figure 4.18 Comparison of small crack growth data against long crack data generated at R=0.1 and R=0.7 a) 8090 and b) 8091 (long crack data after Peacock and Martin, 1989).

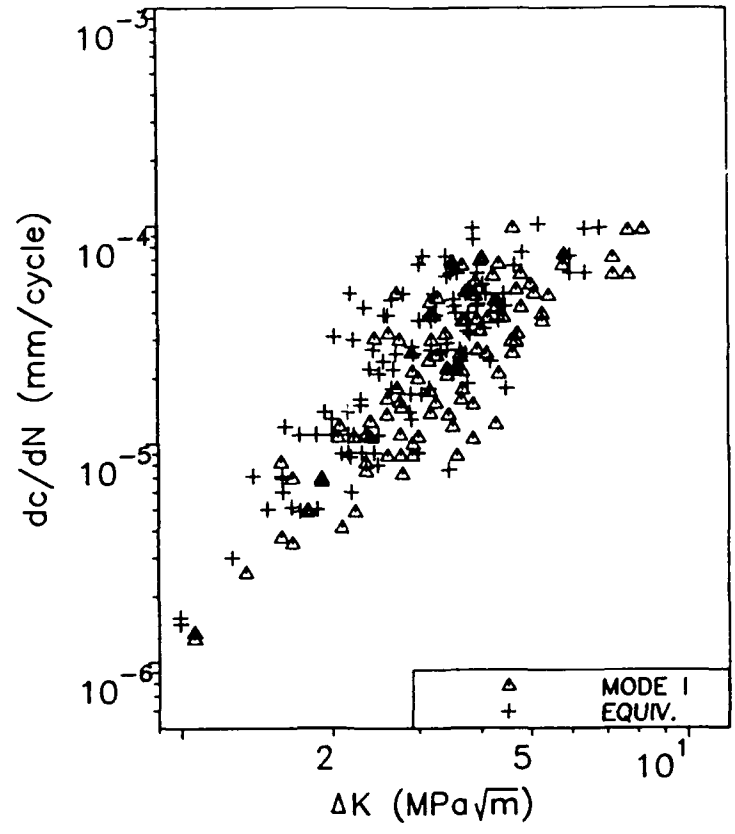

Figure 4.19 Comparison of crack growth rates correlated with ΔK_I and ΔK_{eq}.

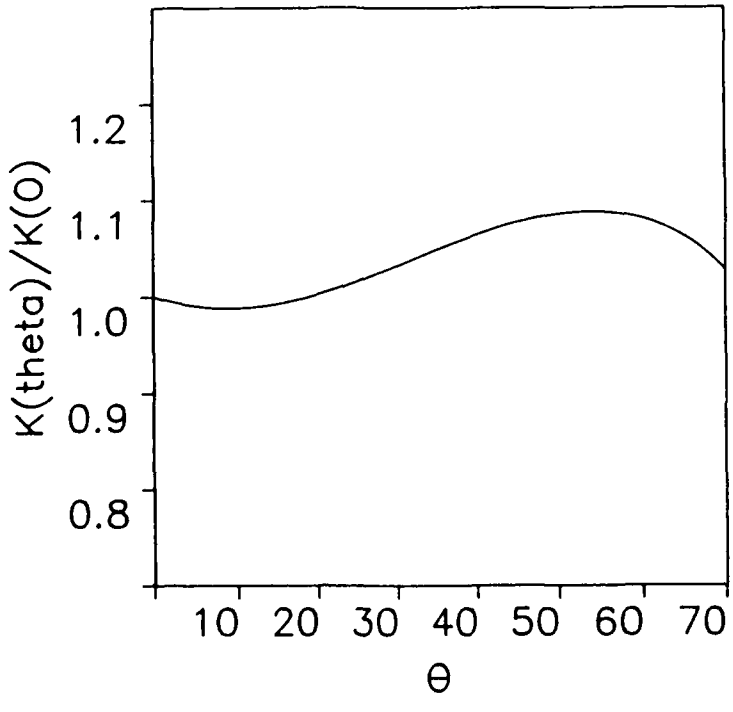

Figure 4.20 K as a function of the angle of crack inclination (θ).

Material	R_L
8090 peak aged, stretched 6%	1.25
"	1.19
"	1.17
"	1.15
"	1.17
8090 peak aged, unstretched	1.39
"	1.52
"	1.30
8090 peak aged, duplex aged	1.28
"	1.47
8091 peak aged, stretched	1.15
"	1.25
"	1.17
8091 peak aged, unstretched	1.38
"	1.20
"	1.26
8091 peak aged, duplex	1.48
"	1.24
8091 underaged, stretched	1.17
8091 overaged, stretched	1.15
"	1.17
8091 underaged, unstretched	1.34
"	1.59

Table 4.1 Lineal roughness parameter (R_L) data for various materials.

CHAPTER 5

THE EFFECT OF PLASTICITY ON SMALL CRACK GROWTH

5.1 INTRODUCTION

The main objective of this work was to relate the microstructure, emphasizing its effect on slip distribution, to the growth of small cracks in fatigue. As, however, the cracks studied in this work were mechanically small, it was likely that their behaviour would be affected by the extensive plasticity ahead of the crack tip. Potentially, the effects of microstructure could be altered or obscured altogether. The purpose of this chapter is to discuss the effects of plasticity both to better understand the microstructural effects and for the inherent interest of the mechanical effects.

This chapter begins with the theoretical calculation and experimental measurement of the plastic zone size. The size of the plastic zone will then be used to characterize more clearly the effect of the plastic zone on small fatigue crack behaviour and to show how the role of microstructure on small fatigue crack behaviour is affected. Because the small scale yielding assumption was violated for the small fatigue cracks studied in this work, the use of the elastic-plastic parameter, ΔJ, will be discussed. Two approaches for estimating ΔJ will be presented, along with experimental results. Next, it will be demonstrated that low cycle fatigue behaviour is related to small fatigue crack behaviour. This relationship will be used to understand microstructural effects on small fatigue crack behaviour more clearly. Finally, observations on small fatigue cracks will be used to comment on apparent fatigue mechanisms for both long and small fatigue cracks.

5.2 PLASTIC ZONE SIZE

The size of the plastic zone relative to the size of the crack is the basis for the anomalous behaviour of mechanically small cracks. In this section, the effect of the higher order terms in the solution for the stresses around the crack tip will be shown to be relevant to the size of the plastic zone associated with small fatigue cracks. Estimates of plastic zone size will be compared to experimental measurements. Finally, possible correlation of long and small fatigue crack data using plastic zone size information will be discussed along with the implications of large scale yielding for the role of the microstructure.

5.2.1 THEORETICAL CALCULATION OF PLASTIC ZONE SIZE

As described in Chapter One, the size of the plastic zone may be calculated by equating the stresses around a crack tip to a yield criterion and solving the resulting expression for the distance from the crack tip at which yielding occurs. The LEFM solution for the stresses around a crack tip is given by Equation 5.1.

$$\sigma_{yy} = \frac{\sigma_{app}\, a^{1/2}}{(2r)^{1/2}} \left[1 + \frac{3}{2}(r/2a) - \frac{5}{8}(r/2a)^2 + \frac{7}{16}(r/2a)^3 \ldots \right] \qquad (5.1)$$

When the plastic zone is small compared with the crack size the higher order terms in this equation can be neglected. Equation 5.1 then becomes

$$\sigma_{yy} = \frac{\sigma (a)^{1/2}}{(2r)^{1/2}} \qquad (5.2)$$

Equating σ_{yy} to σ_{ys} and solving for the plastic zone size (r_p) we get

$$r_p/a = \frac{\sigma^2}{\sigma_{ys}^2} \qquad (5.3)$$

Equation 5.3 can be put into slightly more familiar terms by substituting in the definition of K.

$$r_p = (1/Y)^2 \frac{K^2}{\sigma_{ys}^2} \qquad (5.4)$$

Both of these equations assume that the higher order terms in Equation 5.1 can be neglected. As will be shown in the following section, however, the plastic zone associated with the small cracks studied in this work was a significant fraction of the size of the crack itself. This is a common feature of small cracks as has been pointed out by Lankford and Davidson (1984) among others.

To circumvent this problem, Allen and Sinclair (1982) used the Westergaard expression below for the stresses ahead of the crack tip. This expression includes the effect of the higher order terms on the stresses ahead of the crack tip.

$$\sigma_{yy} = \frac{\sigma_{app}(r/a + 1)}{((r/a)^2 + 2(r/a))^{1/2}} \qquad (5.5)$$

Use of Equation 5.5 for the stresses ahead of the crack tip resulted in the following expression for the plastic zone size.

$$r_p/a = \frac{\sigma^2}{\sigma_{ys}^2 - \sigma^2} \qquad (5.6)$$

Comparison of Equation 5.6 with Equation 5.3 shows that the effect of including the higher order terms is to increase the size of the plastic zone, particularly if the applied stress is a significant fraction of the yield stress. This is particularly relevant to small fatigue cracks as high stresses are normally required for initiation and growth.

Allen and Sinclair's approach for calculating plastic zone size was used in this work. However, the small fatigue cracks studied in this work were semi-elliptical and in a finite plate rather than the straight, through-thickness cracks in an infinite plate assumed by Allen and Sinclair. The stresses ahead of a semi-elliptical crack were estimated from Equation 5.7 which is identical to that used by Allen and Sinclair (Equation 5.5) with the exception that a geometric

term B has been introduced. B is defined as $B=Y/(\pi)^{1/2}$ where Y is the geometric correction for a semi-elliptical crack.

$$\sigma_{yy} = \frac{B\sigma_{app}(r/a + 1)}{((r/a)^2 + 2(r/a))^{1/2}} \qquad (5.7)$$

Integrating this equation between 0 and 2r and equating the result with $2\sigma_y r$, as Allen and Sinclair did, results in the following expression for r_p

$$r_p/a = \frac{B^2\sigma^2}{\sigma_{ys}^2 - B^2\sigma^2} \qquad (5.8)$$

This equation can also be expressed as

$$r_p/a = \frac{1}{1-(B\sigma/\sigma_{ys})^2} - 1 \qquad (5.9)$$

In the derivation of Equation 5.9, the assumptions were that plane stress conditions existed and that the stresses ahead of the crack tip are redistributed because of local yielding. These assumptions appear to be reasonable for small surface cracks. From this equation it can be seen that plastic zone size depends only on the length of the crack and σ/σ_{ys}. It was for this reason that the small crack fatigue tests in this work were always conducted at given fractions of the yield stress. The intent was to keep the effects of plasticity constant so that microstructural effects would not be obscured.

5.2.2 MEASUREMENT OF PLASTIC ZONE SIZE

The size of the plastic zone was measured for the small fatigue cracks studied in this work using selected area channelling patterns (SACP's). As mentioned in section 3.5.2, this technique uses degradation of the SACP as an indication of plastic deformation. More specifically, for this work, plastic deformation was said to occur when the fourth order {111} line disappeared. According to Tekin and Martin (1989) this corresponds to about 1.5% plastic

deformation. It follows, then, that this technique will slightly underestimate the size of the plastic zone. Plastic zones sizes were not measured for samples which had been stretched during thermo-mechanical treatment as the plastic deformation due to stretching would be indistinguishable from plastic deformation associated with the crack. Unfortunately, this meant that it was not possible to characterize the effects of slip distribution on plastic zone size as slip was inhomogeneously distributed for both the unstretched and the duplex aged alloys.

The experimental results are given in full in Table 5.1. The scatter in the results is probably due to variations in yield strength within individual grains and the influence on slip length of the distance to the nearest grain boundary. Below, a summary of the experimental results is compared with theoretical calculations based the equations in the previous sections both including and excluding the effects of higher order terms.

σ/σ_{ys}	Exp. r_p/a	Theor. r_p/a based on ΔK	Theor. r_p/a incl. effect of H.O.T.
0.7	0.48	0.25	0.33
0.85	0.64	0.36	0.58

These data show that the actual plastic zone size is twice as large as the estimate based on ΔK. The inclusion of the effect of the higher order terms does not eliminate the discrepancy although it does reduce it. The data also confirm that the small cracks studied in this work were mechanically small since the plastic zone size is a significant fraction of the crack length. Finally, they show that plastic zone size, not unexpectedly, is a function of σ/σ_{ys}. Thus, the appropriateness, when investigating microstructural effects, of applying a constant fraction of the yield stress rather than a constant stress to all materials is confirmed.

It remains that inclusion of the effect of higher order terms on the plastic zone size still results in an underestimation of the plastic zone size. This is probably due to an overestimation in the yield stress. Equation 5.9 (which calculates r_p/a) is very sensitive to errors in the yield stress. If the actual yield stress were 5% lower than the measured yield stress r_p/a (so that $\sigma/\sigma_{ys} = 0.895$ rather than 0.85) the calculated r_p/a would change from 0.57 to 0.68. It is reasonable that measurements of the yield strength from tensile specimens would systematically overestimate the yield strength of the material locally ahead of the crack due to the reduced constraint associated with proximity to a free surface and to the likelihood that the crack exploits local weaknesses.

5.2.3 THE EFFECT OF PLASTIC ZONE SIZE ON SMALL FATIGUE CRACK BEHAVIOUR

Allen and Sinclair (1982) defined an effective K as

$$K_{eff} = \left(\frac{1}{1-(\sigma/\sigma_{ys})^2} \right)^{1/2} K \qquad (5.10)$$

This equation corrects K for the effect of the higher order terms on the stresses around a crack tip. Adding the geometric factor B to Equation 5.10 to reflect the fact that the cracks studied in this work were semi-elliptical results in

$$K_{eff} = \left(\frac{1}{1-(B\sigma/\sigma_{ys})^2} \right)^{1/2} K \qquad (5.11)$$

Alternatively, the experimentally measured plastic zone can be used to calculate a ΔK_{eff} as expressed in Equation 5.12 if it is assumed that the plastic zone size is proportional to ΔK^2. $r_{p,exp}$ is the experimentally measured plastic zone size and $r_{p,K}/a$ is the size of the plastic zone based on the definition of K (i.e. based on Equation 5.4).

$$K_{eff} = \left(\frac{r_{p,exp}/a}{r_{p,K}/a} \right)^{1/2} K \qquad (5.12)$$

These expressions were used to calculate the values of K_{eff}/K tabulated below.

σ/σ_{ys}	K_{eff}/K (Eq. 5.11)	K_{eff}/K (Eq. 5.12)
0.7	1.15	1.33
0.85	1.26	1.39

In Figure 5.1, where long and small crack growth data are compared as a function of a corrected ΔK based on Equation 5.12, it can be seen that the discrepancy between long and small fatigue crack growth rates remains.

A possible deficiency in the approach just described is that no allowance is made for the fact that the long fatigue crack data were generated under plane strain conditions while the small fatigue crack data were generated under plane stress conditions. The additional constraint of plane strain conditions reduces the size of the plastic zone. To remedy this deficiciency, plastic zone sizes were calculated as described below.

From LEFM, the plastic zone size under plane strain conditions is given by

$$r_p = \frac{1}{3\pi} \left(\frac{K_I}{\sigma_{ys}} \right)^2 = .106 \left(\frac{K_I}{\sigma_{ys}} \right)^2 \qquad (5.13)$$

For the specimen geometry used in this work and the range of crack sizes studied, the Newman-Raju equation used to calculate K can be reduced, with at most a 3% error, to

$$K = 1.26\sigma a^{0.5} \qquad (5.14)$$

Restricting this approach to tests where $\sigma/\sigma_{ys}=0.85$ and rearranging the result to solve for the crack length, a, results in Equation 5.15.

$$a = .873 \left(\frac{K}{\sigma_{ys}} \right)^2 \qquad (5.15)$$

At σ/σ_{ys}=0.85 the estimate of r_p/a (0.58) given by Equation 5.9 agreed quite well with that actually measured for small fatigue cracks. Therefore, combining this estimate for r_p/a with Equation 5.15 results in Equation 5.16.

$$r_p = .51 \left(\frac{K}{\sigma_{ys}} \right)^2 \qquad (5.16)$$

Small and long fatigue crack growth rates plotted versus plastic zone size are compared in Figure 5.2. Calculation of plastic zone size for long fatigue cracks was based on Peacock and Martin's (1989) long fatigue crack data which correlated crack growth rate with ΔK. The correlation between long and small crack growth rates now appears to be quite reasonable especially when the small fatigue crack data are compared with the long fatigue crack data generated at R=.7 where closure effects are eliminated. This is, perhaps, not surprising since crack growth rate and plastic zone size are manifestations of the same driving force.

These data, however, raise the issue as to the effect of constraint on fatigue crack growth. Small fatigue cracks are generally under plane stress conditions since they are so near to a free surface and long fatigue cracks are generally under plane strain conditions. This difference would be expected to affect the plastic zone size. Recently, it has been shown, for example, that surface grains accumulate approximately three times as much strain as the bulk (Keller and Gerberich, 1989). Since there are models in which fatigue crack growth is related to damage accumulation and plastic zone size, it is not unreasonable to conclude that fatigue crack growth should be affected as well. The data generated in this thesis are certainly consistent with this concept and appear to show that the difference in constraint between long and small fatigue

cracks is a major reason for the observed discrepancy between their respective growth rates.

Based on this reasoning, it would be expected that long fatigue crack growth rates would depend on specimen thickness as that also affects the state of stress. Unfortunately, the limited data in this area is conflicting (Dover and Boutle, 1978). Partially, this may be due to the complicating effect of increased plasticity induced closure under plane stress conditions (Schijve, 1977). These complications would not be significant for small fatigue cracks since the effects of closure on small fatigue crack growth are minor.

5.2.4 MICROSTRUCTURAL IMPLICATIONS

The preceeding discussions have shown that plastic zone size is a function of σ/σ_{ys}. The last table, however, shows that corrections to ΔK are similar whether at σ/σ_{ys} equal to 0.85 or 0.7. Therefore, it appears that the fraction of the yield stress is not critical to the effectiveness of ΔK as a correlating parameter in the range $0.7 \leq \sigma/\sigma_{ys} \leq 0.85$. This is confirmed by Figure 5.3 where it is shown that small crack growth rates correlated with ΔK at $\sigma/\sigma_{ys}=0.85$ are comparable to small crack growth rates at $\sigma/\sigma_{ys}= 0.7$. It appears that small crack growth rates correlated with ΔK are independent of the fraction of the yield stress of the material applied over the range examined. Hudak et al (1988) have reported only a minor dependence over the much larger range $0.8 \leq \frac{\sigma}{\sigma_{ys}} \leq 1.6$

This observation is important from a microstructural standpoint. In small fatigue crack tests the local yield stress may be reduced for a number of microstructural reasons such as weakly oriented grains or local dissolution of precipitates in a slip band. If the yield stress has little effect on the rate of crack growth then

these microstructural changes will similarly have little effect on crack growth. Thus, small crack growth rates will be relatively insensitive to microstructural changes that influence the weakness of the grains or the propensity for the dissolution of precipitates within slip bands. This is in agreement with the lack of an effect on small crack growth behaviour of changing precipitate size and distribution through underageing and the thermo-mechanical treatments described in Chapter Four.

Furthermore, the influence on the crack driving force of including the higher order terms appears to be similar for σ/σ_{ys} values between 0.7 and 0.85. This implies that, from the standpoint of neglection of the higher order terms and their influence on plastic zone size, the use of ΔK has not affected the observation of microstructural influences on small crack growth.

5.3 ΔJ AS A CORRELATING PARAMETER

Another issue is whether ΔK, a term based on LEFM, is at all suitable for the characterization of the behaviour of mechanically small cracks. As was shown in the preceeding section, the plastic zones associated with the small cracks studied in this work were about one half of the size of the cracks themselves. Clearly the assumption of small scale yielding, implicit with the use of ΔK, is violated.

This suggests the use of an elastic-plastic parameter such as CTOD or ΔJ. The advantage of using tne CTOD is that it is a measure of conditions in the immediate vicinity of the crack tip. This renders irrelevant issues such as the requirement for path independence of global parameters. The disadvantage is that it must be measured locally rather than derived from the externally applied

stresses and geometric factors (including the crack size). CTOD's have been successfully measured using a stereo-imaging technique (Lankford and Davidson, 1984). This work showed that the CTOD's associated with small fatigue cracks are larger than those associated with long fatigue cracks under the same nominal ΔK (Lankford and Davidson, 1984). No attempt, however, has been made to measure CTOD in this work.

Instead, effort focussed on the use of ΔJ. As mentioned in section 1.3.4, J is a non-linear elastic parameter that, strictly speaking, can only be applied to plastically deforming materials where there is no unloading. To circumvent this restriction Lamba (1975) proposed a ΔJ integral where the terms in the definition of J are replaced with their respective ranges. The relationship between stress and strain is determined from a cyclic stres-strain curve so that the relationship between stress and strain is independent of history.

The use of ΔJ may still be criticized on the grounds that it has been shown to be dependent on the path of integration for both long and small cracks (Chan, 1986). This means that calculation of ΔJ from macroscopic parameters may not accurately reflect the crack driving force within the plastic zone. Nevertheless, ΔJ has been found to improve the correlation between long and small crack growth rates (Dowling, 1977) and it will be used here as a useful approach for accounting for the effects of large scale yielding.

5.3.1 ESTIMATION OF ΔJ

From Chapter One the ΔJ integral is defined as

$$\Delta J = \int_{\Gamma} \Delta w \, dy - \Delta T \frac{\partial \Delta u}{\partial x} ds \qquad (5.17)$$

Unfortunately, no rigorous solution for ΔJ has been developed for a semi-elliptical crack under bending and so an approach for estimating the solution was sought. One approach from the literature is based on relating the area under the cyclic stress-strain curve to ΔJ (Dowling, 1977). Another approach is based on calculation of the crack tip opening displacement for the Dugdale crack (Chan, 1986). Other approaches in the literature are either based on finite element models (eg Nikishkov and Athuri, 1988) or on direct measurement of displacements around the crack tip using stereo-imaging techniques (Chan et al, 1986). Finite element approaches and direct measurement of displacements were considered to be beyond the scope of this thesis. Therefore, Dowling's (1977) and Chan's (1986) approaches for estimating ΔJ were adopted for this work. These derivations will be presented in some detail here both to show the principles upon which they are based and because slightly different forms of these equations were derived for use in this work to estimate ΔJ.

In Dowling's approach a line contour along the crack surfaces is considered as shown in Figure 5.4. $\Delta\sigma_{ij}$ equals zero along such a contour which simplifies Equation 5.17 to

$$\Delta J = \Delta W h \qquad (5.18)$$

where ΔW is the area under the stress-strain curve shown in Figure 5.5 and h is the crack face separation. It is important to note that the stress range for this curve is twice the applied stress. The reason for this is that ΔJ is being evaluated locally within the reversed plastic zone and thus the stresses are varying from the negative of the applied stress to the positive. As illustrated in Figure 5.5, ΔW can be approximated by summing the elastic strain energy density and the cyclic plastic work density associated with

the hysteresis loop at the crack tip. Based on this concept and Shih and Hutchinson's (1975) solution for J, Dowling suggested the following estimate for ΔJ.

$$\Delta J = 2\pi Q^2[\Delta W_e + f(s)\Delta W_p]\, a \qquad (5.19)$$

where Q is the geometric correction factor used to correct K and f(s) is a function of the cyclic strain hardening exponent. From Figure 5.5, ΔW_e can be seen to be given by

$$\Delta W_e = \Delta\sigma^2/2E = 2\sigma^2/E. \qquad (5.20)$$

For an exponentially hardening material ΔW_p is given by

$$\Delta W_p = \frac{(\Delta\sigma\Delta\epsilon_p)}{s+1} \qquad (5.21)$$

Remembering that $\Delta\sigma$ is twice the stress applied and using the approximation suggested by Mowbray (1976) and employed by El Haddad and Miettinen (1982) for f(s)/(s+1), Equations 5.19, 5.20 and 5.21 can be combined to produce the following equation (after rearrangement).

$$\Delta J = \frac{4Q^{2D}\sigma^2\pi a}{E} + \frac{7.7\Delta\epsilon_p Q^2\sigma a}{s^{1.5}+s^{0.5}} \qquad (5.22)$$

Equation 5.22 can derived in terms of ΔK by using the definition of ΔK (i.e. $Q^2\Delta\sigma^2\pi a = \Delta K^2$).

$$\Delta J = \frac{4\Delta K^2}{E} + \left(\left(\frac{2.45\Delta K^2}{s^{1.5}+s^{0.5}}\right)\left(\frac{\Delta\epsilon_p}{\sigma}\right)\right) \qquad (5.23)$$

Equation 5.23 can also be stated in terms of ΔJ_e by substituting in $\Delta K^2/E = \Delta J_e$.

$$\Delta J = \Delta J_e\ 4 + \left(\left(\frac{2.45}{s^{1.5}+s^{0.5}}\right)\left(\frac{E\Delta\epsilon_p}{\sigma}\right)\right) \qquad (5.24)$$

Equation 5.24 apparently predicts that for the purely elastic case $\Delta J = 4\Delta J_e$. This contradiction results from the assumption of a reversed plastic zone. In the purely elastic case there is no reversed plastic zone and so the equation above is inapplicable. For the small cracks studied a reversed plastic zone is expected and so there should be no objection.

Chan (1986) pointed out that, under the nominally elastic conditions that were typically used for small fatigue crack studies, ΔJ should be equivalent to ΔK ($\Delta J=\Delta K^2/E$). Furthermore, from measurements of displacements on various contours around the crack tip, Chan et al (1986) had shown that ΔJ was not path independent. Based on these observations, Chan argued that calculation of ΔJ should be based on the local parameter of the CTOD.

In Chan's approach, as in Dowling's, a line contour along the crack surfaces is considered (Figure 5.4). ΔJ for a Dugdale crack is given by

$$\Delta J = \Delta\sigma(\delta)\ \delta \qquad (5.25)$$

where δ is the cyclic crack tip opening displacement. Assuming that the crack tip stress range is constant at twice the yield strength, and thus independent of δ, this equation can be stated as

$$\Delta J = 2\sigma_y\delta \qquad (5.26)$$

For small scale yielding δ is given by (Kanninen and Popelar, 1985)

$$\delta_{ssy} = \frac{16\ \sigma_y a}{\pi E}\left(\ln\ \sec\left(\frac{\pi\sigma}{4\sigma_y}\right)\right) \qquad (5.27)$$

To account for the high levels of plasticity, δ_{ssy} is multiplied by a plasticity correction factor equal to the ratio of the monotonic crack tip opening displacement for a Dugdale crack to the monotonic δ_{ssy}. The resulting equation is

$$\Delta J = \frac{256\sigma_y^4 a}{\pi^3\sigma^2 E}\left(\ln\ \sec\left(\frac{\pi\sigma}{4\sigma_y}\right)\right)\left(\ln\ \sec\left(\frac{\pi\sigma}{2\sigma_y}\right)\right) \qquad (5.28)$$

Extending Equation 5.28 to general geometries by again multiplying by Q^2 and substituting in $Q^2\sigma^2\pi a = K^2$, Equation 5.29, which is in terms oF ΔK, is derived.

$$\Delta J = \frac{256}{\pi^4}\left(\frac{\sigma_y}{\sigma}\right)^4\left(\frac{\Delta K^2}{E}\right)\left(\ln\ \sec\left(\frac{\pi\sigma}{4\sigma_y}\right)\right)\left(\ln\ \sec\left(\frac{\pi\sigma}{2\sigma_y}\right)\right) \qquad (5.29)$$

In terms of ΔJ_e this becomes

$$\Delta J = \frac{256}{\pi^4}\left[\frac{\sigma_y}{\sigma}\right]^4\left[\ln \sec\left(\frac{\pi\sigma}{4\sigma_y}\right)\right]\left[\ln \sec\left(\frac{\pi\sigma}{2\sigma_y}\right)\right]\Delta J_e \qquad (5.30)$$

5.3.2 CORRELATION OF LONG AND SMALL FATIGUE CRACK GROWTH DATA

Having derived expressions for ΔJ based on Dowling's and Chan's approaches, the estimates of ΔJ from each can be compared. The cyclic stress-strain data necessary for Dowling's approach were obtained from the cyclic stress-strain curves shown in Figure 4.5. Whether based on Dowling's or on Chan's approach the estimates of ΔJ can be expressed in the form $\Delta J = C\Delta K^2$. The values of the coefficient C for both approaches, the various stress levels and the various thermo-mechanical treatments are given in Table 5.2. In Figures 5.6 and 5.7, small and long fatigue crack growth data are compared as a function of ΔJ. The long fatigue crack data were calculated from Peacock and Martin's (1989) data correlating crack growth rates in 8090 and 8091 with ΔK using the relation $J=K^2/E$. From Figure 5.6 and 5.7, it appears that while both approaches improve the correlation between long and small fatigue crack growth rates, Dowling's approach is particularly effective. Once again, however, the correlation is best when the small fatigue crack data is compared to the long fatigue crack data generated at R=0.7.

The factors so far discussed in this work that contribute to the rapidity of small fatigue crack growth as compared with long fatigue crack growth include differences in closure levels, higher applied stress levels, the large size of the plastic zone and the proximity of small cracks to a free surface. From this work, it appears that the effect of closure level must be included regardless of the correlating parameter used. This may be done by either

calculating an effective K for long fatigue cracks or by generating the long fatigue crack data at a high stress ratio. Although there are techniques that may be employed to correct ΔK for the other factors, it was previously shown that they did not completely eliminate the discrepancy between long and small fatigue crack growth rates. Such corrections are not necessary or applicable when ΔJ is used as the correlating parameter because the underlying assumptions are different. For this reason and because the best correlation between long and small fatigue crack growth data was achieved using ΔJ, ΔJ appears to be superior to ΔK when comparing long and small fatigue crack growth rates.

Potentially, the use of Dowling's approach for calculating ΔJ introduces microstructural effects because quantities that are microstructurally dependent, such as the strain hardening exponent and the plastic strain for a given stress, are explicitly included in the calculation of ΔJ. However, plotting small fatigue crack growth data versus ΔJ does not change the earlier conclusions as to the lack of an effect of slip distribution on small fatigue crack growth (see Figure 5.8). Furthermore, none of the factors affecting comparison of long and small fatigue crack data has been found to compromise the ability of ΔK, as a measure of the crack driving force, to characterize microstructurally related changes in small crack growth rates. From these observations, it does not appear that ΔJ is superior to ΔK for characterizing microstructural effects on small fatigue crack growth.

5.4 MODELS BASED ON LOW CYCLE FATIGUE

In section 1.2, S-N curves were discussed as a design tool. A common practice is to plot the number of cycles to failure as a

function of strain amplitude rather than stress amplitude. The resistance of a metal to cyclic straining can be represented as the sum of its resistance to plastic straining and to elastic straining (Hertzberg, 1983). Thus, fatigue life can be related to strain by the following equation (commonly called the strain-life relationship) where ϵ_T is the total strain, ϵ_e is the elastic strain, ϵ_p is the plastic strain, σ_f' is the fatigue strength coefficient, N_f is the number of cycles, b is the fatigue strength exponent, ϵ_f' is the fatigue ductility coefficient, and c is the fatigue ductility exponent.

$$\Delta\epsilon_T/2 = \Delta\epsilon_e/2 + \Delta\epsilon_p/2 = (\sigma_f'/E)(2N_f)^b + \epsilon_f'(2N_f)^c \quad (5.31)$$

A schematic of how this equation represents the fatigue life data is shown in Figure 5.9. The region to the left of the intersection of the two lines in Figure 5.9 is defined as the low cycle fatigue (LCF) regime. In the LCF regime, the contribution of the plastic strain dominates and the strain-life relationship given above can be simplified to the Coffin-Manson relationship i.e.

$$\Delta\epsilon_T = e_f'N_f^c \quad \text{or equivalently} \quad \Delta\epsilon_T N_f^n = C \quad (5.32)$$

5.4.1 RELEVANCE OF LCF TO SMALL FATIGUE CRACK BEHAVIOUR

Typically, cracks are initiated very early in the lifetime of an LCF specimen. Crack growth occurs under the cyclic loading until a crack is large enough to cause failure of the specimen. Since the crack initiation time is insignificant, the LCF life is defined by the length of time for a crack to grow to a critical size. Therefore, there must be a relationship between crack propagation behaviour and LCF behaviour. Several models for LCF behaviour are based on this relationship.

In particular, however, LCF should be related to the propagation behaviour of <u>small</u> fatigue cracks. The stresses used in

LCF tests are relatively high so that the critical crack lengths at which fracture occurs are relatively small. Therefore, cracks in LCF specimens are small for the majority of their existence. Murakami (1988) has observed that cracks as large as the grain size existed very early in the fatigue life ($N<0.02N_f$) and that for more than 90% of their total life the cracks were less than 1 mm long.

The relation between LCF behaviour and small fatigue crack behavior is confirmed by the similarity of the effects of microstructure for each case. Decreasing grain size, for example, has been shown in other work, and was shown in this work, to decrease small crack propagation rates. If small fatigue crack behaviour and LCF behaviour are related, then decreasing small crack propagation rates should imply longer LCF lifetimes. And, indeed, longer LCF lifetimes are observed for small grained materials (Starke and Lutjering, 1978) especially if slip in the alloy is relatively planar. Secondly, slip distribution (which can be related to precipitate distribution) has been shown in this work to have little effect on small crack growth. It has also been reported to have little effect on LCF behaviour although it does affect crack nucleation (Starke and Lutjering, 1978).

Having established that LCF behaviour and small fatigue crack behaviour are related, the issue remains of whether this relationship can be exploited to better understand small fatigue crack behaviour. Some models have used LCF behaviour to understand fatigue crack propagation although this has been primarily done for long cracks. It has been argued (eg Chakrabortty, 1979) that during the fatigue process the material ahead ot the crack tip is gradually exhausted (the exhaustion mechanism of fatigue will be further discussed in section 5.5.1). Therefore, the material ahead of the crack tip has

been likened to a miniature LCF specimen that ultimately reaches its fatigue life. McEvily (1983) has strongly criticized this approach, pointing out that LCF life is a function of crack initiation and propagation not a function of the material in the specimen becoming "exhausted".

There are, however, other approaches that use LCF response to explain small fatigue crack behaviour. It has already been shown that microstructural features have similar effects on LCF and small fatigue crack behaviour. It should be possible to predict microstructural effects on small fatigue crack rates from a knowledge of microstructural effects on LCF life. The accumulated knowledge of LCF behaviour can be regarded, then, as a data bank from which small crack behaviour may be predicted. In addition, LCF data could be used to confirm the presence of a trend observed in small fatigue crack behaviour. It is possible that LCF data may reveal microstructural effects more precisely since an LCF lifetime would effectively be an average of the small fatigue crack growth rates over a large number of cycles. This is likely to reduce the scatter typical of small fatigue crack data.

Another approach that can be used to interpret small fatigue crack behaviour in terms of LCF behaviour is to compare the equations that govern each type of behaviour. The growth rates of small fatigue cracks as a function of ΔK obey the Paris law. LCF lifetimes are characterized by the Coffin-Manson relation. As LCF behaviour is related to crack propagation behaviour, it is reasonable to expect that the Coffin-Manson relation should be related to the Paris law. It is the purpose of the next section to discuss that relationship and describe its implications.

5.4.2 A COMPARISON OF THE EQUATIONS GOVERNING LCF AND SMALL FATIGUE CRACK BEHAVIOUR

There have been several researchers, at least as far back as Tomkins (1968), who have, from Paris law type equations, derived Coffin-Manson type laws for LCF. A good example is given by the following derivation (Murakami, 1988). Murakami observed that small fatigue crack growth appeared to follow the relation in Equation 5.33.

$$\frac{da}{dN} = C_1(\Delta\epsilon_p)^m \, a \qquad (5.33)$$

If Equation 5.33 is integrated then the result is that

$$\Delta\epsilon_p^m(N_f-N_o)=C_2 \, f(a_f,a_o) \qquad (5.34)$$

Taking N_o, the time required to initiate a crack, as negligible for LCF tests and combining a_f, a_o and C_2 into a single constant, Equation 5.34 can be expressed as

$$\Delta\epsilon_p^m N_f=C_3 \qquad (5.35)$$

This equation can be rearranged into the Coffin-Manson equation.

$$\Delta\epsilon_p N_f^n=C_4 \qquad (5.36)$$

Small fatigue crack growth in this work was observed to follow the Paris law (i.e.)

$$\frac{da}{dN} = C_1(\Delta K)^p \qquad (5.37)$$

Linear regression was used to identify the value of the exponent p for 8090 and 8091. For 8090 the exponent was determined to be 2.07 with a correlation of 0.86 and for 8091 the exponent was determined to be 1.72 with a correlation of 0.78. These data are consistent with the observation that generally small fatigue crack growth rates are proportional to ΔK^2 (Wojcik et al, 1988). Considering the scatter in the results and the probability that the exponent in the Paris law equation is actually the same for 8090 and 8091, it appears that the small fatigue crack growth rates observed in this work follow the

relation

$$\frac{da}{dN} = C_1(\Delta K)^2 \qquad (5.38)$$

Equation 5.38 is not the same as the equation that Murakami (1988) used (Equation 5.33) to describe the growth behaviour of small fatigue cracks. That difference will now be examined more closely to see how the derivation of the Coffin-Manson relation is affected.

If the definition of ΔK is substituted into Equation 5.38 the result is

$$\frac{da}{dN} = C_2(\Delta\sigma)^2 a \qquad (5.39)$$

Equation 5.39 only differs from Equation 5.33 in that the exponent is specified as two and $\Delta\sigma$ is used instead of $\Delta\epsilon_p$. $\Delta\sigma$ can be related to $\Delta\epsilon_p$ through the following equation that describes the cyclic stress-strain behaviour.

$$\Delta\sigma = k' \Delta\epsilon_p^{n'} \qquad (5.40)$$

Substituting Equation 5.40 into 5.39 results in

$$\frac{da}{dN} = C_3(\Delta\epsilon_p)^{2n'} a \qquad (5.41)$$

Integrating this equation to derive the Coffin-Manson equation results in

$$\Delta\epsilon_p N_f^{1/2n'} = C_4 \qquad (5.42)$$

The problem with this equation is that unrealistically high exponents for N_f are predicted. Using the value of n' observed in this work (approximately 0.1), $1/2n'$ would equal 5. This is well outside the normal range for the Coffin-Manson exponent (0.5 to 0.7).

This problem emerges because the plastic strains in small fatigue crack characterization are typically small in magnitude as compared to the elastic strains. For example, using the cyclic stress-strain data discussed in section 4.2.2, the plastic strain for unstretched 8091 at $\sigma/\sigma_{ys} = 0.85$ is 3.4×10^{-4} whereas the elastic strain is over an order of magnitude greater at 4.6×10^{-3}.

The elastic strains contribute significantly to the driving force for crack propagation.

The observation that, for the small fatigue cracks studied in this work, the global elastic strains were larger than the global plastic strains is important because in LCF the plastic strains are normally much larger than the elastic strains. This raises the question of whether small fatigue crack behaviour is truly comparable with LCF behaviour. It is still true that LCF life is dominated by the crack propagation rate of small cracks. However, in LCF the small fatigue cracks are propagated under higher stresses where plastic strain dominates. The key issue that must be addressed, then, is whether the small fatigue cracks in LCF specimens (where plastic strains are high) behave differently from the small fatigue cracks studied in this work (where the plastic strains were small).

The amount of plastic strain will be a function of the stress level. In this work, no effect of stress level on small fatigue crack propagation was observed in the range $0.7 \leq \sigma/\sigma_{ys} \leq 0.85$. The effect of stress level has been examined over a wider range by Hudak et al (1988). Their data indicate that small fatigue crack behaviour is insensitive to the fraction of the yield stress employed up to about $\sigma/\sigma_{ys}=1.1$. Small fatigue cracks appeared to grow very slightly faster at $\sigma/\sigma_{ys}=1.6$ but the considerable data scatter makes this conclusion doubtful. In no case, however, did the exponent in the Paris law relation appear to change. Based on these observations, it seems reasonable to conclude that small fatigue crack behaviour would be the same for the conditions typical of LCF and for the conditions typical of small fatigue crack characterization.

It also appears to be reasonable, then, to take the critical

parameter as being the total strain. In the LCF regime this would be approximately equal to the plastic strain and in the small fatigue crack regime this is approximately equal to the elastic strain. Therefore, instead of using Equation 5.40, which related $\Delta\sigma$ to Δe_p, it would be appropriate to relate $\Delta\sigma$ to the total strain. Because the plastic strains are so small compared with the elastic strains, they will be neglected which reduces the relation betwen stress and strain to Hooke's law i.e.

$$\Delta\sigma = E\Delta\epsilon \qquad (5.43)$$

Substituting equation 5.43 into 5.39 results in the following expression.

$$\frac{da}{dN} = C_3(\Delta\epsilon)^2 a \qquad (5.44)$$

If this equation is integrated and rearranged Equation 5.45 is derived.

$$\Delta\epsilon N_f^{1/2} = C_4 \qquad (5.45)$$

This equation is compatible with the expected value of the exponent in the Coffin-Manson relation (0.5 to 0.7).

Thus, it has been demonstrated that the Paris law equation which describes small fatigue crack growth in this work can be used to derive the Coffin-Manson relation for LCF. Furthermore, it is apparent that the exponent in the Coffin-Manson relation is approximately the inverse of the exponent observed in the Paris law expression describing small fatigue crack growth rates. Theories based on fundamental principles have been proposed for both the exponent in the Paris Law equation (see Section 5.5.1) and for the exponent in the Coffin-Manson relation. In the following section, the theories relating the exponent in the Coffin-Manson relation to cyclic stress-strain behaviour will be discussed. The coefficients in the Paris law and the Coffin-Manson relation are also related but since

they are purely empirical parameters in both cases, it is doubtful that any useful information can be derived from their relationship.

5.4.3 THE RELATION BETWEEN CYCLIC STRESS-STRAIN BEHAVIOUR AND SMALL FATIGUE CRACK BEHAVIOUR

Two quantities that describe cyclic stress-strain curves are the cyclic strain hardening coefficient (k') and the cyclic strain hardening exponent (n'). Of these two quantities, only n' has been related to fatigue behaviour. Tomkins (1968), for example, used the Dugdale model of a crack to derive the following equation which relates the cyclic strain hardening exponent (n') to the Coffin-Manson exponent (m).

$$m = \frac{1}{1 + 2n'} \qquad (5.46)$$

A similar semi-quantitative expression (Morrow, 1965) which appears to agree more closely with experimental data (Grosskreutz, 1971) is given by

$$m = \frac{1}{1 + 5n'} \qquad (5.47)$$

Previously in this chapter it was argued that the exponent in the Paris law expression describing small fatigue crack growth is the inverse of the exponent in the Coffin-Manson relation. Therefore, the exponent in the Paris law for small fatigue cracks should be related to the cyclic strain hardening exponent by Equation 5.48 where c is either two or five depending on whether Equation 5.46 or 5.47 is assumed to be correct.

$$p = 1 + cn' \qquad (5.48)$$

In order to examine the validity of this expression, variations in the cyclic strain hardening exponent were desired. As can be seen from the following table, the values of n' associated with underaged alloys were significantly higher than those associated

with peakaged alloys. It can also be seen that duplex ageing and stretching had no significant effect on n'. A comparison of the associated cyclic stress-strain curves for the peak aged and underaged alloys is shown in Figure 5.10.

Alloy	n'
8090 stretched, peakaged	0.08
8090 unstretched, peakaged	0.10
8090 duplex aged, peakaged	0.09
8091 stretched, peakaged	0.08
8091 unstretched, peakaged	0.08
8091 duplex aged, peakaged	0.11
8091 stretched, underaged	0.18
8091 unstretched, underaged	0.24

Based on these data an average n' for the peakaged materials was taken as 0.09 while for the underaged materials the average n' was taken as 0.24. If c is taken to be 5, as has been found to more closely agree with experiment (Grosskreutz, 1971), then the estimates of p would be 1.45 for the peakaged materials and 2.20 for the underaged materials. The actual measurements of p (see section 5.4.2) were 2.07 for peakaged 8090 and 1.72 for peakaged 8091 and it was felt that the true value of p for the peakaged materials was close to two. Therefore, equation 5.48 somewhat underestimates p for the peakaged materials.

Furthermore, the expectation that an increase in n' will lead to a higher Paris law exponent for small fatigue cracks was not suppported by the experimental evidence in this work. Comparison of small fatigue crack growth in peakaged and underaged materials in section 4.3.4 found no significant differences between small fatigue crack growth rates. It should be pointed out, however, that the predicted difference is not great and the data on underaged materials is somewhat limited.

5.5 MECHANISMS OF FATIGUE CRACK GROWTH

As the conclusion of this thesis is approached, it is worthwhile speculating on how small fatigue crack behaviour might illuminate fatigue crack growth in general. In this section, the general principles of the current theories of fatigue crack propagation will be briefly described. Then, features of small fatigue crack behaviour will be used to provide a perspective on fatigue crack growth mechanisms in general.

5.5.1 DESCRIPTION OF FATIGUE MECHANISMS

There are basically two schools of thought as to the mechanism for fatigue crack propagation. One is that the ductility of the growth process results from the plastic shearing off of material immediately ahead of the crack tip. A second is that the material ahead of the crack tip loses the capacity to resist further deformation over a period of time and eventually fractures resulting in an increment of crack growth. Both of these theories have a certain physical appeal and both have evidence backing them up. Therefore, both will be discussed beginning with theories based on ductility exhaustion.

When postulating an exhaustion mechanism for crack growth a criterion for exhaustion is implicit. Weertman (1978), in a review of fatigue mechanisms, identified the criteria as accumulated plastic strain and accumulated plastic displacement. If the stress is assumed to be constant within the plastic zone these criteria are equivalent to accumulated plastic work density and accumulated plastic work respectively. If either accumulated plastic strain or accumulated plastic work density is taken as the criterion for exhaustion, crack growth rate is expected to be proportional to ΔK^2.

On the other hand adoption of the accumulated plastic displacement or accumulated plastic work criteria lead to crack growth rate being proportional to ΔK^4.

The shear sliding model is based on successive shear on planes angled to the crack plane followed by reversed shear on the same or parallel planes (see Figure 5.11). If this model is assumed, it seems reasonable to conclude that crack growth rate will be dependent on geometry. On this basis, Liu (1961) suggested that the crack growth rate must be proportional to the length of the crack itself because in large specimens the crack length is the only geometrical factor. Alternatively, it has been suggested that the crack growth rate should be related to the CTOD (Beilon and Antolovich, 1983). In either case it is predicted that the crack growth rate will be proportional to ΔK^2.

Perhaps the strongest support for this model is the direct observations made by Neumann (1974) of fatigue crack growth on {001} planes in single crystal copper samples. The slip was confined to a {111} plane on each side of the crack. There was virtually no slip in a triangular shaped region in the direction of crack propagation. He also observed that the crack tip closed in compression by slip reversal. Other support for this model can be found in the work of Garrett and Knott (1976) who annealed a specimen containing a fatigue crack to remove any damage caused by the fatigue and then continued with the fatigue test. Ductility exhaustion theories would predict a pause in the crack growth rate while damage accumulated ahead of the crack tip. Sliding off theories would not require a pause and, in fact, no pause was observed.

One criticism of the shear sliding model is that the supporting

evidence was generated on pure metals and may not apply to commercial materials where slip is complicated by microstructural features such as precipitates. A second is that the supporting evidence was also generated at high rates of crack growth so that the crack growth mechanism could be better observed. Laird (1978) has countered these criticisms by arguing that as long as sufficient ductility exists to counter static modes of failure, there is no reason to expect crack tip geometries in commercial materials to be different. He has also observed that striations appear much the same at high growth rates as at low growth rates and thus there is no reason to expect a different mechanism - again, of course in the absence of static modes of failure. Nonetheless, the issue of the mechanism responsible for fatigue is still in dispute.

It is worthwhile emphasizing that the mechanisms discussed in this section were suggested with application to long cracks. That is, as Weertman (1978) pointed out, the fatigue crack is assumed to be infinitely deep to reduce the problem to two dimensions, and small scale yielding is assumed. However, striations have been observed in both long and small cracks which indicates that the fundamental mechanism of crack growth might nonetheless be the same. In the next section, aspects of small fatigue crack growth will be examined that pertain to crack growth mechanisms.

5.5.2 THE BEHAVIOUR OF SMALL FATIGUE CRACKS

The Paris law exponent for the small fatigue cracks studied in this work was determined to be two (see section 5.4.2). Unlike long fatigue cracks, a value of two for the Paris law is a very common result in work on small fatigue cracks (Wojcik et al, 1988). As it has already been shown that the exponent in the Coffin-Manson

expression should be the inverse of the exponent in the Paris law expression for small fatigue cracks, it is also consistent with the frequent observation of about 1/2 for the Coffin-Manson exponent. Finally, it has been observed that small fatigue crack data sets generated on FCC single crystals tend to overlap one another (Brown and King, 1986). These observations suggest that there is a single, fundamental fatigue mechanism responsible for small fatigue crack growth. Examination of small fatigue crack behaviour, then, should improve our understanding of this fatigue mechanism.

One characteristic of small fatigue crack growth, already discussed, is the Paris law exponent of two. This characteristic is consistent with the sliding off mechanism where the crack extension should be proportional to the CTOD (CTOD is proportional to ΔK^2). It is also consistent with the exhaustion mechanism if the criterion for exhaustion is either plastic strain or accumulated plastic work density. It is, however, inconsistent with the exhaustion criteria of accumulated plastic displacement or accumulated plastic work.

Another widespread characteristic of small fatigue crack growth is the tendency to propagate along slip bands. The importance of the slip band is highlighted by the success of models that predict small fatigue crack retardation on the basis of slip band blocking (Tanaka and Nakai, 1983). Similarly, the dependence of small fatigue crack growth on grain size can be related to slip band length. This tendency suggests that it is the shear stresses ahead of the crack tip that are important to the growth of small fatigue cracks. This conclusion is supported by the observation of crack growth primarily at oblique angles to the applied stresses or, in other words, near to planes where the shear stresses are maximized.

The importance of shear stresses may also partially explain the relative rapidity of small fatigue crack growth as compared with long fatigue crack growth. Previously, it has been mentioned that small fatigue cracks are typically surface cracks and, so, under conditions of plane stress. Under plane stress conditions, one of the principal stresses is zero and so the shear stresses are higher than those found in plane strain conditions which are typical for long fatigue crack growth experiments.

Unfortunately, while the tendency to propagate along slip bands appears to be a characteristic of the mechanism of small fatigue crack growth, it cannot be used in the same way as the Paris law exponent to distinguish between the shear sliding model and the damage accumulation model. In the shear sliding model, crack growth is produced by the movement of dislocations along slip bands and so it is reasonable that crack growth would also favour slip planes. In the damage accumulation model, it seems reasonable that damage would accumulate predominantly along slip bands and so, once again, crack growth on slip planes would be favoured.

A final characteristic of small fatigue crack growth is the relative insensitivity of growth rate to precipitate distribution. This observation is consistent with the relative insensitivity of LCF to precipitate distribution previously discussed. The insensitivity of small fatigue crack growth to precipitate distribution is interesting as it suggests that there is little that can be done to improve a material's resistance to small fatigue crack growth, with the possible exception of refining the grain size. Like the tendency of small fatigue cracks to propagate along slip bands, however, it is difficult to see how this observation could be used to distinguish between the shear sliding and exhaustion models of fatigue as both processes

occur on a larger scale than precipitate distributions.

5.5.3 RELEVANCE TO LONG FATIGUE CRACK GROWTH

Having discussed the characteristics of the mechanism responsible for small fatigue crack growth, it remains to relate those characteristics to long fatigue crack growth. Similarity of long and small fatigue crack growth mechanisms might be expected since both have been associated with the formation of striations. If so, it implies that the characteristics of small fatigue crack growth should also apply to long fatigue crack growth.

There are, however, several differences, even discounting the difference in rapidity, between small and long fatigue crack growth behaviour. Firstly, for long fatigue cracks, Paris law exponents have been measured over a range from 2-4 or even higher (Lindley et al, 1976). Secondly, long fatigue crack growth is generally macroscopically smoother and the cracks are often Mode I in nature as opposed to small fatigue cracks which are typically crystallographic. Thirdly, long fatigue crack rates are sensitive to precipitate size and distribution whereas small fatigue crack rates are not.

The range of Paris law exponents characteristic of long fatigue cracks is troubling to those attempting to find a fundamental mechanism for fatigue crack growth as it would seem that if there is a fundamental fatigue mechanism, there should be a unique power law relation between crack growth rate and the crack driving force. The range of Paris law exponents observed in long cracks also makes evaluation of proposed models for fatigue difficult as there is always a set of data that fits the model (Birol, 1989). The lack of consistency in Paris law exponents suggests that more than one

mechanism may be responsible for long fatigue crack growth. This seems reasonable as changes in the slope of da/dN vs ΔK curves for long cracks at high values of ΔK are attributed to the crack growth mechanism changing to a static mode such as void nucleation ahead of the crack tip. It is, therefore, suggested that the existence of multiple exponents in the Paris law describing long fatigue crack growth implies the existence of multiple mechanisms responsible for long fatigue crack growth. Furthermore, it is suggested that, when the Paris law exponent describing long fatigue crack growth rates is approximately two, it is likely that the mechanism of fatigue is the same as typically observed for small fatigue cracks.

It has been mentioned that long fatigue crack paths tend to be smoother than small fatigue crack paths. This is quantifiably confirmed in the table below where the roughness parameters (R_L) observed for the small fatigue cracks in this work are compared with the roughness parameters associated with long fatigue cracks (R=0.7) in the same materials (Peacock and Martin, 1989).

Material	Long fatigue crack R_L	Small fatigue crack R_L
8090 stretched	1.10	1.19
8090 unstretched	1.15	1.40
8090 duplex aged	1.24	1.38
8091 stretched	1.04	1.19
8091 unstretched	1.06	1.28
8091 duplex aged	1.19	1.36

The smoother crack path under mode I loading, typical of long fatigue cracks, is likely to be a function of the state of stress ahead of the crack tip. It has already been pointed out the shear stresses ahead of a small fatigue crack would be expected to be higher because one of the principal stresses is zero. This would encourage fatigue mechanisms that depended upon shearing ahead of the crack tip. This may also indicate why a wider variety of fatigue

mechanisms is seen in long fatigue cracks. The stresses ahead of a long fatigue crack are triaxial and all in tension. The hydrostatic stresses would encourage alternative mechanisms such as void formation and coalescence.

Finally, the relative insensitivity to precipitate size and distribution of small fatigue crack growth as compared to long fatigue crack growth may be a function of the influence of closure on fatigue crack growth. In long fatigue cracks the effect of roughness-induced closure is reduced at high stress ratios where closure levels are reduced. Similarly, in small fatigue cracks closure levels are low and so the effect of preciptate distribution is reduced. This may be particularly emphasized in small fatigue cracks as the proximity of small fatigue cracks to a free surface may reduce slip reversibility, as discussed in Chapter Four, which also would relate fatigue crack growth rate to precipitate size and distribution.

Despite these differences, the study of small fatigue crack behaviour is relevant to understanding long fatigue crack behaviour. Because both mechanisms have been observed to result in striations, it seems likely that the same mechanism responsible for small fatigue crack growth applies to long fatigue crack growth. In small fatigue cracks, however, the mechanism appears to be more universal. As indicated previously, this may be partly due to the plane stress conditions ahead of the crack tip which encourage fatigue mechanisms based on shear. In small fatigue cracks, there is also the advantage that phenomena such as crack closure and slip reversibility, which might obscure observation of a basic fatigue mechanism, are reduced.

Although the above discussion failed to define a unique

mechanism of fatigue, several points emerging from that discussion are worth emphasizing. Firstly, the mechanism of small fatigue crack growth is inconsistent with the plastic displacement and the accumulated plastic work criteria for exhaustion. Secondly, the studies of small crack growth and LCF behaviour suggest that a Paris law exponent of two may be characteristic of a fundamental fatigue mechanism. Thirdly, this fatigue mechanism appears to be insensitive to precipitate structure. This suggests that the primary effect of precipitate structure is on extrinsic phenomena such as closure. Furthermore, the relative insensitivity of the mechansism responsible for small fatigue crack growth rates to precipitate structure suggests that, in order to produce materials with improved long or small fatigue crack growth resistance, particular emphasis must be placed on increasing levels of closure.

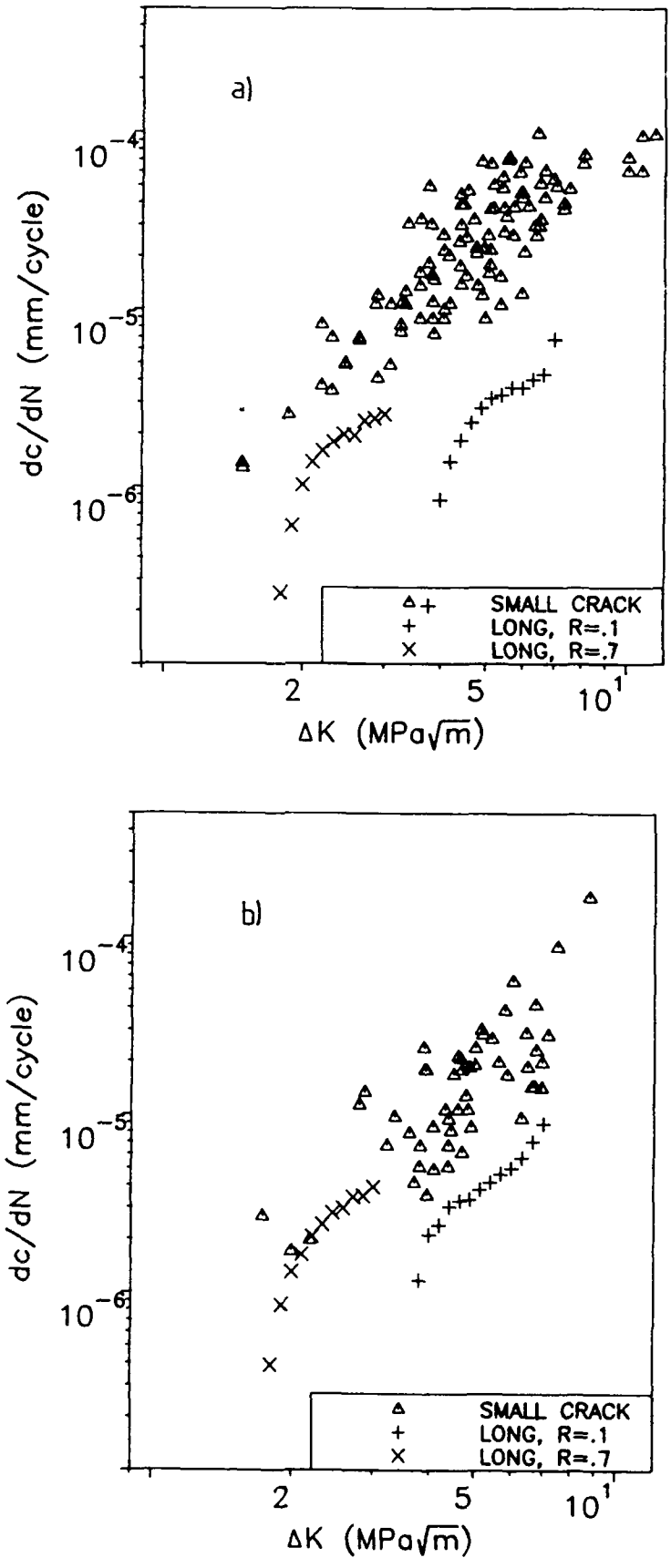

Figure 5.1 Comparison of long and small fatigue crack data using a ΔK corrected for the the effect of higher order terms for a) 8090 b) 8091.

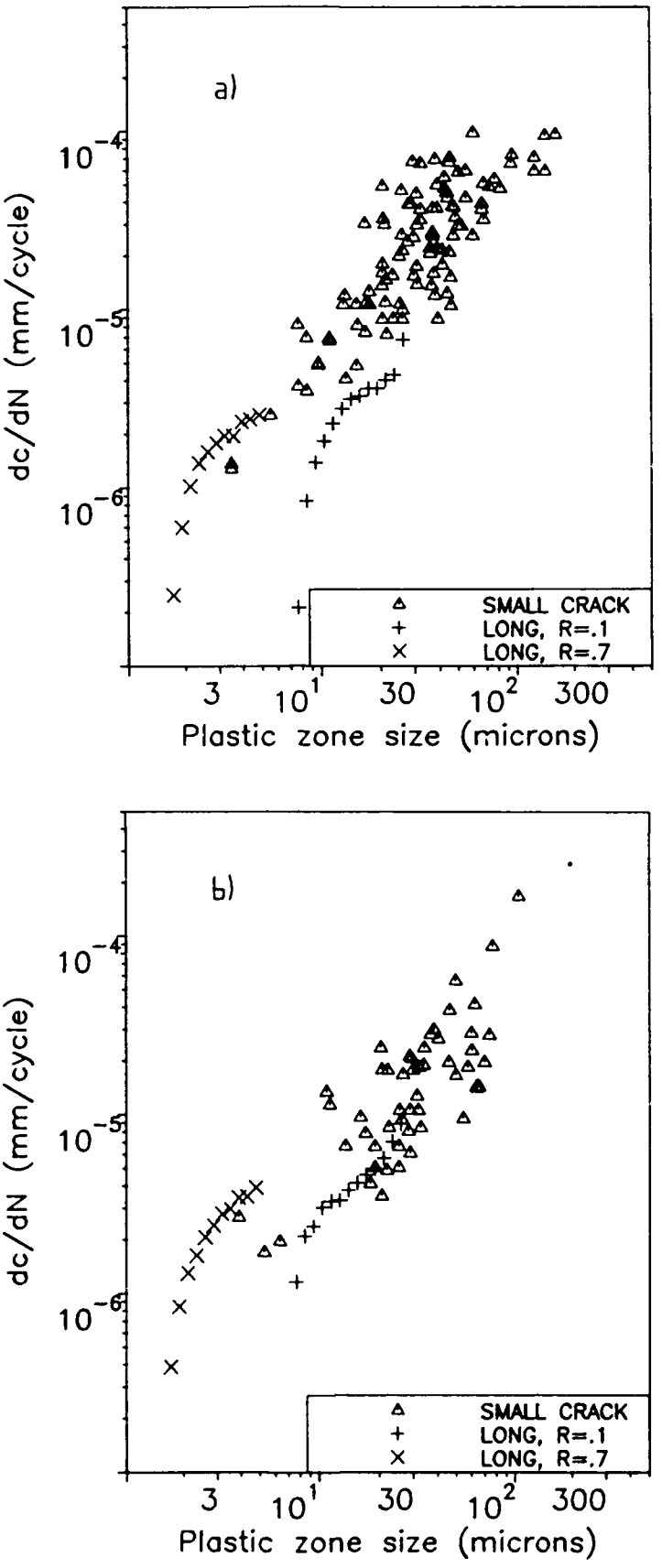

Figure 5.2 Comparison of long and small fatigue crack data using plastic zone size a) 8090 b) 8091.

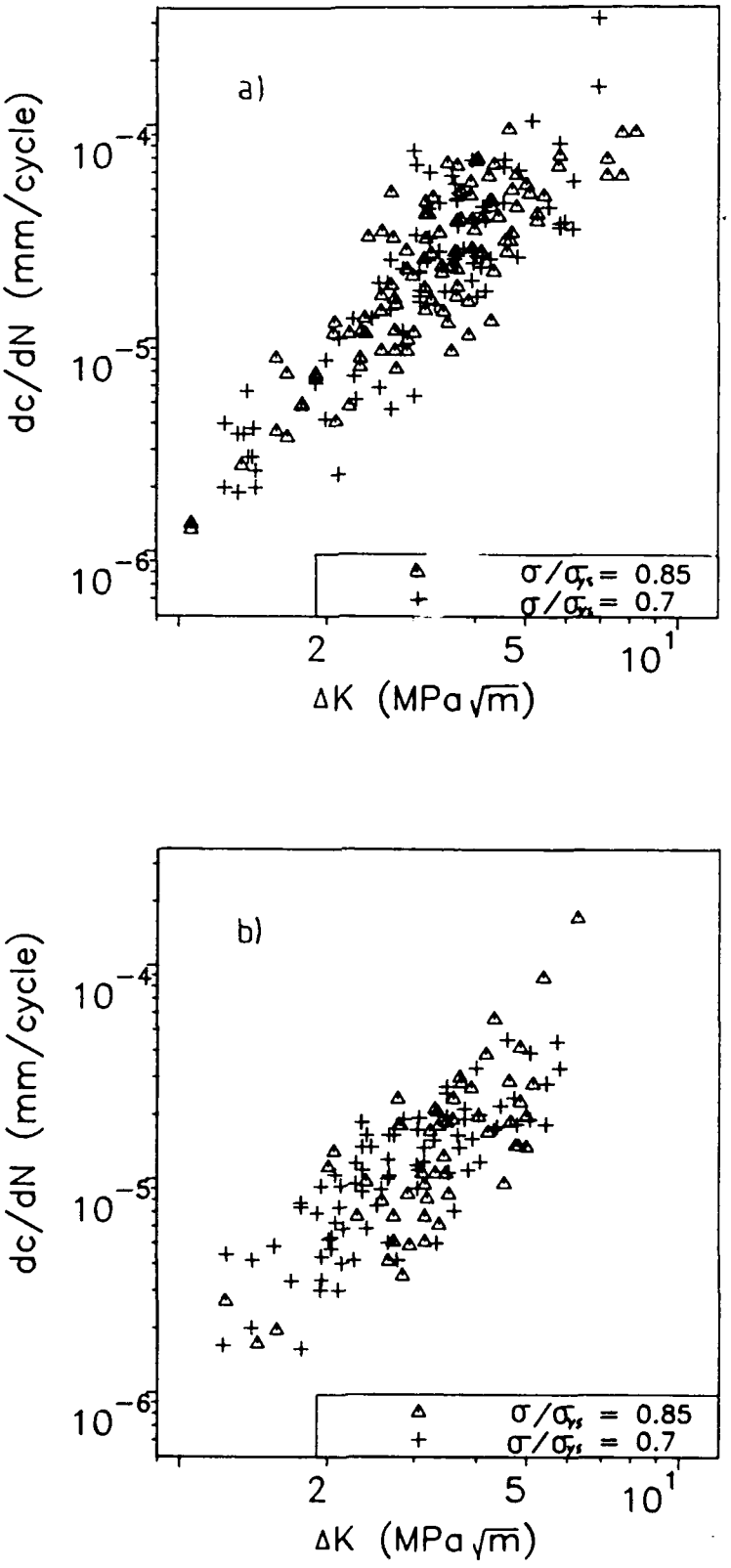

Figure 5.3 Comparison of small fatigue crack data generated at σ/σ_{ys}=0.7 and 0.85 for a) 8090 b) 8091.

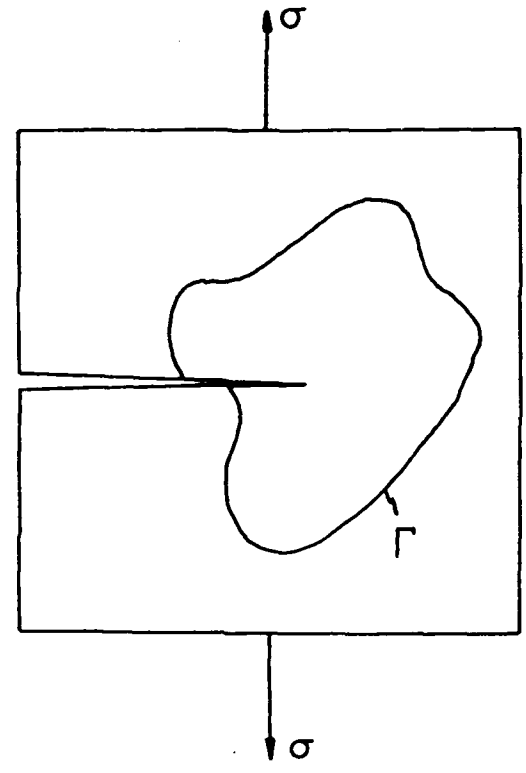

Figure 5.4 Illustration of line contour around crack tip.

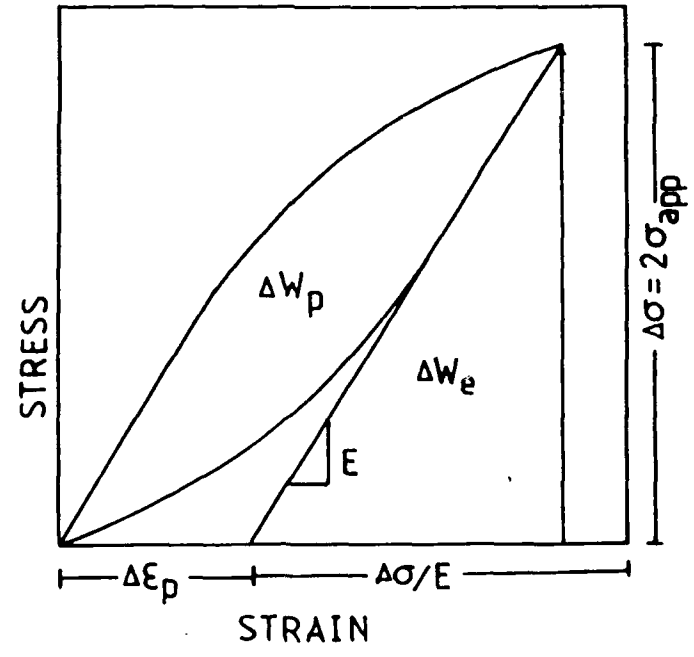

Figure 5.5 Schematic showing plastic and elastic contributions to cyclic stress-strain behaviour (after Dowling, 1977).

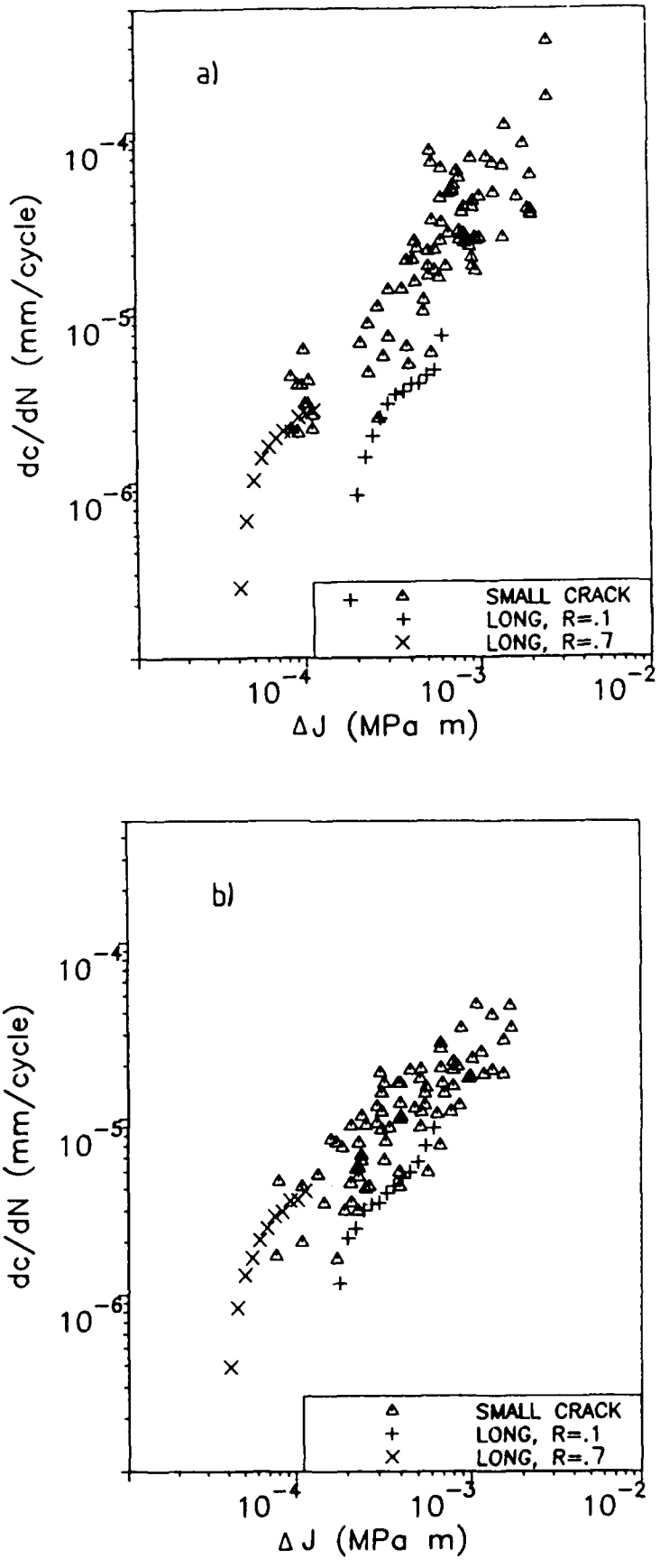

Figure 5.6 Comparison of long and small fatigue crack data using ΔJ based on Dowling's approach for a) 8090 b) 8091.

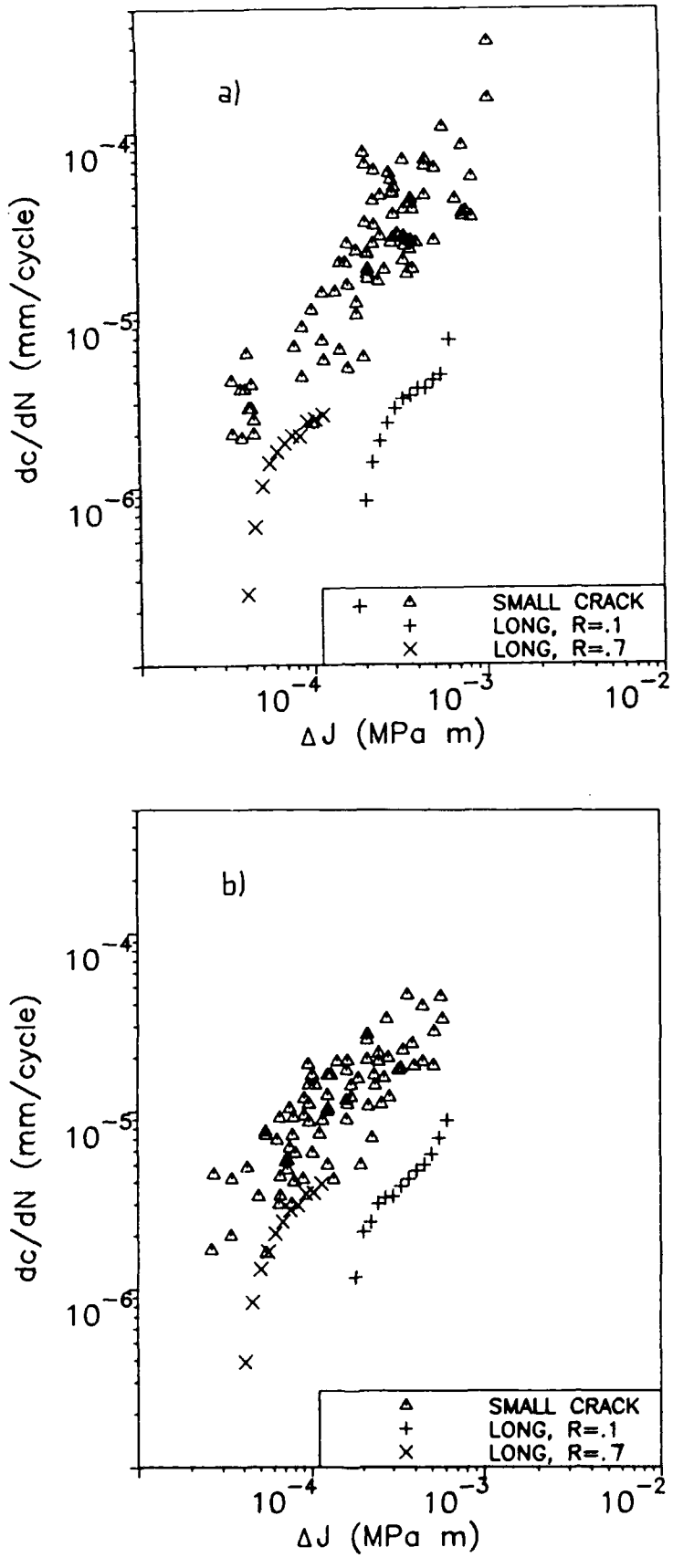

Figure 5.7 Comparison of long and small fatigue crack data using ΔJ based on Chan's approach for a) 8090 b) 8091.

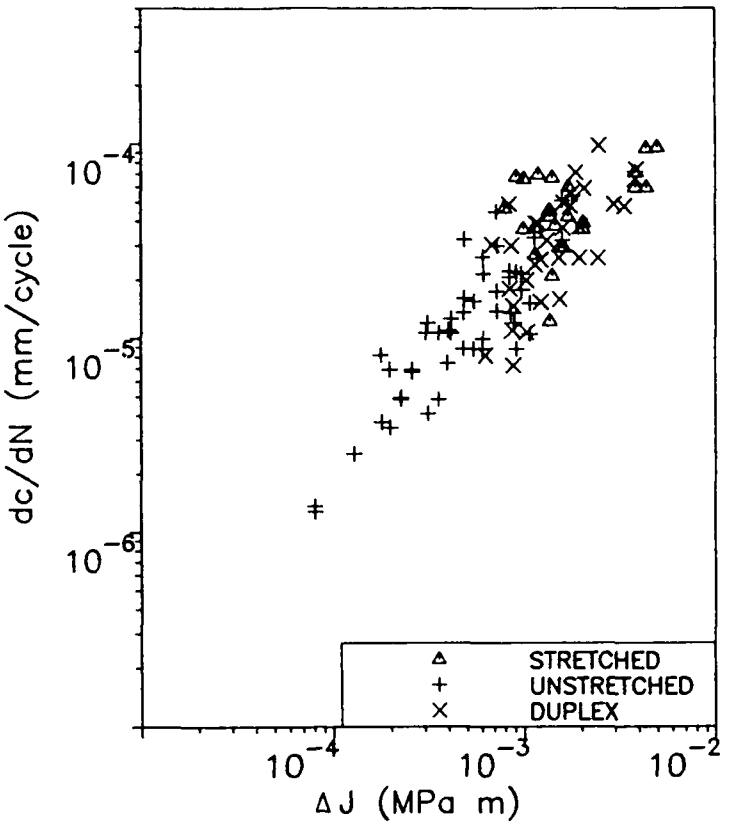

Figure 5.8 Comparison of small fatigue crack data using ΔJ for 8090.

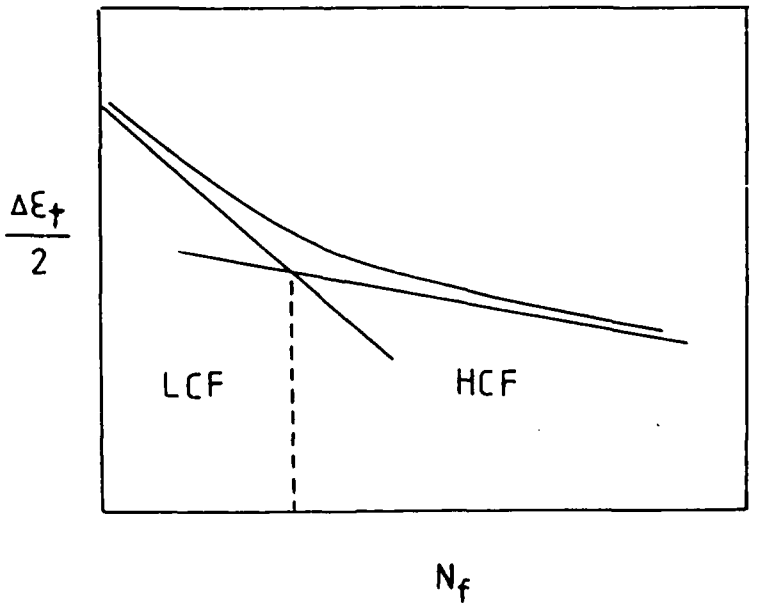

Figure 5.9 Illustration of strain life curve showing low cycle fatigue regime.

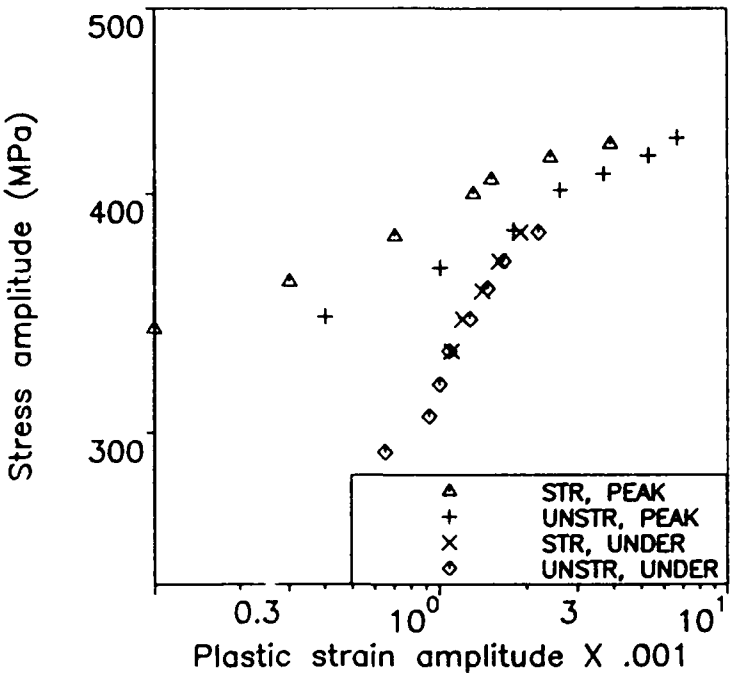

Figure 5.10 Cyclic stress-strain data for underaged and overaged 8091 compared with peak aged 8091.

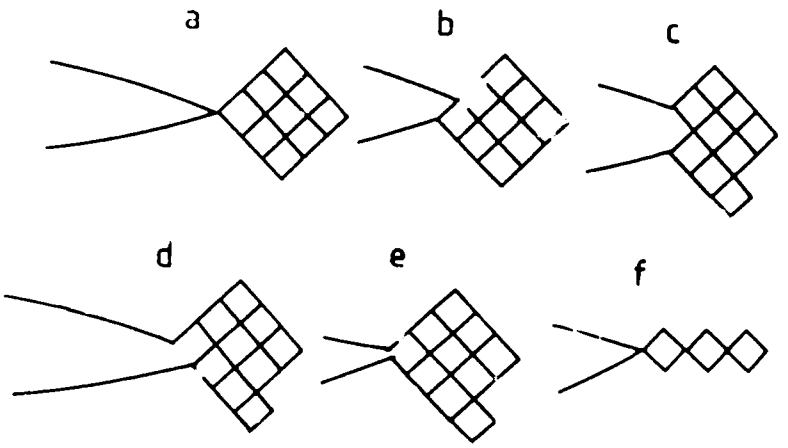

Figure 5.11 Illustration of the shear sliding mechanism of fatigue crack growth. Tensile loading results in crack blunting in a-c. Compressive loading closes crack in d and e but crack has advanced one block. Crack advance after a number of cycles is shown in f (After Weertman, 1978).

Material	σ/σ_{ys}	r_p/a
8090 unstretched	0.85	0.60
8090 unstretched	0.85	0.45
8090 unstretched	0.85	0.76
8090 unstretched	0.85	0.79
8090 duplex aged	0.85	0.66
8091 duplex aged	0.85	0.52
8090 unstretched	0.70	0.52
8091 unstretched	0.70	0.35
8091 duplex aged	0.70	0.45
8091 duplex aged	0.70	0.47
8091 duplex aged	0.70	0.45
8091 duplex aged	0.70	0.62
8091 duplex aged	0.70	0.57

Table 5.1 Compilation of plastic zone size data gathered from SACP measurements.

Material	σ/σ_{ys}	Approach used	C $x10^{-5}$
8090 stretched	0.85	Dowling	7.39
8090 unstretched	0.85	Dowling	7.17
8090 duplex aged	0.85	Dowling	11.5
8091 stretched	0.85	Dowling	6.44
8091 unstretched	0.85	Dowling	6.97
8091 duplex aged	0.85	Dowling	7.97
8090 stretched	0.7	Dowling	5.33
8090 unstretched	0.7	Dowling	5.48
8090 duplex aged	0.7	Dowling	5.98
8091 stretched	0.7	Dowling	5.20
8091 unstretched	0.7	Dowling	5.18
8091 duplex aged	0.7	Dowling	5.59
All materials	0.85	Chan	2.22
All materials	0.7	Chan	1.74

Table 5.2 Compilation of coefficient C's for calculation of ΔJ using the expression $\Delta J = C\Delta K^2$.

CHAPTER 6

CONCLUSIONS AND FUTURE WORK

6.1 CONCLUSIONS

At the end of Chapter Two several research objectives for this work were outlined. In this section, these objectives will be restated for reference and discussed on the basis of the results of this thesis. For clarity the objectives will be underlined and are stated exactly as they were originally stated in Chapter Two.

Define the relation between the behaviour of small fatigue cracks and the size and distribution of precipitates. Particular emphasis will be placed on the distribution of slip and on the role of slip reversibility on small fatigue crack behaviour.

In this work stretching and duplex ageing were used to vary the distribution of the slip homogenising S' phase and thus the distribution of slip. TEM observations confirmed that in the stretched and duplex aged materials there was a relatively uniform distribution of S' while, in the unstretched materials, the S' was heavily concentrated on grain and subgrain boundaries. Mechanical testing and measurements of the lineal roughness parameters of small cracks showed that the slip was more homogeneous in the stretched alloys than in the unstretched or the duplex aged alloys. The lack of slip homogeneity in the duplex aged materials was surprising in view of the uniformity of the S' distribution. This was found to be due to the small diameter of the S' precipitates in the duplex aged materials. A model was developed that showed that the precipitates in the duplex aged materials would be sheared rather that looped by dislocations and thus lost effectiveness as slip homogenisers.

In neither 8090 or 8091 was any effect of slip distribution on

small fatigue crack growth observed. This is in sharp contrast to long fatigue crack behaviour where increased planarity of slip increases fatigue crack growth resistance. Primarily, the lack of an effect of slip distribution is attributed to reduced closure levels in small fatigue cracks. Secondarily, the proximity of the plastic zone associated with a small crack to a free surface inhibits slip reversibility which, in long fatigue cracks, also contributes to the effect of slip distribution on crack propagation rate.

In addition, the effect of overageing and underageing 8090 and 8091 on small fatigue crack growth was examined. Here also, the alterations to the precipitates had no effect on small fatigue crack growth. Therefore, it is concluded that small fatigue crack growth is insensitive to precipitate size and distribution.

Compare the behaviour of small fatigue cracks in 8090 and 8091. Explain differences in small fatigue crack behaviour based on the differences in grain size, texture and copper content for the two alloys.

Small fatigue cracks in 8091 grew approximately twice as fast as small cracks in 8090. The differences between the two alloys were a higher copper content in 8091, different grain size, and a modest difference in texture. The primary effect of the higher copper content would be to encourage the precipitation of S' and T_1, both of which would have slip homogenising effects. As was just discussed, however, the distribution of slip had no effect on small fatigue crack behaviour. Thus, copper content is unlikely to be responsible for the variation in small fatigue crack propagation rate in these alloys. The difference in texture between the two alloys was minor and did not cause any apparent differences in the crack path. Furthermore, small crack fatigue tests on T-L specimens of

8091 showed no effect of texture on crack propagation rates. Therefore, texture seems unlikely to be responsible for the difference in crack growth rate between 8090 and 8091. By elimination, this leaves the grain size as the most likely explanation. While no experiments were done to prove this conclusively, other work has shown that small fatigue crack growth rates are affected by grain size. This work highlighted, in particular, the importance of the smallest grain size measurement. In this case, the grain size in the S direction was identified as the critical factor.

Examine the suitability of using ΔK as a correlating parameter when investigating microstructural effects on small cracks. This will include examining the method of calculating ΔK and determining whether the use of ΔK for physically and mechanically small cracks obscures microstructural effects.

Two approaches were used in this work to calculate ΔK. One approach was based on a crack shape projected on to the plane normal to the applied stress. The other attempted to incude the effects of crack branching and inclination through calculating K_I, K_{II} and K_{III} and then combining them into a single term. Both approaches resulted in the same relationship between small crack growth rate and ΔK and there was little effect on data scatter. This was primarily attributed to the observation that the steep angle of crack inclination toward the centre-line of the specimen made crack kinking and inclination on the surface virtually irrelevant to the calculation of ΔK. Nevertheless, the results of this thesis indicate that the method used to calculate ΔK has no significant effect on the results obtained and, therefore, the method used to calculate ΔK does not affect the suitability of ΔK for observing microstructural effects.

The primary effect of physical smallness is to reduce closure levels. While this certainly reduces the influence of microstructurally induced closure on small fatigue crack growth, the effect is real and not an artifact introduced by the the use of ΔK. *Therefore, physical smallness is unlikely to affect the suitability of* ΔK for characterizing microstructural effects on small crack growth.

Mechanical smallness, the proximity of the crack to the surface and the high stresses required to initiate and propagate small cracks all lead to large scale yielding. Calculations of the plastic zone based on K were shown to be inaccurate, primarily because of the effect of the higher order terms in the solution for the stresses around the crack tip. However, the error in using ΔK was consistent for the materials examined. Furthermore, while the elastic-plastic parameter ΔJ was superior to ΔK as a correlating parameter when comparing long and small fatigue crack growth rates, the use of ΔJ did not change any conclusions as to the effect of microstructure. Therefore, the large scale yielding present in the small cracks studied in this work does not affect the suitability of ΔK when characterizing microstructural effects.

Compare long and small fatigue crack growth rates under nominally the same ΔK. Determine the causes of any differences in behaviour and if any other correlating parameters (eg ΔJ) are more effective when comparing long and small fatigue crack growth behaviour.

In this work, small fatigue crack growth rates were found to be significantly faster than long fatigue crack growth rates under the same nominal ΔK. In addition, the small fatigue cracks showed no sign of the fatigue threshold observed in long fatigue cracks. The differences between long and small fatigue crack behaviour were

shown to be partially caused by reduced closure levels in small fatigue cracks. Because of this, long and small crack growth rates were more similar when small fatigue crack growth rates were compared with long fatigue crack growth rates generated at R=0.7 (where closure levels are also small).

In addition, the proximity of small fatigue cracks to the surface, the high stresses applied in small fatigue crack testing and the comparability of plastic zone size and crack size. This violation of the small-scale yielding assumption also contributed to the observed differences between long and small fatigue crack behaviour. Correcting ΔK for the effect of the higher order terms in the solution for the stresses around a crack tip improved the correlation between long and small fatigue crack growth rates slightly. A better correlation, however, was obtained when ΔJ was used as the correlating parameter.

Plastic zone sizes for long and small cracks were calculated based on corrections for the higher order terms and for the different states of stress associated with small cracks as opposed to long cracks. When long and small fatigue crack growth rates were plotted as a function of the calculated plastic zone sizes, they were comparable. This suggests that the plane stress conditions typical for small fatigue cracks contributes to the discrepancy between long and small fatigue crack growth rates.

Examine the interplay between the physical "smallness", mechanical "smallness" and the effect of the microstructure on small fatigue crack behaviour.

As discussed previously, the primary effect of physical smallness is to reduce closure levels. Since one of the principal effects of the microstructure on long fatigue cracks is to affect the amount of

closure, the importance of the microstructural factors controlling closure is minor for small fatigue cracks.

On the basis of this thesis, it appears that the mechanical smallness and the reduced constraint near a free surface may also reduce the importance of the microstructure to small fatigue crack growth. Both the large scale yielding and the reduced constraint encourage activation of multiple slip systems despite the precipitate structure. Furthermore, the emergence of dislocations onto free surfaces forming steps that are unable to reverse their path reduces the slip reversibility independently of the microstructure.

Examine the relationship between low cycle fatigue, cyclic stress-strain behaviour, and small fatigue crack behaviour for micro-structural implications.

Since the time for crack initiation is insignificant for LCF behaviour, LCF life is a function of crack propagation behaviour. Since the cracks in LCF specimens are "small" for the majority of the life of an LCF specimen, LCF behaviour is specifically linked to small fatigue crack behaviour. This assertion is further confirmed by the similarity of microstructural effects on LCF and small fatigue crack growth rates. This latter observation is potentially significant since it may be possible to use LCF testing to characterize small fatigue crack behaviour without the somewhat tedious procedures necessary for direct observation of small fatigue cracks. Furthermore, the observed behaviour of small fatigue cracks may be independently verified by examination of the LCF behaviour.

It was also shown that the Paris law type expression describing the small fatigue crack growth behaviour observed in this work resulted in the prediction of a Coffin-Manson type relation for LCF. In that derivation the importance of the elastic component of

the strain to small fatigue crack growth was highlighted. The exponent in the Coffin-Manson expression was confirmed to be the inverse of the exponent in the Paris law expression.

Expressions relating cyclic stress-strain behaviour to the Coffin-Manson relation and thus to small fatigue crack behaviour were discussed. It was shown that changes in the cyclic strain hardening exponent, as were produced in underaged materials, should produce changes in the exponent observed in the Paris law relation describing small fatigue crack growth rates. Over the limited range investigated in this work, however, no such dependence of Paris law exponent on the cyclic strain hardening exponent was observed.

Examine the mechanism of small crack growth, the implications for general fatigue mechanisms and any implications for alloy development where small fatigue crack growth is a concern.

The small fatigue crack growth behaviour in this work was characterized by a Paris law exponent of two. A Paris law exponent of two appears to be a widespread characteristic of small fatigue crack growth. This is relatively consistent with the range of exponents observed in LCF for the Coffin-Manson relation (~0.5). The consistency of the exponent suggests that the mechanism of fatigue in small fatigue cracks is more uniform than that for long fatigue cracks where a wider range of exponents is observed. Contributing factors may include the reduction of such extrinsic effects, such as closure, and the planarity of stress ahead of small fatigue cracks specifically encouraging a single, shear dependent mechanism of fatigue.

The characteristics of the fatigue mechanism associated with small fatigue cracks include the proportionality of growth rate to

ΔK^2, an insensitivity to precipitate structure and a preference to propagate along slip bands. The proportionality of crack growth rate to ΔK^2 is inconsistent with the exhaustion mechanism of fatigue when the criterion for exhaustion is based on accumulated plastic work/plastic displacement. It is, however, consistent with either the shear sliding mechanism of fatigue or with the exhaustion mechanism when the criterion for exhaustion is accumulated plastic work density/plastic strain. The insensitivity of small fatigue crack behaviour to precipitate structure suggests that there is little that can be done to improve a material's resistance to small fatigue crack growth, with the possible exception of reducing the grain size. The tendency of small fatigue cracks to propagate along slip bands at oblique angles suggests that the mechanism is dependent upon shear stresses ahead of the crack tip.

The literature suggests that the fatigue mechanism responsible for small fatigue crack growth may sometimes be responsible for long fatigue crack growth since striations have been observed for both long and small fatigue cracks and a Paris law exponent of two is sometimes observed in long fatigue cracks. Since small fatigue cracks are less affected by such extrinsic phenomena as closure and slip reversibility, the study of this fatigue mechanism may be easier in small fatigue cracks than in long fatigue cracks.

6.2 FUTURE WORK

Although the results obtained were found to be relatively insensitive to the method of calculating ΔK and da/dN used in this work, this remains a major issue in the characterization of the behaviour of small fatigue cracks. Without standard procedures, comparability between the work of different laboratories will always

be an issue. Therefore, work is required to establish these standard procedures.

A related issue is the effect of crack shape on small fatigue crack growth. Some aspects of this, such as crack inclination and crack branching were referred to in this thesis. Other aspects such as deviations from a semi-elliptical shape, crack shape changes with growth, and variations in growth rate along the crack front perimeter should be addressed. This may be a suitable application for the acoustic microscope.

It is not always possible in practical applications to stretch materials prior to artificial ageing. For that reason, duplex ageing represents an important alternative. In this work, duplex ageing was not found to homogenise slip. This was due to the small diameter of the S' precipitates in the duplex aged alloys that allowed shearing rather than Orowan looping of the precipitates. It was also shown in this work, however, that changing the artifical ageing temperature affected the precipitate diameters and the slip homogenising capability of S'. Other processing variables, such as the solution treatment temperature or the length of the natural age could also have significant effects on precipitate size. Work is required to explore optimum treatments for various mixes of mechanical properties.

In this work and the work of others, the strain hardening rate has been found to be substantially higher in underaged materials. It has been hypothesized but not proven that this is due to the distribution of slip in the underaged materials (Jata and Starke, 1986). In view of the similarity of the work hardening rates in stretched and unstretched materials observed in this work, this explanation seems unlikely. More work is required to explain the

mechanism for this phenomenon.

A link between LCF behaviour and small fatigue crack behaviour has been established. Further work is required to compare microstructural effects on small fatigue crack and LCF behaviour. Additional work may show that, from the design standpoint, a knowledge of LCF behaviour is sufficient. This would avoid the rather arduous task of collecting small fatigue crack data. Finally, the amount of scatter typical for small fatigue cracks may be reduced as observation of LCF lifetimes would, in effect, average out crack growth rates over a number of cycles.

In this work, a tentative conclusion was reached that small fatigue crack behaviour was, at best, only weakly related to cyclic stress-strain behaviour. Further work, examining wider ranges of strain hardening exponents is required to confirm this conclusion.

The finding in this work that long and small fatigue crack growth rates were indistinguishable when plotted versus plastic zone size suggests that the state of stress is important to fatigue crack growth rates. Conflicting results have been obtained from long fatigue crack work done to determine the effect of the state of stress through changing specimen thickness. Therefore, further work is required to establish the reasons for the conflicting reports as to the effect of the state of stress on fatigue crack growth.

Finally, further work should be done to determine the mechanism for small fatigue crack growth. The literature contains many different models for fatigue and there is data to support each model. Small fatigue cracks may represent a regime where the fatigue mechanism is relatively simple partially due to the lack of the complicating effects of closure. It is likely that such work will also be applicable to fatigue crack growth in general.

REFERENCES

Agyekum, E. Ruch, W., Starke, E.A. Jr., Jha, S.C. and Sanders, T.H. (1986) *Aluminium-Lithium Alloys III*, eds. C. Baker, et al, Inst. of Metals, London, 448

Allen, R.J. and Sinclair, J.C. (1982) *Fat. Eng. Mat. Struct.*, 343

ASTM (1987) *1987 Annual Book of ASTM Standards*, ASTM, 3.01:199

Andrade, A., Freitas, M. (1987) *Fatigue 87*, R.O. Ritchie and E.A. Starke, Jr eds, EMAS, 271

Ardell, A.J. and Huang, J.C. (1988) *Phil. Mag. Letters*, 58:189

Banerjee, S. (1984), *A Review of Crack Closure*, AFWAL TR-84-4031

Baumann, S.F and Williams D.B. (1984) *Aluminum-Lithium Alloys II*, eds T. H. Sanders and E.A. Starke Jr. TMS-AIME, 17

Baxter, W.J. (1986) *The Behaviour of Short Fatigue Cracks*, K.J. Miller and E.R. de los Rios eds., Mech. Eng. Pub., 93

Beilon, J-P. and Antolovich, S.D. (1983) *ASTM STP 811*, AIME 313

Birol, Y. (1989) *J. of Mat. Sci.*, 24:2093

Bischler, P. and Martin, J.W. (1987) *4th Int. Aluminium Lithium Conf.*, eds G. Champier et al, les editions de physique, 761

Blom, A.F. (1986) *Small Fatigue Cracks*, R.O. Ritchie and J. Lankford eds, AIME, 623

Bolingbroke, R.K. and King, J.E. (1986) *The Behaviour of Short Fatigue Cracks*, K.J. Miller and E.R. de los Rios eds., Mech. Eng. Pub., 101

Breat, J.L., Mudry, F. and Pineau, A. (1983) *Fat. Eng. Mat. Struct.*, 6:349

Brechet, Y. and Livet, F. (1987) *4th Int. Aluminium Lithium Conf.*, eds G. Champier et al, les editions de physique, 717

Broek, D. (1978), *Elementary Engineering Fracture Mechanics*, Sijthoff & Noordhoff Publishers, The Netherlands, 3

Broussard, F. and Thomas, M. (1986) *Aluminium-Lithium Alloys III*, eds. C. Baker, et al, Inst. of Metals, London, 442

Brown, C.W. and Hicks, M.A. (1983) *Fat. Eng. Mat. Struct.*, 6:67

Brown, C.W., King, J.E. and Hicks, M.A. (1984), *Metal Science*, 18:374

Brown, C.W. and King, J.E. (1986), *Small Fatigue Cracks*, R.O. Ritchie and J. Lankford eds, AIME, 73

Brown, M.W. (1986), *The Behaviour of Short Fatigue Cracks*, K.J. Miller and E.R. de los Rios eds., Mech. Eng. Pub., 423

Cassada, W.A., Shiflet, G.J. and Starke, E.A. Jr. (1987) *4th Int. Aluminium Lithium Conf.*, eds G. Champier et al, les editions de physique, 397

Chakraborrty, S.B. (1979) *Fat. Eng. Mat. Struct.*, 2:331

Chan, K.S. (1986) *Small Fatigue Cracks*, R.O. Ritchie and J. Lankford eds, AIME, 407

Chan, K.S., Lankford, J., and Davidson D.L. (1986) *Trans. of the AIME*, 108:206

Chan, K.S. (1987) *Fatigue 87*, eds R.O. Ritchie and E.A. Starke, EMAS, 1801

Chan, K.S. and Lankford, J. (1988), *Acta Metallurgica*, 36:193

Cooke, R.J. and Beevers, C.J. (1974) *Mat. Sci. and Eng.*, 13:201

Coyne, E.J., Sanders, T.H. Jr., and Starke, E.A., Jr. (1981) *Proc. 1st Int. Aluminum-Lithium Conf.*, eds T.H. Sanders Jr. and E.A. Starke Jr., 293

Davidson, D.L. and Lankford, J. (1986) *Small Fatigue Cracks*, R.O. Ritchie and J. Lankford eds, AIME, 455

Davidson, D.L. (1988) *Acta Metallurgica*, 36:2275

Di, Z. Saji, S. and Hori, S. (1987) *4th Int. Aluminium Lithium Conf.*, eds G. Champier et al, les editions de physique, 753

Dover, W.D. and Boutle, N.F. (1978) *J. of Strain Analysis*, 13:129

Dowling, N.E. (1977), *ASTM STP 637*, ASTM, 97

Duga, J.J., Fisher, W.H., Buxbaum, R.W., Rosenfield, A.R., Buhr, A.R. Honton, E.J. and McMillan, S.C. (1983), *The Economic Effects of Fracture in the United States*, Battelle's Columbus Laboratories,

El Haddad, M.H., Smith, K.N., Topper,T.H. (1979), *J. of Eng. Mat and Tech.*, 101:42

El Haddad, M.H. and Miettinen, B.I. (1982), *Fatigue Thresholds*, J. Backland ed, EMAS, 827

Elber, W. (1970) *Engineering Fracture Mechanics*, 2:37

Ewalds, H.L. and Wanhill, R.J.H, (1985), *Fracture Mechanics*, Edward Arnold Ltd.

Farcy, L. Carre, C., Clavel, M., Barbaux, Y. and Aliaga, D. (1987) *4th Int. Aluminium Lithium Conf.*, eds G. Champier et al, les editions de physique,

Flower H.H., Gregson, P.J., Tite, C.N.J. and Mukhopadhay, A.K. (1986) *Al Alloys-Phys. and Mech. Prop.*, eds E.A. Starke and T.H. Sanders, 2:743

Flower, H.M. and Gregson, P.J. (1987) *Mat. Sci. and Tech.*, 3:81

Fox, A.G. and Fisher, R.M. (1988) *J. of Mat. Sci. Letters*, 7:301

Garret, G.G. and Knott, L.F. (1976) *Metall. Trans. A*, 7:884

Gentzbittel, J.M. and Fougere, R. (1987) *Scripta Metallurgica*, 21:1411

Gerdes, C., Gysler, A. and Lutjering, G. (1984), *Fatigue Crack Threshold Concepts*, D.L. Davidson and S. Suresh, AIME, 465

Gregson, P.J. and Flower, H.M. (1985) *Acta Metallurgica*, 33:527

Griffith, A.A. (1920) *Phil. Trans., Royal Society of London*, A221:163

Grosskreutz, J.C. (1971) *Phys. Stat. Sol. B*, 47:359

Gu, B.P. Mahalingham, K., Liedl, G.L. and Sanders, T.H. Jr (1986) *Aluminium-Lithium Alloys III*, eds. Baker, C. et al, Inst. of Metals, London, 360

Guillet, L. and LeRoux, R. (1967) *Intermetallic Compounds*, ed J.H. Westbrook, Wiley, 453

Gungor, S. and Edwards, L. (1989) *Proc Int Conf on Fracture VII*, eds K. Solomon et al, Houston, Pergammon Press, 2:1171

Gupta, A.K., Gaunt. P. and Chatuverdi, M.C. (1987) *Phil. Mag. A*, 55:375

Harris, S.J., Noble, B. and Dinsdale, K. (1987) *4th Int. Aluminium Lithium Conf.*, eds G. Champier et al, les editions de physique, 415

Hertzberg, R.W. (1983) *Deformation and Fracture Mechanics of Engineering Materials*, Wiley Inc., 497

Hicks, M.A. and Brown, C.W. (1984) *Fatigue 84*, ed C.J. Beevers, EMAS, 3:1337

Hornbogen, E. and Zum Gahr K-H. (1976) *Acta Metallurgica*, 24:581

Huang, J.C. and Ardell, A.J. (1987) *4th Int. Aluminium Lithium Conf.*, eds G. Champier et al, les editions de physique, 373

Hudak, S.J. Jr. and Chan, K.S. (1986) *Small Fatigue Cracks*, R.O. Ritchie and J. Lankford eds, AIME, 379

Hudak, S.J. Jr, Davidson, D.L. and Chan, K.S. (1988), *Growth of Small Cracks in Aeroengine Disk Materials*, AFWAL-TR-88-4090

Inglis, C.E. (1913) *Trans. of the Inst. of Naval Architects*, 55:219

Irwin, G.R. (1948) *Fracturing of Metals*, ASM, 147

Irwin, G.R. (1957) *Journal of Applied Mechanics*, 24:361

Irwin, G.R. (1964) *Applied Materials Research*, 3:65

Irwin, G.R. (1968) *Eng. Fract. Mech.*, 1:241

James, M.R. (1987) *Scripta Metallurgica*, 21:783

Jata, K.V. and Starke E.A. Jr (1986) *Aluminium-Lithium Alloys III*, eds. Baker, C. et al, Inst. of Metals, London, 247

Jensrud, D. (1986) *Aluminium-Lithium Alloys III*, eds. C. Baker et al, Inst. of Metals, London, 411

Kanninen, M.F. and Popelar, C.H. (1985) *Advanced Fracture Mechanics*, Oxford University Press, 173

Keller, R. and Gerberich, W.W. (1989) Scripta Metallurgica., 23:1115

Kendall, J.M. and King, J.E. (1988) *Int. J. of Fatigue*, 10:163

Khireddine, D., Rahoudj, R. and Clavel M. (1989) *Acta Metallurgica*, 37:191

Kitagawa, H. and Takahashi, S. (1976), *Proc. 2nd Int. Conf Mech. Behaviour of Materials*, Boston, 627

Kulwicki, J.H. and Sanders, T.H. Jr. (1984) *Aluminum-Lithium Alloys II*, eds T. H. Sanders and E.A. Starke Jr. TMS-AIME, 31

Laird, C. (1967) *ASTM STP 415*, ASTM, 131

Laird, C. (1978) *Fatigue and Microstructure*, Papers presented at a 1978 ASM materials science seminar, ASM, 149

Lamba, H.S. (1975), *Eng. Fract. Mech.*, 5:693

Lankford, J. (1982), *Fat. Eng. Mat. Struct.*, 5:233

Lankford, J. and Davidson, D.L. (1984) *Fatigue Crack Threshold Concepts*, AIME, 447

Lankford J., Davidson, D.L. and Chan, K.S. (1984), *Metall. Trans. A*, 15A:1579

Lankford, J. and Davidson D.L. (1986) *Small Fatigue Cracks*, R.O. Ritchie and J. Lankford eds, AIME, 51

Lankford, J. and Davidson, D.L. (1987) *Fatigue 87*, eds R.O. Ritchie and E.A. Starke, EMAS, 1769

Lapasset, G. and Loiseau, A. (1987) *4th Int. Aluminium Lithium Conf.*, eds G. Champier et al, les editions de physique, 489

Larsen, J.M. (1987) PhD Thesis, Carnegie Mellon University

Lendvai, J., Gudladt H-J. and Gerold V. (1988) *Scripta Metallurgica*, 22:1755

Lindley, T.C., Richards, C.E. and Ritchie, R.O. (1976) *Metallurgia and Metal Forming*, 268

Liu, H.W. (1961) *J. of Basic Engineering, Trans. of the AIME*, 83:23

Mahmoud, M.A. and Hosseini A. (1986) *Eng. Fract. Mech.*, 24:207

Martin, J.W. (1980) *Micromechanisms in particle-hardened alloys*, Cambridge University Press, 51

McAlister, A.J. (1982) *Bull. Alloy Phase Diagrams*, 3:177

McDarmaid, D.S. (1985) *RAE Technical Report 85016*

McEvily, A.J. (1983) ASTM STP 811, 283

Meier, B. and Gerold, V. (1987) *Fatigue 87*, 323

Miller, W.S., White, S., and Lloyd, D.J. (1987) *4th Int.Aluminium Lithium Conf.*, eds G. Champier et al, les editions de physique, 139

Morris, W.L. (1980), *Metall. Trans. A*, 11A:1117

Morrow, J. (1965) ASTM STP 378, 45

Mowbray, D.F. (1976) ASTM STP 601, ASTM, 33

Mughrabi, H., Wang, R., Differt, D., Essmann, U. (1983) *ASTM STP 811*, ASTM, 5

Muller, W. et al (1986) *Aluminium-Lithium Alloys III*, eds. C. Baker et al, *Inst. of Metals, London*, 435

Murakami, Y. (1986) ASTM STP 942, ASTM, 1048

Murakami, Y. (1987) *Stress Intensity Factors Handbook*, Pergamon Press, 2:712

Murphy, O.R. and Martin J.W. (1986) *Aluminum Technology*, ed T. Sheppard, Inst. for Metals, 429

Neumann, P. (1974) *Acta Metallurgica*, 22:1155

Newman, J.C. Jr and Raju, I.S. (1981) *Eng. Fract. Mech.*, 15:185

Newman, P. and Beevers, C.J. (1986) *Small Fatigue Cracks*, R.O. Ritchie and J. Lankford eds, AIME, 97

Nicholas, T. (1989) Personal communication

Nikishkov, G.P. and Athuri, S.N. (1988) *Eng. Fract. Mech.*, 29:81

Niskanen, P. and Sanders, T.H. Jr. (1982) *Corrosion Science*, 22:283

Noble, B. and Thompson, G.E. (1972) *Met. Sci. J.*, 6:167

Noble, B., Harris, S. J. and Dinsdale, K. (1982) *J. of Mat. Sci.*, 17:461

O'Dowd, M.E., Ruch, W. and Starke, E.A. Jr. (1987) *4th Int. Aluminium Lithium Conf.*, eds G. Champier et al, les editions de physique, 565

Orowan, E. (1948) *Rep. on Prog. in Physics*, 12:185

Owen, N.J., Field, D.J. and Butler, E.P. (1986) *Mat. Sci. and Tech.*, 2:1217

Paris, P.C., Gomez, M.P. and Anderson, P. (1961) *The Trend in Engineering*, 13:9

Paris, P.C. (1964) *Proc. 10th Sagamore Conf.*, Syracuse Univ. Press, 107

Paris, P.C., Bucci, R.J., Wessel, E.T., Clark, W.G. and Mager, T.R. (1972) ASTM STP 513, ASTM, 141

Peacock, H.D., and Martin, J.W. (1989) *5th Int. Aluminium Lithium Conf.*, eds T.H. Sanders Jr and E.A. Starke Jr, MCEP Ltd, 2:1013

Pearson, S. (1975) *Eng. Fract. Mech.*, 7:235

Peel, C.J., Evans, B. and McDarmaid, D. (1986) *Aluminium-Lithium Alloys III*, eds. C. Baker et al, Inst. of Metals, London, 26

Peters, M., Bachmann, V. and Welpmann, K. (1987) *4th Int. Aluminium Lithium Conf.*, eds G. Champier et al, les editions de physique, 785

Peterson, R.E. (1974) *Stress Concentration Factors*, Wiley Inc., 23

Plumbridge, W.J. and Ryder, D.A. (1969) *Metallurgical Reviews*, Review #136, 14:119

Pridham, M., Noble, B. and Harris, S.J. (1986) *Aluminium-Lithium Alloys III*, eds. Baker, C. et al, Inst. of Metals, London, 547

Quist, W.E., Narayanan, G.H. and Wingert, A.L. (1984), *Aluminum-Lithium Alloys II*, eds T.H. Sanders and E.A. Starke Jr. TMS-AIME, 313

Radmilovic, V., Thomas, G., Shiflet, G. J. and Starke, E.A. Jr (1989) *Scripta Metallurgica*, 23:1141

Rice, J.R., (1968) *Journal of Applied Mechanics*, 35:379

Ritchie, R.O., Yu, W., Blom, A.F., Holm, D.K. (1987) *Fat. Eng. Mat. Struct.*, 10:343

Sainfort, P. and Guyot, P. (1986) *Aluminium-Lithium Alloys III*, eds. C. Baker et al, Inst. of Metals, London, 420

Sanders, T.H. Jr. (1981) (1981) *Proc. 1st Int. Aluminum-Lithium Conf.*, eds T.H. Sanders Jr. and E.A. Starke Jr., 63

Schijve, J. (1977) *Report LR-254*, Delft Univ. Of Technology, 35

Schneider, J., Gudladt, H.-J. and Gerold, V. (1987) *4th Int. Aluminium Lithium Conf.*, eds G. Champier et al, les editions de physique, 745

Scott, P.M. and Thorpe, T.W. (1981) *Fat. Eng. Mat. Struct.*, 4:291

Shah, R.C. and Kobayashi, A.S. (1975) *Int. Journ of Fracture*, 9:133

Shih, C. F. and Hutchinson, J.W. (1975) *Report #DEAP-S-14*, Harvard University

Silcock, J.M. (1959) *J. Inst. Metals*, 89:203

Smith, I.F.C. (1986) *The Behaviour of Short Fatigue Cracks*, K.J. Miller and E.R. de los Rios eds., Mech. Eng. Pub., 15

Socie, D.F., Hua, C.T. and Worthem, D.W. (1987) *Fat. Eng. Mat. Struct.*, 10:1

Starke, E.A. Jr. and Lutjering, G. (1978) ASTM STP , ASTM, 205

Suresh, S. (1983) *Metall. Trans. A*, 14A:2375

Suresh, S. and Ritchie, R.O. (1984) *Int. Metals Reviews*, 29:45

Suresh, s. and Ritchie, R.O. (1986) *Small Fatigue Cracks*, R.O. Ritchie and J. Lankford eds, AIME, 227

Suresh, S., Vasudevan, A.K. and Bretz, P.E. (1984) *Metall. Trans. A*, 15A:369

Suresh, S. and Shih, C.F. (1986) *Int. Journ of Fracture*, 30:237

Tanaka, K., Nakai, Y. and Yamashita, M. (1981) *Int. Journ. of Fracture*, 17:519

Tanaka, K. and Nakai, Y. (1983) *Fatigue Crack Threshold Concepts*, eds D.L. Davidson and S. Suresh, AIME, 497

Tanaka, K. (1986) *Small Fatigue Cracks*, R.O. Ritchie and J. Lankford eds, AIME, 343

Taylor, D. and Knott, J.F. (1981), *Fat. Eng Mat. Struct.*, 4:147

Tekin, A. and Martin, J. W. (1989) *Metallography*, 22:1

Tintillier R., Yang, H.S., Ranganathan, N. and Petit, J. (1987) *4th Int. Aluminium Lithium Conf.*, eds G. Champier et al, les editions de physique, 777

Tomkins, B. (1968) *Philosophical Magagazine*, 18:1041

Trantina G.G. and de Lorenzi H.G. (1982) *Proc. Army Symp. on Solid Mech*, AMMRC Report # MS 82-4, 203

Vasudevan, A.K. and Suresh, S. (1985) *Metall. Trans A*, 16A:475

Vasudevan, A.K. and Doherty, R.D. (1987) *Acta Metallurgica*, 35:1193

Vecchio, R.S. and Hertzberg, R.W. (1985), *Eng. Fract. Mech.*, 22:1049

Venkateswara Rao, K.T., Yu, W. and Ritchie, R.O. (1986) *Small Fatigue Cracks*, R.O. Ritchie and J. Lankford eds, AIME, 623

Wagner, L. and Lutjering, G. (1987) *Fatigue 87*, R.O. Ritchie and E.A. Starke, Jr eds, EMAS, 1819

Wanhill, R.J.H (1986) *The Behaviour of Short Fatigue Cracks*, K.J. Miller and E.R. de los Rios eds., Mech. Eng. Pub., 27

White J. and Miller, W.S. (1987) *4th Int. Aluminium Lithium Conf.*, eds G. Champier et al, les editions de physique, 425

Wells, A.A. (1963) *British Welding Journal*, 10:563

Weertman, J. (1978) *Fatigue and Microstructure*, Papers presented at a 1978 ASM materials science seminar, ASM, 279

Wöhler A. (1860) *Zeitschrift fur Bauwesen*, Vol. 10

Wojcik, C.G., Chan, K.S. and Koss, D.A. (1988) *Acta Metallurgica*, 36:1261

Xia, X. and Martin, J.W. (1989) *5th Int. Aluminium Lithium Conf.*, eds T.H. Sanders Jr and E.A. Starke Jr, MCEP Ltd, 1:315

Xiao, Y. and Bompard, P. (1987) *4th Int. Aluminium Lithium Conf.*, eds G. Champier et al, les editions de physique, 737

Yoder, G.R., Pao, P.S., Imam, M.A. and Cooley, L.A. (1988) *Scripta Metallurgica*, 22:1214

Zurek, A.K., James, M.R. and Morris, W.L. (1983) *Metall. Trans A*, 14A:1697